Vol. 04 No. 02 2026

RiESTech

JOURNAL RECENT IN ENGINEERING SCIENCE AND TECHNOLOGY

MBI

E-ISSN : 2985-704X

P-ISSN : 2985-8321

Recent in Engineering Science and Technology (RiESTech)
PT MENCERDASKAN BANGSA INDONESIA (MBI)
Available online at: http://www.mbi-journals.com/index.php/riestech

E-ISSN : 2985-704X
P-ISSN : 2985-8321

Recent in Engineering Science and Technology (RiESTech)

Volume 4 No 2 April 2026

FOCUS AND SCOPE

RIESTECH

Recent in Engineering Science and Technology **(RiESTech):** I*SSN: 2985-704X (print), ISSN: 2985-8321 (online)* a peer-reviewed quarterly engineering journal, publishes theoretical and experimental high-quality papers to promote engineering and technology's theory and practice. In addition to peer-reviewed original research papers, the Editorial Board welcomes original research reports, state-of-the-art reviews, and communications in the broadly defined field of recent engineering science and technology. **RiESTech** covers topics contributing to a better understanding of engineering, material science, computer science, environmental science, and their applications. **RiESTech** is concerned with scientific research on mechanical and civil engineering, Electrical/Electronics and Computer Engineering, and Metallurgical and Materials Engineering with specific analytical techniques and/or computational methods.

The frequency of RiESTech publications is four times a year namely in January, April, July, and October. The scope of RiESTech includes a wide spectrum of subjects namely:

Mechanical and Civil Engineering (Automotive Technologies; Construction Materials; Design and Manufacturing; Dynamics and Control; Energy Generation, Utilization, Conversion, and Storage; Fluid Mechanics and Hydraulics; Heat and Mass Transfer; Micro-Nano Sciences; Renewable and Sustainable Energy Technologies; Robotics and Mechatronics; Solid Mechanics and Structure; Thermal Sciences)

Electrical/Electronics and Computer Engineering (Instrumentation; Coding, Cryptography, and Information Protection; Communications, Networks, Mobile Computing, and Distributed Systems; Compilers and Operating Systems; Parallel Processing, and Dependability; Computer Vision and Robotics; Control Theory; Electromagnetic Waves, Microwave Techniques and Antennas; Embedded Systems; Integrated Circuits, VLSI Design, Testing, and CAD; Microelectromechanical Systems; Microelectronics, and Electronic Devices and Circuits; Power, Energy and Energy Conversion Systems; Signal, Image, and Speech Processing; Machine Learning and Data Science)

E-ISSN : 2985-704X
P-ISSN : 2985-8321

Metallurgical and Materials Engineering (Advanced Materials Science; Ceramic and Inorganic Materials; Electronic-Magnetic Materials; Energy and Environment; Materials Characterization; Metallurgy Extractive; Polymers and Nanocomposites)

Environmental Science and Engineering (Waste Management, Climate Change, Zero Waste, Environmental Disaster Management, Circular Economy, Sustainable Development, Environmental Security, Environmental Management, Environmental Ecology, Conservation of Natural Resources And Environment, Environmental Impact Analysis, Planning and Environmental Administration, Environmental Health, Environmental Pollution, Environmental Accounting, and Environmental Information Systems)

Recent in Engineering Science and Technology (RiESTech)
PT MENCERDASKAN BANGSA INDONESIA (MBI)
Available online at: http://www.mbi-journals.com/index.php/riestech

E-ISSN : 2985-704X
P-ISSN : 2985-8321

Recent in Engineering Science and Technology

(RiESTech)

Volume 4 No 2 April 2026

Recent in Engineering Science and Technology (RiESTech)
PT MENCERDASKAN BANGSA INDONESIA (MBI)
Available online at: http://www.mbi-journals.com/index.php/riestech

E-ISSN : 2985-704X
P-ISSN : 2985-8321

Layout and Typesetting:

Imam Sapto Nugroho, Universitas Indonesia (Alumni), Indonesia
Kamil Raihan Permana, Universitas Indonesia, Indonesia
Raihan Trinanda Agsya, Politeknik Negeri Jakarta, Indonesia

PUBLISHER
PT MENCERDASKAN BANGSA INDONESIA (MBI)
Address : 4th Floor Gedung STC Senayan Room 31-34, Jl. Asia Afrika Pintu IX, Jakarta 10270, Indonesia.

Recent in Engineering Science and Technology (RiESTech)
PT MENCERDASKAN BANGSA INDONESIA (MBI)
Available online at: http://www.mbi-journals.com/index.php/riestech

E-ISSN : 2985-704X
P-ISSN : 2985-8321

Recent in Engineering Science and Technology (RiESTech)

Volume 4 No 2 April 2026

PREFACE

Journal RiESTech (e-ISSN: 2985-704X (online), p-ISSN: 2985-8321 (print); is a peer review journal published by PT Mencerdaskan Bangsa Indonesia. The RiESTech journal is published four times a year in January, April, July, and October. This journal provides direct open access to its content on the principle that making research freely available to the public supports a greater global exchange of knowledge within the engineering field. This journal aims to provide a place for academics, researchers, and practitioners to publish original research articles or review articles. The scope of articles published in this journal relates to various topics in the field of outcomes of research activities.

The RiESTech journal publishes papers strictly following the RiESTech guidelines and templates for manuscript preparation. All submitted manuscripts will go through a double-blind peer review process. The paper is read by members of the editor (according to the area of specialization) and will be screened by the Managing Editor to meet the criteria required for RiESTech publication. Manuscripts will be sent to two reviewers based on their historical experience in reviewing manuscripts or based on their areas of specialization. RiESTech has review forms to keep the same item reviewed by two reviewers. Then the editorial board makes a decision on the comments or suggestions of the reviewers.

Reviewers provide an assessment of originality, clarity of presentation, contribution to the field/science. This journal publishes research articles, review articles/literature reviews, case reports and concept/policy articles, in all fields of Computer Science, Informatics Engineering, Multimedia, Arts. The article to be published is an original work and has never been published. Incoming articles will be reviewed by the reviewer team.

The Editorial Board will try to continue to improve the quality of the journal so that it can become an important reference in the development of engineering sciences. The greatest appreciation and gratitude to Mitra Bestari along with members of the Editorial Board and all parties involved in the publication of this journal. Complete writing instructions are displayed on the portal of this journal.

Regards,

Chief Editor

Recent in Engineering Science and Technology (RiESTech)
PT MENCERDASKAN BANGSA INDONESIA (MBI)
Available online at: http://www.mbi-journals.com/index.php/riestech

E-ISSN : 2985-704X
P-ISSN : 2985-8321

Recent in Engineering Science and Technology (RiESTech)

Volume 4 No 2 April 2026

Contents

Articles

RiESTech
Recent in Engineering Science and Technology

MBI

Article

Measuring Thermal Conductivity and Magnetic Strength Using Low-Cost Sensors Based on an Open-Source Platform Arduino

Nazhmi Fadhila [1], Filia Solagratia Takasumiang [1], Hanandira Wistikhirana [1], Yudha Dewangga [1], Rafi Pradaya Andareska [1], Agus Edy Pramono [2,*], Iman Setiyadi [2]

[1] Study program of Applied Bachelor of Manufacturing Technology, Politeknik Negeri Jakarta, Indonesia
[2] Magister Program in Applied Manufacturing Technology Engineering, Politeknik Negeri Jakarta, Indonesia
* Correspondence: agus.edypramono@mesin.pnj.ac.id

Abstract: The use of low-cost sensors controlled by an open-source microcontroller (Arduino) is investigated in this study to measure electrical, thermal, and magnetic parameters, and to evaluate the feasibility of using these sensors for future extraction of intrinsic material properties such as thermal conductivity and magnetic response. The MAX6675 and HMC5883L sensors, together with an SS49E Hall sensor, were used to monitor a carbon rod supplied with 29.9 V DC. The MAX6675 thermocouple sensor recorded surface temperatures in the range of 48–50 °C, showing consistent trends when cross-checked against multimeter readings. The HMC5883L magnetic sensor measured an average magnetic field strength of approximately 8.65 G, remaining within stable control limits across all trials. Meanwhile, the electrical current recorded manually from the digital display of the power supply due to the absence of an installed current sensor averaged 0.21 A during testing. Minor signal interference was observed when multiple sensors operated simultaneously, indicating the need for electrical isolation or signal multiplexing in future designs. These findings demonstrate that low-cost open-source sensors can produce consistent and interpretable data for basic material characterization, supporting the development of affordable instrumentation as a practical alternative to commercial measurement systems. Accordingly, this work emphasizes sensor consistency and measurement feasibility rather than reporting final thermal conductivity values.

Keywords: Low-cost sensors; Arduino; Thermal conductivity; Magnetic strength

Citation: Fadhila, N., Takasumiang, F. S., Wistikhirana, H., Dewangga, Y., Andareska, R. P., Pramono, A. E., Setiyadi, I. (2026). Measuring Thermal Conductivity and Magnetic Strength Using Low-Cost Sensors Based on an Open-Source Platform Arduino. Recent in Engineering Science and Technology, 4(02), 59–72. Retrieved from https://www.mbi-journals.com/index.php/riestech/article/view/118.

Academic Editor: Vika Rizkia

Received: 16 June 2025
Accepted: 3 February 2026
Published: 30 April 2026

Publisher's Note: MBI stays neutral with regard to jurisdictional claims in published maps and institutional affiliations.

1. Introduction

Many researchers have been using low-cost sensors controlled by cheap microcontrollers as an economical alternative to expensive commercial tools over the years [1], [2], [3], [4], [5], [6]. A common microcontroller used is open-source platform Arduino that can be used for many purposes. Arduino project itself has many board models, one of which is Arduino UNO. Arduino UNO is a microcontroller board based on ATmega328P microcontroller. It has 14 digital pins, 6 analog pins, 5V and 3.3V rail, 3 ground pins, for I2C communications SDA and SCL pin and a USB connection to connect to a computer. Arduino IDE is used to write and upload code to the board.

Some low-cost sensors incorporate hall elements, such as Allegro™ ACS712 current sensor. ACS712 has a copper conduction path inside which current flows and generates magnetic field. Hall IC then converts the magnetic field into proportional voltage. There are 3 variants of ACS712 which have different current sensing ranges from 5A, 20A and 30A. ACS712 has been used as an economical choice for measuring AC or DC current. A study used ACS712 to measure current discharged by Battery Discharger Board (BDB), a device that allows discharging Li-ion cells with a programmable profile. While ACS712 is low-cost, the measurements are noisy. In order to filter the noise, Kalman Filter (KF) a linear quadratic estimation is used and the signal produced becomes smooth [7]. The high

noise recorded using ACS712 in some cases are thoroughly considered. An example is in this study that develops a test bench for checking the quality of electric vehicle chargers. A range of sensors are used and ACS712 is considered for AC and DC current measurements. However, the author noted that the hall-effect principle is not suitable for AC current measurement and used OP-AMP 358 in a non-inverting amplifier mode instead. Filter circuits are used for both AC and DC measurements. A DHT11 temperature sensor is also used to monitor internal components of the charger [8]. Current and other parameters produced by photovoltaic panels need to be monitored and, in this study, an ESP32 board and ACS712 30A are used with additional Bluetooth features. The study showed that the ACS712 experienced intense noise of 130 mA. To filter the noise, instead of using KF, an alternative simple method is proposed using 470nF capacitor. The result shows the system is able to monitor photovoltaic panels especially in isolated places where the internet network is absent [9]. An ESP32 board is also used in this study developing an IoT system to monitor batteries used in electric vehicles. ACS712 30A is used to measure current and LM35, a high voltage analog temperature sensor is also used. The study designed a voltage divider network consisting of 1kΩ and 2kΩ resistors to achieve a full scale reading of 30A within the 3.3V maximum limit of I/O pins and the ADC input. A Sallen-Key active low pass filter is used to achieve precise and accurate current measurements within short durations (below 10ms). A noticeable difference is observed after the filter is installed [10]. Voltage irregularities are often responsible for damaging electrical equipment. In order to protect the equipment, an experimental system was developed using Arduino UNO board, ZMPT101B for measuring voltage and ACS712 for measuring AC current. The system helps protect overvoltage and undervoltage conditions in a single-phase power supply [11]. This study used ACS712 5A sensor to monitor current consumed by Dynamixel MX 64 AT servo motor used in mobile robotic platforms. The system used Arduino Mega 2560 board and ADS1115, a 16-bit ADC, to improve the resolution and measure currents in the order of tens of milliamps. The experiment showed that the largest error for ACS712 compared to a multimeter is 13.75% and the lowest error at 0.38% [12]. This wide range of accuracy error trend would continue to this study of comparing the measurements from ACS712 controlled by ATMega328P to a high precision network power analyzer Chauvin Arnoux C.A 8335. The largest error observed is 19.38%. In home appliances including hot dryer, fluorescent lamp, heater and a laptop the largest accuracy error is 3.43% [13]. ACS712 is also used in the machining industry. A device using ACS712, and an Arduino board is developed to measure RMS current in drilling machines. The measurements are taken every 50ms and recorded with the help of LabView. The study explored ways to monitor drill bit condition and using current signature can effectively detect tool wear. ACS712 is able to detect current rising with respect to increased friction as drilling depth increases. Rate of current also rises high during initial wear of the drill bit. With more usage, the current amplitude increases thus indicating wear [14].

Another example of a low-cost sensor using hall elements is SS49E. SS49E are small devices that are commonly used to detect magnetic field. It has a wide magnetic range of ±1000G with a supply voltage of 5V. Unlike ACS712, the SS49E doesn't require filtering circuit due to the integrated circuitry that features low noise output and an additional amplifier to strengthen the signal. A demonstration of the capability of the SS49E is showed in this study of recording the magnetic field produced by underwater cable. Four SS49E sensors and a DS18B20 temperature sensor are used in this experiment. DS18B20 is used to account for temperature variations and thus make the magnetic field measurements more accurate. Arduino Nano board is chosen as the microcontroller and an additional feature of a microSD card module to record data. The difference between the theoretical magnetic field and the measured magnetic field is within range considered admissible. The results are that the underwater measurements are very accurate ±0.3% on average and both in and out of salt water. The study showed that the device could work

and store magnetic field measurements up to 150 m under the sea [15]. Other studies have shown that SS49E is a perfectly viable alternative to measure magnetic field strength in a wide range of applications. This study used SS49E and Arduino board to control the magnetic field of a MAGLEV system to be constant by adjusting current running through the coil. Magnetic field strength generated by a ferrosilicon core with 1250 turns and a current of 0.58A is measured by SS49E sensor to be 0.0811T or 811G and be able to levitate a body of 0.1 kg [16]. In thermodynamics field, SS49E also saw usage. The magnetic field affecting the performance of thermoelectric cooler is measured using SS49E and an Arduino Mega 2560 board. LM35 temperature sensor is also used. To simulate the magnetic field, a system is built consisting of two magnetic coils to produce 2T of magnetic intensity. The result of the study shown that coefficient of performance (COP) increases with the magnetic field. From 0.875T to 1.25T, the maximum enhancement of COP can be found at 1.25T [17]. In the food industry, SS49E and Arduino Nano board is used to measure EMF to evaluate its effects to the quality of the cocoa beans from the fermentative process. To generate the EMF, lab scale Helmholtz coils are used to generate variable density magnetic field of 1 to 120mT. The measurements are read using LabView. The result of the study revealed that magnetic field densities of 5 to 42mT improves yield and flavor of the cocoa beans and 80mT correlates to low yield and bitterness [18]. In another study, a 49E sensor which is similar to SS49E and a small neodymium magnet is integrated to a DIY filament extruder machine. Arduino Nano board is used to process the output from the sensor and control the extruder speed. The change of the filament diameter can be calculated by detecting the magnetic field strength. The experiment showed that the obtained tolerance of the filament diameter is ±0.1 mm. However, the produced filament is not up to the industry standards of tolerance up to ±0.05 mm for precision FDM printing [19]. An alternative to SS49E sensor is MLX-90215 sensor. In this study, the sensor is used with a 16-bit ADC USB-6210 to measure magnetic strength of iron oxide nanoparticles coated with either SiO^2 and TiO^2. The measurements are compared to the SQUID magnetometer model MPMS-XL. At the saturation region, the largest error is at 10% and the lowest at 0.4% [20]. A1302 sensor is also a popular alternative to SS49E. A study used A1302 and LMT86 temperature sensor with additional components such as a solar panel and a network system to monitor structural crack in a monumental architecture. The system could detect displacement and measure in tens of micrometers [21].

Another parameter, besides current and magnetic strength, commonly measured using low-cost sensor is temperature. There are various types of temperature sensors, from NTC thermistor, resistance temperature detectors (RTDs), thermocouples and semiconductors. One of which is easy to interface using Arduino boards are thermocouples using a MAX6675 that digitize signal from type-K thermocouple. This converter outputs the measurements in resolution up to 0.25°C and is able to read maximum temperatures of 1024°C. To interface with an Arduino board, SPI communication is used. There are several studies using MAX6675 and demonstrated its capabilities in lab and even in industrial scale. MAX6675 has a similarity with ACS712, with them being noisy. However, several studies have proven that either with or without an additional circuit to improve the accuracy of the sensors by filtering the noise or by adding Analog-to-Digital Converter (ADC) to improve resolution, the measured data is deemed accurate enough for it to be reliable. Four type-K thermocouples with MAX6675 each are used with Arduino Mega 2560 board and a microSD card module to measure temperatures of a water in a heater controlled using a voltage regulator in this study. Similar to ACS712, KF is used to improve the readings accuracy and reduce the noise [22]. This study discusses the application of a low-cost smart system for a heat treatment of AISI 1040 steel. To monitor the temperatures, a type-K thermocouple with MAX6675 is connected to an Arduino UNO board with an additional feature of wireless communications using NRF240L01 receiver and ESP8266 board. Using the smart system, the hardness of AISI 1040 is measured at 232 HV whilst from traditional normalizing heat

treatment process measured at 234 HV. The temperature error observed is ±3oC with no additional filtering process required [23]. This study explored the efficiency in energy of thermoelectric devices (TEDs) when operated as thermoelectric coolers (TECs). To measure temperature, the author used 3 MAX6675 connected to an ESP32 board to measure the hot side of the TEC. Due to MAX6675 not able to read below 0°C, to measure the cold side the author proposed MAX31855, which is similar to MAX6675, but deemed too difficult to use with the SPI interface and DS18B20 is used instead requiring only one digital pin and is also more affordable [24]. This study developed an IoT device to use with any commercial furnace lab or oven to measure temperatures using MAX6675. The system helps the user observe real-time temperature data and can detect fire or overheating. The average reading compared to commercial thermometer difference is observed at 0.34% which is accurate enough for this safety system [25]. This study uses MAX6675 and an Arduino board to control the heater temperature of a filament extruder. A simple bang-bang control is implemented to control the heater if it has reached the desired temperature to extrude the filament [26]. This study utilized MAX6675 to measure the temperature of the pot in a design of smart electric cooking stove. There are several problems regarding the temperature readings, including a lag in actual change of temperature and the study suggests that direct contact of the sensor to the heating surface is required and also coating the thermocouple with heat insulation material to avoid convectional heat to affect the thermocouple [27]. A unique implementation of MAX6675 is in this study used for temperature control of electrically floated samples with a thermocouple in direct contact with it. The device is electrically insulated from the CVD chamber and the Arduino UNO board is connected to a ZigBee Wi-Fi unit. The difference between thermocouple reading and an infrared pyrometer can be +25°C at 140-minute mark while the temperature reading of the MAX6675 stays constant at 650°C throughout the experiment. The study revealed that this error is due to a change in emissivity [28]. This study developed a system using MAX31855K to digitize signal from type-K thermocouple and Arduino to process it. The system is used to measure the temperature of a ladle transporting molten steel and the performance of the system is evaluated under harsh environments. The system shows great durability and did not fail while measuring up to 1250°C temperatures at prolonged periods of time and the accuracy of the data meets the industry quality standards [29]. A study developed a system that was developed for characterization of thermoelectric generators (TEGs) for energy harvesting using MAX31855 for temperature measurements and ACS712 5A sensor for current acquisition. It's shown that the temperature error reaches 12% while the current measurements have an error of 4%, both without calibration measures [30].

The aim of this study is to make a low-cost and easy to fabricate device, based on affordable sensors and an Arduino board to measure thermal conductivity and magnetic strength of a material. While low-cost sensors have been used to easily measure parameters in a range of applications, few have been used to process and calculate from the data to obtain material properties, especially in thermal conductivity [31].

Accordingly, this study aims to develop a low-cost and easy-to-fabricate Arduino-based instrumentation prototype (GTAM) and to evaluate its feasibility for future extraction of intrinsic material properties especially for thermal conductivity and magnetic response). In this work, feasibility is assessed by demonstrating synchronized monitoring of thermal, magnetic, and electrical parameters under controlled DC excitation and by examining measurement consistency during repeated trials.

This work contributes (i) an integrated multi-sensor prototype built from affordable modules, (ii) a practical acquisition workflow that includes real-time display and automatic CSV data logging to support repeatable experiments and post-processing, and (iii) a stability summarization approach using control-chart boundaries (CL, UCL, and LCL) to describe sensor consistency across trials. The observed interference and

placement sensitivity indicate that isolation/multiplexing and fixed sensor mounts are needed to improve future measurements.

2. Design, Material and Construction method

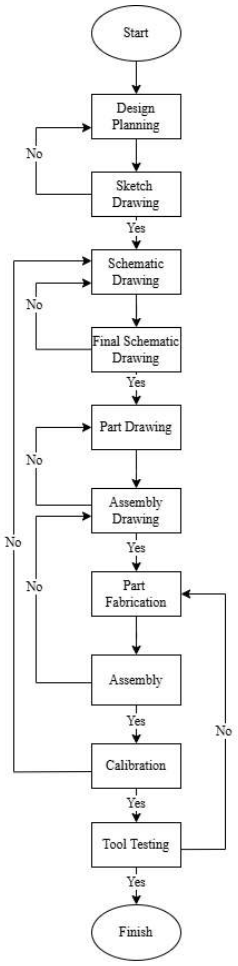

Figure 1. Stages of design and construction of the GTAM

In designing this measuring instrument, several software are used to help, such as Solidworks (SW) to help design, in addition because this measuring instrument is based on Arduino, Arduino IDE is used to help in the electrical field. Figure 1 explains more clearly about the flow of design and construction stages.

- Design planning, initial design planning that includes objectives, tool specifications, and system requirements, which will produce output in the form of an initial design planning document (design brief).
- Sketch drawing means making a rough sketch to express ideas and concepts for the physical form of the tool.
- Schematic drawing, creating a schematic diagram of the electrical system and sensors. The output produced is a wiring diagram shown in Figure 3.
- Part drawing, steps for making technical drawings of each component of a measuring instrument.
- Assembly drawing, a drawing that shows how all the components are assembled and produces output in the form of an exploded view as shown in figure 2.
- Part fabrication, the process of physically making each component based on the drawings that have been made.
- Assembly, assembling all mechanical and electronic parts into one unit.

- Calibration is required to set the initial value and system settings to comply with measurement standards.
- Tool testing, comprehensive testing of tool functionality to ensure all systems work as they should.

3. Results and Discussion

3.1. Visual Design and System Diagrams

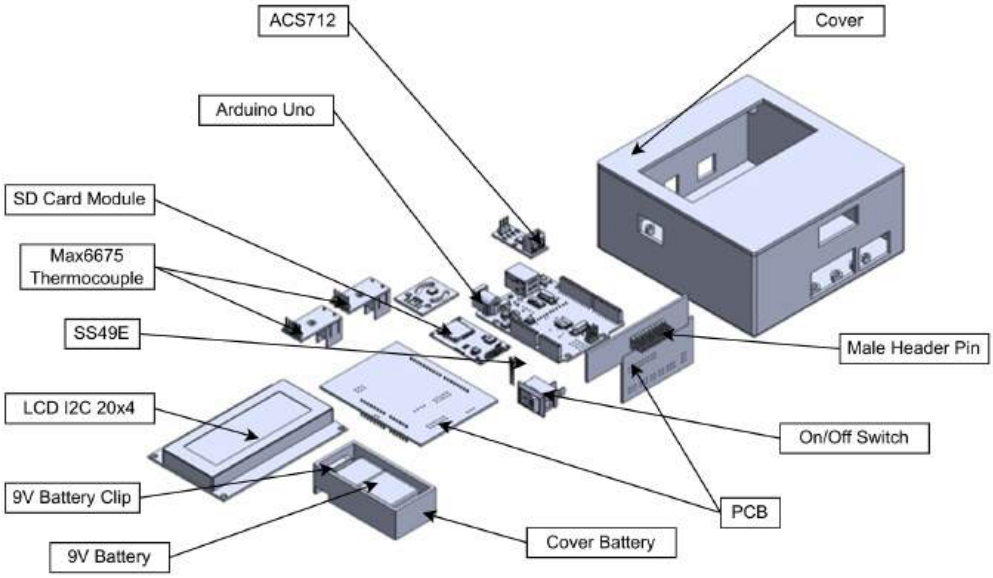

Figure 2. Exploded of GTAM

The design of the measurement device results in the exploded view configuration shown in Figure 2. In the exploded view, the dimensions of each component are intentionally omitted as a form of copyright protection by the designer. Several components in this design are commercially available modules, while others—such as the casing, PCB, and battery cover—are custom-fabricated parts developed to support the system's integration and portability.

This design article groups the components of the measurement device into several major categories:

a) Electronic Module Components
The electronic module components of the measurement device consist of several integrated modules that support the system's functionality. The Arduino Uno serves as the central microcontroller, responsible for acquiring data from various sensors and executing control operations. Temperature measurement is handled by the MAX6675 Thermocouple Module, which interfaces with the Arduino via the SPI communication protocol for accurate thermal readings. The ACS712 current sensor is used to measure the electric current in the circuit, while the SS49E magnetic sensor captures magnetic field intensity in analog form, allowing for precise detection of magnetic variations. To log data, the device uses an SD Card Module, which stores the collected sensor information for further analysis or archival. Real-time readings are presented through the LCD I2C 20x4 display, which uses the I2C communication interface to efficiently communicate with the Arduino, minimizing the use of digital pins and simplifying wiring.

b) Power Supply Components
The system is powered using a 9V battery connected via a 9V battery clip, with an on/off switch integrated on the PCB to control power flow to the Arduino and modules. This ensures ease of operation and portability without the need for external power adapters.

c) Mechanical & Structural Components

The mechanical and structural components of the device are designed to provide a stable foundation and protective enclosure for all electronic modules. The Printed Circuit Board (PCB) serves as the primary base, facilitating the physical arrangement and electrical interconnection of all sensors and modules. Male header pins are integrated onto the PCB to allow modular, plug-and-play connections, simplifying assembly and maintenance. The entire system is enclosed within a custom-designed cover, which not only protects the internal components from mechanical impact and environmental exposure but also features cutouts that ensure accessibility to the LCD display, power switch, and sensor interfaces. Additionally, a dedicated battery cover secures the 9V battery in place, ensuring both safety and ease of replacement. This structural integration enhances both the functionality and durability of the measurement device.

All components are arranged in a compact and modular layout to ensure easy maintenance, future upgrades, and reliable field operation. The enclosure ensures durability and ease of use in various environmental conditions.

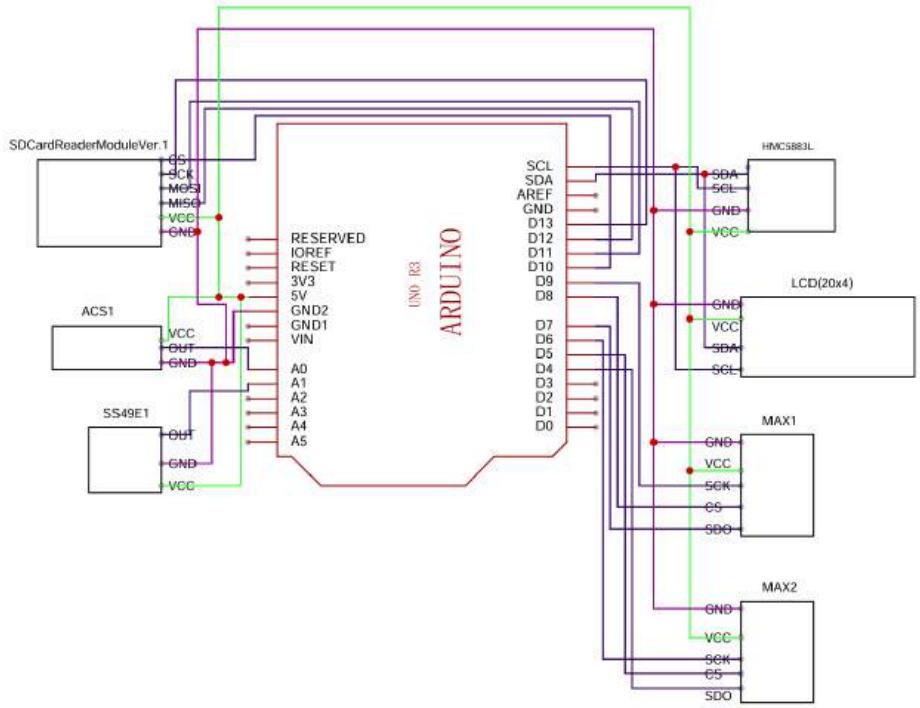

Figure 3. Wiring Diagram of GTAM

The Arduino Uno serves as the central controller, receiving a 5V power supply. The SD Card Reader Module is connected via SPI (pins D10–D13) to store data in CSV format. The LCD 20x4 uses I2C communication (SDA: A4, SCL: A5) to display real-time readings. The HMC5883L magnetic field sensor also uses I2C protocol (SDA: A4, SCL: A5). Two MAX6675 thermocouple modules are connected via SPI using separate CS pins (D2 and D3). Analog sensors, ACS712 (current sensor) and SS49E (hall-effect magnetic sensor), are connected to analog pins A0 and A1 respectively. This configuration allows synchronized acquisition and logging of temperature, magnetic field, and current data.

3.2. System Testing Result and Analyst

Table 1. Data of Experience

Experiment	Ampere (A)	T1 (°C)	T2 (°C)	Gauss (G)	X (mT)	Y (mT)	Z (mT)
1	0,21	48,75	37,25	8,45	-18,09	4,9	17,6
2	0,22	49	37,25	8,55	-18,09	4,9	17,53
3	0,2	49,5	37,5	8,73	-17,91	4,8	17,44
4	0,2	49,5	37	8,64	-18,55	5	17,55
5	0,21	49,75	37,75	8,91	-18,18	5,1	17,44
6	0,22	49,75	37,75	8,82	-18	5,31	17,53
7	0,22	49,25	37,5	8,64	-17,82	5	17,6
8	0,21	49,75	37,25	8,36	-17,91	5,1	17,48
9	0,2	49,75	37,25	8,45	-18,09	4,9	17,44
10	0,21	50	37,25	8,36	-18,09	5	17,58
11	0,22	50	37,25	8,55	-17,91	5	17,58
12	0,21	50	37	8,82	-18,36	5,1	17,51
13	0,2	49,75	37,25	8,73	-18,18	4,9	17,48
14	0,22	49,5	37,25	8,91	-18,45	5,2	17,48
15	0,21	50,25	37,25	8,82	-18,55	5,2	17,46

The test was conducted by passing DC current through the carbon rod using a regulated power supply at 29,9V. The MAX6675 thermocouple sensor was mounted directly on the rod to measure the surface temperature, while the HMC5883L magnetic field sensor was positioned approximately 15 cm next to the rod. Each trial data of temperature, magnetic field, and current values were recorded simultaneously every 1 second.

Among all the sensors installed, only the thermocouple (MAX6675) produced stable and interpretable readings. The dual thermocouple setup experienced interference when both were installed simultaneously on the carbon rod, so it was decided to rely on only one sensor for valid data, in this experiment the thermocouple sensor relied on was the one shown in column T1.

It should be noted that the current readings in the table do not come from the system's internal sensors, but are taken manually from the current display on the power supply during testing.

Based on the collected test data, visualization is carried out in the form of graphs for each measurement parameter, namely electric current (amperes) shown in figure 4, temperature from the T1 sensor (MAX6675), gauss from HMC5883L sensor, and magnetic field components on the X, Y, and Z axes from SS49E sensor. The magnetic field components on the X, Y, and Z axes are expressed in millitesla (mT), which is a standard SI-derived unit used to represent magnetic flux density. Current data is recorded manually from the power supply display, while other data is obtained from automatic sensor readings.

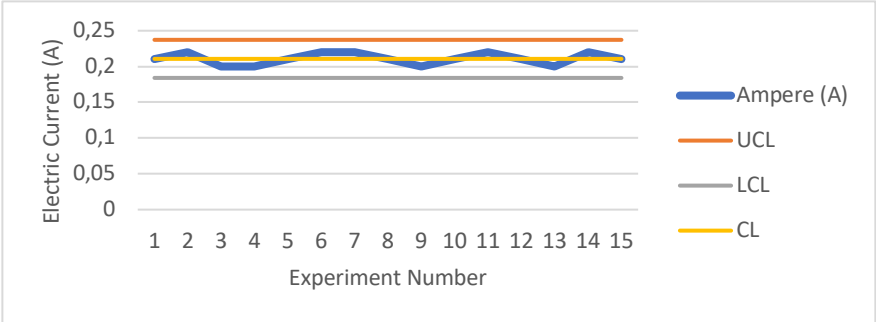

Figure 4. Graph of Ampere Measurement

The control chart shown in Figure 4, Figure 5, Figure 6 and Figure 7 use three reference lines, namely the Center Line (CL), Upper Control Limit (UCL), and Lower Control Limit (LCL), to evaluate the stability of the measurement results. The CL represents the average value of the observed data and reflects the normal operating condition of the system. The UCL and LCL define the upper and lower boundaries of acceptable data variation, respectively, which are statistically determined based on the dispersion of the measured values. Data points falling within these limits indicate that the system operates under stable and controlled conditions, while points exceeding the UCL or falling below the LCL suggest potential anomalies, disturbances, or measurement errors. In this experiment that shown in Figure 4, all current data remain within the control limits, indicating consistent and reliable system performance.

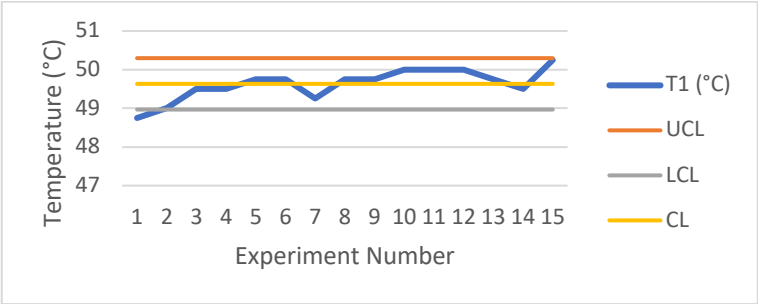

Figure 5. Graph of T1 Measurement

From the temperature graph of the T1 sensor shown in Figure 5, the measured temperature generally exhibits a stable and gradual increase over the experimental trials and remains within the defined control range. One data point, observed in the first trial, falls outside the control limits, indicating a deviation from both the Upper Control Limit (UCL) and Lower Control Limit (LCL). This deviation is attributed to the initial transient condition of the system, where the temperature had not yet reached a steady-state after power-up. Following the first trial, all subsequent temperature readings fall within the control limits, demonstrating stable system performance and reliable surface temperature measurement of the carbon rod under DC current excitation.

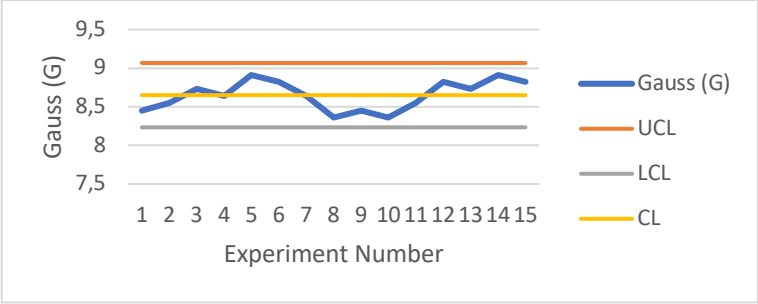

Figure 6. Graph of Gauss Measurement

Magnetic field measurements were carried out using the HMC5883L sensor placed at a distance of about 15 cm next to the carbon rod. The data obtained were in the form of magnetic field strength values (in Gauss units). The measurement results showed that all magnetic field strength values were within the control limits (UCL and LCL), with an average of 8.649 Gauss. As shown in Figure 6, no data was found that deviated from the control limits (CL), indicating that the sensor provided relatively stable and acceptable results for the purposes of observing the trend of magnetic field changes due to current flow in the carbon rod.

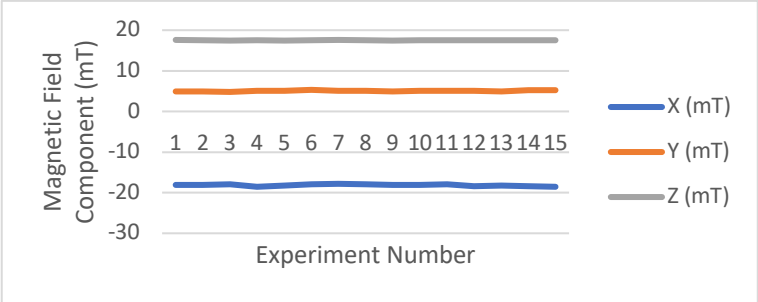

Figure 7. Graph of Magnetic Field Measurement

The measurement data of magnetic field components on the X, Y, and Z axes shown in figure 7 relatively small and stable fluctuations in value throughout 15 experiments. However, although the graph shows relative stability, it should be noted that the sensor position has not been permanently fixed. The sensor is only placed at a distance of about 15 cm next to the carbon rod without using a jig. Therefore, the use of a jig is highly recommended in further testing to improve the accuracy and repeatability of vector magnetic field component measurements.

Overall, this work goes beyond reporting raw sensor outputs by demonstrating a complete measurement workflow, including real-time monitoring, automatic CSV logging, and post-processed stability evaluation using control limits (CL/UCL/LCL). The consistent trends observed across trials indicate that this integrated workflow is practical for repeatable low-cost instrumentation prototyping.

3.3. Technical Issues and Solutions

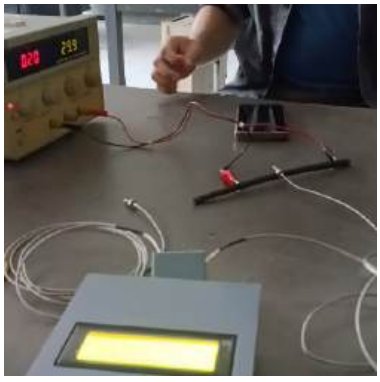

Figure 8. Documentation of Experiment

During the system assembly and testing process, several technical issues were found that affected the quality and consistency of the data. One of the main obstacles occurred in the use of two MAX6675 thermocouple sensors simultaneously attached directly to the carbon rod. The test results showed that one of the sensors could not provide a valid temperature reading or experienced interference (error). This is thought to be caused by signal interference due to the installation position being too close, as well as possible conflicts in data communication from the sensors. To overcome this, it was decided to use only one thermocouple sensor (T1) which was proven to provide the most stable and reliable results.

The next problem is related to reading the current value. In this system, there is no ACS712 current sensor installed due to device and time limitations. Instead, the current value is taken directly from the digital display on the power supply used to flow current to the carbon rod. Although this method is not an automatic reading through the system, the current value from the power supply is quite stable and is used as a reference in

recording data. The use of accurately calibrated current sensors is still recommended for future tool development.

Another problem was found in the installation position of the HMC5883L and SS49E magnetic field sensors. Both sensors were simply placed next to the carbon rod at a distance of about 15 cm without using a jig or fixed support. This unfixed position has the potential to cause small variations in orientation and distance between experiments, which can affect the results of the magnetic field readings, especially in the X, Y, and Z axes. Although the graph shows general data stability, the use of a jig is essential to ensure the accuracy and repeatability of the measurement results in further testing.

In addition, in the first experiment, the temperature reading by the T1 sensor showed a value that was outside the upper control limit (UCL). This is thought to have occurred because the system had not reached a stable thermal condition when data collection began. Therefore, it is recommended to provide a pre-heating period before data recording begins to ensure that all components are in a steady-state condition.

Overall, various technical problems found have been identified and analyzed. Temporary solutions have been implemented, and several recommendations for improvement have been prepared for the development of the tool to be more stable and accurate in the future.

3.4. Interpretation and Future Improvements

Based on the test results, this measuring instrument system shows quite good performance in recording temperature and magnetic field data simultaneously. The MAX6675 thermocouple temperature sensor provides the most stable results with a measurement range of 48–50°C, especially from the first sensor (T1) which is used as the main reference because readings from two sensors simultaneously cause errors in the measurement.

One of the advantages of this system is the automatic data storage feature. Each measurement result of temperature, magnetic field, and current is displayed in real-time on a 20x4 LCD, and simultaneously stored in CSV format on an SD card, making it easier for users to document and analyze data further.

However, there are still some technical limitations that need to be fixed:

- Current reading is not yet automatic, because internal current sensors such as the ACS712 are not installed on this device due to system limitations, so current data is still recorded manually from the power supply display.
- Calibration of the magnetic field unit has not been carried out, due to limited reference tools or calibration standards. As a result, the displayed gauss value is still relative and its accuracy in international units cannot be guaranteed.
- The absence of a jig to position the magnetic sensor causes possible inconsistencies in position between experiments.

As a future development, several things that are recommended include:

- Addition of an automatic current sensor so that all parameters can be recorded directly by the system.
- Making a jig or fixed mount for the HMC5883L and SS49E sensors to improve accuracy and repeatability.
- Calibration of the magnetic field sensor against a standard magnetic field source or using a verified reference tool.

With these improvements, the measuring instrument that has been developed can be upgraded towards a portable, automatic physical monitoring system that is ready to be used in the context of research, laboratory testing, or simple industrial needs.

4. Conclusions

This study developed and evaluated a low-cost, Arduino-based instrumentation prototype (GTAM) for synchronized monitoring of thermal, magnetic, and electrical parameters on a carbon rod under DC excitation. During system testing, temperature measurements obtained using the MAX6675 thermocouple (T1) were stable and interpretable, with surface temperatures recorded in the range of 48–50 °C, and only an initial transient point outside the control limits before the system reached steady-state behavior. Magnetic measurements using the HMC5883L sensor remained within the control limits across all trials, yielding an average magnetic field strength of 8.649 Gauss and demonstrating consistency for trend observation. The electrical current during testing averaged 0.21 A, but it was recorded manually from the power-supply display because the ACS712 current sensor was not installed in the device at the time of experimentation.

Several practical limitations were identified. The dual MAX6675 configuration showed interference when two thermocouple modules were mounted simultaneously on the rod therefore, a single thermocouple channel (T1) was used for valid temperature acquisition. In addition, magnetic sensor positioning was not fixed using a jig, which may introduce small variations between trials, and magnetic calibration could not be performed due to limited reference standards; thus, the magnetic readings should be interpreted primarily for repeatable trend monitoring rather than absolute calibration-grade measurement.

Overall, the results indicate that low-cost, open-source sensors integrated in a compact platform can produce consistent and interpretable data for basic characterization and instrumentation prototyping. Future improvements should prioritize (i) installing an automatic current sensor for fully integrated electrical monitoring, (ii) applying electrical isolation or signal multiplexing to reduce multi-sensor interference, (iii) implementing fixed-position fixtures (jigs) to improve measurement repeatability, and (iv) conducting sensor calibration against verified reference tools to strengthen quantitative interpretation for future material-property extraction.

Acknowledgments: The designer and author would like to express their gratitude to Mr. Iman Setiyadi who acted as a donor by providing funds for the design and manufacture of this gauss, temperature and ampere (GTAM) measuring instrument.

Conflicts of Interest: "The authors declare no conflict of interest."

References

[1] V. A. Balogun, B. I. Oladapo, A. O. M. Adeoye, J. F. Kayode, and S. O. Afolabi, "Hysteresis analysis of Thornton (IP6, IP12E and TH5V) magnetic materials through the use of Arduino microcontroller," *Journal of Materials Research and Technology*, vol. 7, no. 4. pp. 443–449, 2018. doi: 10.1016/j.jmrt.2017.05.018.

[2] P. F. Pereira and N. M. M. Ramos, "Low-cost Arduino-based temperature, relative humidity and CO2 sensors - An assessment of their suitability for indoor built environments," *Journal of Building Engineering*, vol. 60. 2022. doi: 10.1016/j.jobe.2022.105151.

[3] A. S. Ali, Z. Zanzinger, D. Debose, and B. Stephens, "Open Source Building Science Sensors (OSBSS) A low-cost Arduino-based platform for long-term indoor environmental data," *Build. Environ.*, vol. 100, pp. 114–126, 2016, doi: https://doi.org/10.1016/j.buildenv.2016.02.010.

[4] D. A. McGranahan, "FeatherFlame: An Arduino-based thermocouple datalogging system to record wildland fire flame temperatures in agris," *Rangeland Ecology and Management*, vol. 76. pp. 43–47, 2021. doi: 10.1016/j.rama.2021.01.008.

[5] J. F. D. F. Araujo, E. B. M. Junior, and L. A. F. Mendoza, "A Simple Portable Magnetometer Based on Magnets and Hall-Effect Sensors Capable of Measuring Magnetic Properties," *Appl. Sci.*, vol. 12, no. 24, 2022, doi: 10.3390/app122412565.

[6] E. C. Prima, S. Karim, S. Utari, R. Ramdani, E. R. R. Putri, and S. M. Darmawati, "Heat Transfer Lab Kit using Temperature Sensor based ArduinoTM for Educational Purpose," in *Procedia Engineering*, 2017, pp. 536–540. doi: 10.1016/j.proeng.2017.03.085.

[7] P. L. dos Santos, T. P. A. Perdicoúlis, P. A. Salgado, and J. C. Azevedo, "Kalman filter for noise reduction of Li-Ion cell discharge current," *IFAC-PapersOnLine*, vol. 56, no. 2. pp. 9582–9587, 2023. doi: 10.1016/j.ifacol.2023.10.261.

[8] J. Jency Joseph, F. T. Josh, S. Leander Gilbert, and S. Leander Gilbert, "A test bench on quality checking for electric vehicle chargers," in *Materials Today: Proceedings*, 2021, pp. 8176–8181. doi: 10.1016/j.matpr.2021.02.554.

[9] Z. Didi and I. El Azami, "Experimental Analysis and Monitoring of Photovoltaic Panel Parameters," *Int. J. Adv. Comput. Sci. Appl.*, vol. 14, no. 2, pp. 151–157, 2023, doi: 10.14569/IJACSA.2023.0140219.

[10] S. Haldar, S. Gol, A. Mondal, and R. Banerjee, "IoT-enabled advanced monitoring system for tubular batteries: Enhancing efficiency and reliability," *e-Prime - Adv. Electr. Eng. Electron. Energy*, vol. 9, 2024, doi: 10.1016/j.prime.2024.100709.

[11] D. D. Tung and N. M. Khoa, "An Arduino-Based System for Monitoring and Protecting Overvoltage and Undervoltage," *Eng. Technol. Appl. Sci. Res.*, vol. 9, no. 3, pp. 4255–4260, 2019, doi: 10.48084/etasr.2832.

[12] G. Constantin *et al.*, "Monitoring the Current Provided by a Hall Sensor Integrated in a Drive Wheel Module of a Mobile Robot," *Machines*, vol. 11, no. 3, 2023, doi: 10.3390/machines11030385.

[13] Đ. Lazarević, M. Živković, Đ. Kocić, and J. Ćirić, "The utilizing Hall effect-based current sensor ACS712 for true RMS current measurement in power electronic systems," *Sci. Tech. Rev.*, vol. 72, no. 1, pp. 27–32, 2022, doi: 10.5937/str2201027L.

[14] J. Gokulachandran and B. Bharath Krishna Reddy, "A study on the usage of current signature for tool condition monitoring of drill bit," in *Materials Today: Proceedings*, 2019, pp. 4532–4536. doi: 10.1016/j.matpr.2020.09.696.

[15] V. Luna, R. Silva, E. Mendoza, and I. Canales-García, "Recording the Magnetic Field Produced by an Undersea Energy Generating Device: A Low-Cost Alternative," *J. Mar. Sci. Eng.*, vol. 11, no. 7, 2023, doi: 10.3390/jmse11071423.

[16] A. H. Takinami, R. B. Cruz, B. L. S. de Lima, and F. Jesus de Almeida, "Design, simulation and development of a magnetic levitation system (MAGLEV)," *Results Phys.*, vol. 17, 2020, doi: 10.1016/j.rinp.2020.103115.

[17] M. S. Nassar, A. A. Hegazi, and M. G. Mousa, "Combined effect of pulsating flow and magnetic field on thermoelectric cooler performance," *Case Stud. Therm. Eng.*, vol. 13, 2019, doi: 10.1016/j.csite.2019.100403.

[18] T. M. Guzmán-Armenteros, L. A. Ramos-Guerrero, L. S. Guerra, S. Weckx, and J. Ruales, "Optimization of cacao beans fermentation by native species and electromagnetic fields," *Heliyon*, vol. 9, no. 4, 2023, doi: 10.1016/j.heliyon.2023.e15065.

[19] Z. T. Piotr *et al.*, "Hall effect diameter sensor integration in DIY filament extruder," in *Procedia Computer Science*, 2022, pp. 1437–1445. doi: 10.1016/j.procs.2022.09.200.

[20] J. F. D. F. Araujo, M. C. Costa, S. R. W. Louro, and A. C. Bruno, "A portable Hall magnetometer probe for characterization of magnetic iron oxide nanoparticles," *J. Magn. Magn. Mater.*, vol. 426, pp. 159–162, 2017, doi: 10.1016/j.jmmm.2016.11.083.

[21] T. Addabbo *et al.*, "A low cost distributed measurement system based on Hall effect sensors for structural crack monitoring in monumental architecture," *Meas. J. Int. Meas. Confed.*, vol. 116, pp. 652–657, 2018, doi: 10.1016/j.measurement.2017.11.050.

[22] R. Septiana, I. Roihan, and R. A. Koestoer, "Denoising MAX6675 reading using Kalman filter and factorial design," *Int. J. Electr. Comput. Eng.*, vol. 11, no. 5, pp. 3818–3827, 2021, doi: 10.11591/ijece.v11i5.pp3818-3827.

[23] D. Saber, H. M. Almalki, and K. Abd El-Aziz, "Design and building of an automated heat-treatment system for industrial applications," *Alexandria Eng. J.*, vol. 59, no. 6, pp. 5007–5017, 2020, doi: 10.1016/j.aej.2020.09.023.

[24] N. P. Bayendang, V. Balyan, and M. T. Kahn, "The question of thermoelectric devices (TEDs) in/efficiency—a practical examination considering thermoelectric coolers (TECs)," *Results Eng.*, vol. 21, p. 101827, Mar. 2024, doi: 10.1016/j.rineng.2024.101827.

[25] M. Hassan, A. Bhattacharjee, M. S. Azam, S. Aziz, M. A. Ali Shaikh, and M. S. Islam, "A smart device of data acquisition with emergency safety features for laboratory furnaces," *Results Eng.*, vol. 19, 2023, doi: 10.1016/j.rineng.2023.101357.

[26] S. Nithya Priya, S. Naveen Kumar, S. Prem Kumar, and K. K. Pradeep, "Design and fabrication of filament extruder with spooler," in *Materials Today: Proceedings*, 2021, pp. 221–223. doi: 10.1016/j.matpr.2021.03.103.

[27] C. Svosve and L. Gudukeya, "Design of A Smart Electric Cooking Stove," in *Procedia Manufacturing*, 2020, pp. 135–142. doi: 10.1016/j.promfg.2020.02.127.

[28] T. Shimada, T. Miura, W. Xie, T. Yanase, and T. Nagahama, "A thermocouple-based remote temperature controller of an electrically-floated sample for plasma CVD of nanocarbons with bias voltage," *Meas. J. Int. Meas. Confed.*, vol. 102, pp. 244–248, 2017, doi: 10.1016/j.measurement.2017.02.012.

[29] V. Chang and C. Martin, "An industrial IoT sensor system for high-temperature measurement," *Comput. Electr. Eng.*, vol. 95, 2021, doi: 10.1016/j.compeleceng.2021.107439.

[30] C. L. Izidoro, O. H. Ando Junior, J. P. Carmo, and L. Schaeffer, "Characterization of thermoelectric generator for energy harvesting," *Measurement*, vol. 106, pp. 283–290, Aug. 2017, doi: 10.1016/j.measurement.2016.01.010.

[31] A. Abed Gatea Al-Shammary, A. Caballero-Calvo, H. A. Jebur, M. Ismael Khalbas, and J. Fernández-Gálvez, "A novel heat-pulse probe for measuring soil thermal conductivity: Field test under different tillage practices," *Comput. Electron. Agric.*, vol. 202, 2022, doi: 10.1016/j.compag.2022.107414.

RiESTech
Recent in Engineering Science and Technology

MBI

Article

Applying Structural Reliability to Risk-Based Inspections of Underwater Crude Oil Pipelines

Muhammad Iqbal [1,*], Johny Wahyuadi Soedarsono [2], and Gusti Verhan Pratama [3]

[1] Department of Metallurgical and Materials Engineering, Universitas Indonesia, Indonesia
* Correspondence: muhammad.iqbal410@ui.ac.id

Abstract: This study investigates the application of structural reliability methods in risk-based inspections (RBIs) for subsea crude oil pipelines. Given the increasing reliance on submarine pipeline infrastructure in offshore oil and gas operations, maintaining its integrity is critical to operational safety and environmental protection. This study uses inspection data from smart pigging operations carried out in 2020 and 2024 on 28.7 km of 12-inch underwater pipes. Using API RP 581 (2020) and First-Order Second-Moment (FOSM) structural reliability theory, this study quantitatively assesses the probability of failure (PoF) and the consequence of failure (CoF). Results showed active internal corrosion, with pitting corrosion identified as the dominant degradation mechanism. Risk projections from 2024 to 2030 reveal unacceptable levels of risk in 2030 if mitigation strategies are not implemented. Based on the financial impact and business risk thresholds, a tailored inspection and maintenance strategy is proposed. These findings support the optimization of inspection intervals and highlight the importance of corrosion control measures such as routine pigging and inhibitor injections.

Keywords: Risk-Based Inspection (RBI); Undersea Pipeline; Structural reliability; Internal corrosion; Probability of Failure (PoF); Consequences of Failure (CoF)

Citation: Iqbal, M., Soedarsono, J. W., Pratama, G. V. (2026). Applying Structural Reliability to Risk-Based Inspections of Underwater Crude Oil Pipelines. Recent in Engineering Science and Technology, 4(02), 73–86. Retrieved from https://www.mbi-journals.com/index.php/riestech/article/view/126.

Academic Editor: Noor Hidayati

Received: 2 September 2025
Accepted: 28 Oktober 2025
Published: 30 April 2026

Publisher's Note: MBI stays neutral with regard to jurisdictional claims in published maps and institutional affiliations.

1. Introduction

In the early 1970s, subsea field development began by placing wellheads and production equipment on the seabed. Over the past decades, subsea systems have advanced from manually operated shallow-water setups to remotely controlled installations at depths of up to 3000 m, supported by significant technological progress (Li et al., 2024).

The sustainability and stability of subsea pipelines is a top priority in the oil and gas industry, given their enormous contribution to the economy, the environment, and human life. serves as the primary infrastructure for draining resources from the offshore work area (Offshore Section) to the Receiving Facility (Onshore Section). Given the increasing global demand for oil and gas, ensuring that pipeline transportation capacity is adequate has become an important operational requirement. Therefore, maintaining the structural integrity and safety of pipelines is critical and requires comprehensive and thorough analysis to reduce the risk of failure. Pipeline failures can result in severe environmental consequences and substantial economic losses for operators. In this context, the probabilistic assessment of pipeline failure due to external corrosion has emerged as a key factor in understanding and managing pipeline integrity (Hocine et al., 2024; Seghier et al., 2018).

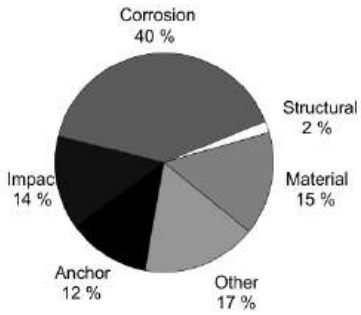

Figure 1. Failure in the Offshore Pipeline System (DNV RP F116)

The reliability and safety of these pipelines is crucial, as failures can lead to environmental damage and large operational losses. Therefore, risk assessment and management are an important part of the design, monitoring, and maintenance of subsea pipelines to prevent problems such as corrosion and damage due to external factors.

Based on the Regulation of the Minister of Energy and Mineral Resources No. 32 of 2021, every equipment and/or installation used in oil and gas business activities must undergo technical inspections and safety inspections. This aims to ensure that the equipment operates in excellent condition, works in safe conditions and minimizes accidents (Kementerian Energi dan Sumber Daya Mineral, 2021). In Indonesia, technical inspections can be carried out using two methods. namely time-based inspection and risk-based inspection (Nurbayanah et al., 2024). The time-based inspection method has the advantage of ease of implementation because it does not require complex technical analysis. However, this approach tends to require higher costs because the entire equipment is inspected at the same interval, without considering the level of risk. Alternatively, a Risk-Based Inspection (RBI) method can be applied that is more focused on risk priorities.

Risk-Based Inspection (RBI) is a systematic and risk-based approach used to design technical inspection programs for equipment in industrial process systems. This approach combines quantitative and/or qualitative evaluation of two main parameters, namely likelihood of failure and consequence of failure, to determine inspection priorities based on the actual level of risk posed by each piece of equipment (American Petroleum Institute, 2020). The RBI aims to allocate inspection resources efficiently, by giving higher priority to equipment with a high level of risk, as well as establishing tailored inspection methods, frequencies, and scopes (American Petroleum Institute, 2020).

Compared to the time-based inspection method, RBI is considered more effective because it takes into account the differences in operating conditions and vulnerabilities of each equipment. Time-based inspections tend to be uniform and do not take into account risk variations, so they can lead to over-inspection of low-risk equipment, and under-inspection of high-risk equipment. In addition, equipment degrades in quality that varies over time due to environmental factors, fluid type, and operating history, making it difficult for time-based approaches to accurately predict potential damage (Hameed et al., 2021).

The implementation of RBI not only provides cost efficiency and reduced downtime, but also improves operational safety, system reliability, and protection of the environment and personnel. Through a comprehensive risk analysis, mitigation and inspection strategies can be designed to maintain equipment performance according to its function (Hameed et al., 2021; Sözen et al., 2022).

Technically, the API RP 581 standard provides a quantitative methodology for calculating Probability of Failure (PoF) and Consequence of Failure (CoF). PoF is calculated through the Damage Factor (DF), formerly known as the Technical Module Sub-Factor (TMSF), while CoF is represented by the Leak Impact Factor (LIF). These factors accommodate the technical aspects of the equipment that affect the probability of

failure as well as its impact on the environment, safety, and economy (American Petroleum Institute, 2020; Haryadi et al., 2020).

The implementation of RBI has been widely carried out in various industrial facilities in Indonesia. A study by Haryadi et al. (2020) on gas piping systems shows that the dominant failure is in the form of thinning, with a moderate risk value and an inspection interval is recommended every three years. Thus, RBI has proven to be a more adaptive, accurate, and efficient approach than conventional inspection methods, and is able to provide technical justification in strategic decision-making related to the inspection and maintenance of critical equipment (Haryadi et al., 2020).

In this study, technical data that includes design data and operational data is collected and analyzed for the subsea pipeline system. The study emphasizes the importance of risk analysis of underwater pipelines, given that their placement on the seafloor makes routine daily monitoring, such as those carried out on onshore pipelines, impossible. The standard used in this study is API RP 581 Third Edition, Addendum 2 of 2020, where the Probability of Failure (PoF) is determined based on the initial identification of the fault mechanism and using the FOSM theory of structural reliability, while the Consequence of Failure (CoF) is calculated based on the highest value of the impact of component damage and its consequences on personnel safety. In addition, the determination of risk limits is used as a reference in the classification of risk levels and inspection planning. This study aims to investigate the application of structural reliability methods in risk based inspection for subsea crude oil pipelines.

2. Experimental Materials and Methods

The researchers focused on the 12" main oil subsea pipeline at PT XYZ which is the design and operating condition based on **Table 1**. This study uses data from in-line inspection (ILI) reports using smart pigging technology. Risk assessment is carried out through a quantitative risk-based inspection methodology (RBI), in accordance with the API 581 standard (2020 edition), by analyzing and evaluating the corrosion rate obtained from the ILI data (American Petroleum Institute, 2020).

Table 1. Pipe Design and Operation

Parameters	Value	Unit
Pipe Identification	12" ABC	-
Total Length	28.7	Kilometer
Material	API-5L- X52	-
SMYS	52.000	Psi
SUTS	60.000	Psi
Design Code	ASME B31.4	-
Pipe Products	Crude oil	-
Nominal OD	12.75	Inch
CA	3.175	Mm
Wall Thickness	0.5	Inch
Design Factor	0.72	-
Design Temperature	200	F
Design Pressure	200	Psi
MAOP	250	Psi
Layer	Creation Layer	-

The subsea pipeline risk method will follow the process as shown in **Fig. 2** below. As seen in **Fig. 2**, risk is the multiplication between the chance of failure (POF) and the impact of failure (COF). This POF x COF product will generate a risk value for each segment of the pipeline regulated every 1 km of pipeline. For this QRA, the risk matrix used follows HSSE PT XYZ.

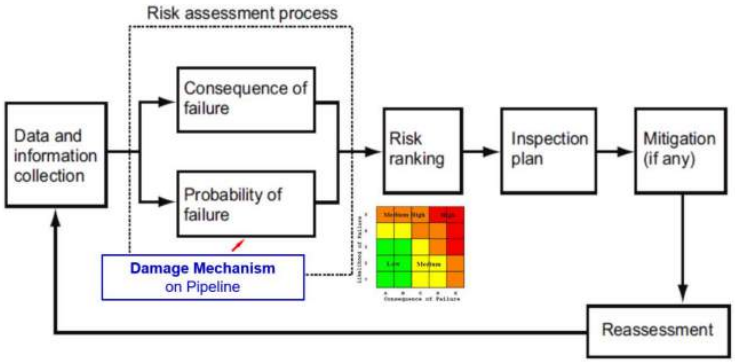

Figure 2. Risk assessment methodology

The risk assessment method, especially the determination of POF uses the FOSM theory of structural reliability, which is an approach from the integrity aspect as a counterpart method or approach from the side of process safety. Risk analysis in this approach is carried out in a quantitative manner, where risk is defined as the result of multiplication between probability and consequence, both of which are expressed in numerical form.

$$R(t) = \text{Pof}(t) \times \text{CoF} \quad (1)$$

The risk that occurs if the risk falls into category V (high-risk), then mitigation must be carried out immediately, if the risk is in category IV moderate to high, then mitigation must be carried out within 1-3 years depending on the remaining age of the pipeline. However, if the risk of falling is category III – I (moderate to low), then in general there is no specific effort that needs to be made, only a monitoring program or routine inspection (Purwidyasari et al., 2023).

Table. 2 Risk matrix untuk penentuan kategori risiko

CONSEQUENCE		PROBABILITY (LIKELIHOOD)					TINGKAT RISIKO
LEVEL	DESCRIPTION	1	2	3	4	5	
		0% < X < 20%	20% < X < 40%	40% < X < 60%	60% < X < 80%	80% < X < 100%	Kategori V Tinggi (15 - 25)
		< 10^{-6} per year	10^{-6} to 10^{-4}/year	10^{-4} to 10^{-2}/year	10^{-2} to 1 / year	> 1 per year	
5	Catastrophic	5	10	15	20	25	Kategori IV Moderat ke Tinggi (10 - 12)
4	Significant	4	8	12	16	20	Kategori III Moderate (5 - 9)
3	Moderate	3	6	9	12	15	Kategori II Rendah ke Moderate (4)
2	Minor	2	4	6	8	10	Kategori I Rendah (1 - 3)
1	Insignificant	1	2	3	4	5	

The implementation of the RBI's analysis requires the collection of data and information relevant to the analyzed subsea pipeline. The data is obtained from an alignment sheet that contains important information about the route and configuration of the subsea pipeline, process flow diagram, piping and instrumentation diagrams, material and construction data, and previous in-line inspection (ILI) reports. The composition of the flowing fluid, design data, operational data, as well as safety systems. All of this collected data will be used in the calculation of probability of failure (PoF), consequence of failure (CoF), and risk level evaluation, and will be the basis for scheduling inspection programs. The probability of failure is sometimes superseded by the rate of accidents, and the COF can be evaluated from the financial or safety losses of the person in terms of the number of deaths. The probability of failure (POF) which is the opposite of reliability (or

the chance of operating without failure), as shown in the simple equation below (American Petroleum Institute, 2020; Purwidyasari et al., 2023).

$$\text{Pof}(t) = \text{GFF} \times \text{DF}(t) \times \text{FM} \quad (2)$$

$$\text{Reliability} = 100\% - \text{Probability of Failure, or } R(t) = 1 - \text{POF}(t) \quad (3)$$

The impact of failure is usually taken into account from aspects; 1) safety, 2) environmental damage and 3) business loss due to oil and gas leakage resulting in financial losses. DNV-RP-F116 explains the division of the losses. For the determination of COF, the worst case scenario principles are usually taken (Norske Veritas, 2010).

During the design phase, the calculation of the design pressure or required thickness is based on a deterministic method, for example when calculating the required pipe thickness, a single sum of SMYS, pressure or otherwise is put into the equation. The risk aspect is only considered by including a few safety factors, such as class location, welding factor or temperature. However, in reality, those parameters are not single values, they always have distributions, and reliability theory takes those distributions into account and incorporates them into the calculations. The concept of structural reliability can be easily explained by the following diagram shown in **Fig. 3**. The probability of failure is described and measured by the area that overlaps between the loading factor and the material's resistance.

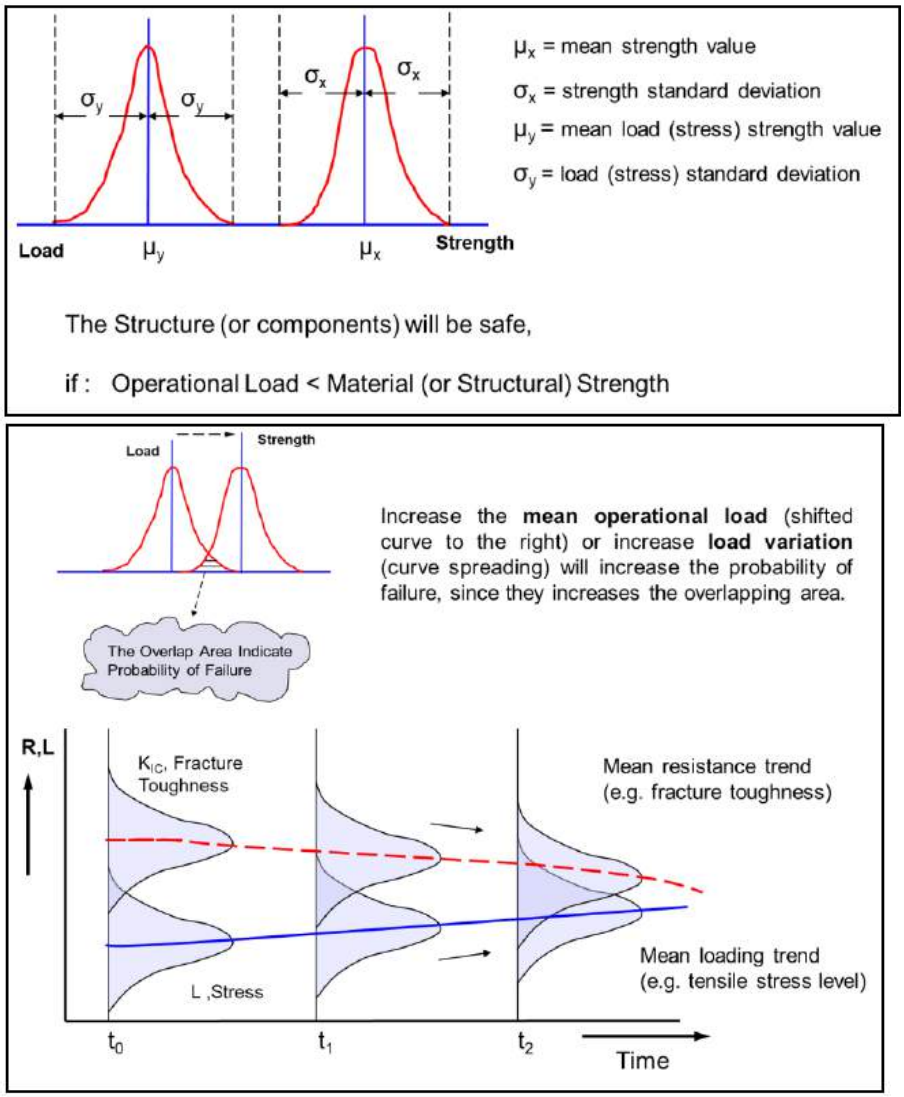

Figure 3. Concept of structural reliability

Probability is defined as the wedge between an increase in the load factor, in this case the tensile stress (and the spread of its curve) and a decrease in the resistance of the material, in this case the strength of the material yield (SMYS) or an increase in its spread (deviation). Without proper action, the likelihood of failure increases over time and the associated risks are increasing, as the area of the slice becomes larger.

To calculate the probability of failure, a linear equation was developed to describe the interference of load resistance or stress strength based on the concept of structural reliability. This is referred to as the finite state function, developed using the second-order moment theory of the first order [4]. The boundary state function is the function, g, which is the difference between resistance and load in the form of a linear equation (Det Norske Veritas, 2017).

$$g = \mathrm{R} - \mathrm{L} \tag{4}$$

g = limit state function

R = material resistance

L = demand, stress intensity factor

The pipe will fail if $g \leq 0$ which means the operating load exceeds the resistance. When the voltage distribution and the power distribution follow the normal distribution function and are independent of each other, by utilizing the Taylor series.

Average Value

$$\mu g \approx \mu R - \mu L \tag{5}$$

Deviation

$$\sigma g = \sqrt{\sigma_R^2 + \sigma_L^2} \tag{6}$$

$$\beta = \frac{\mu R - \mu L}{\sqrt{\sigma_R^2 + \sigma_Y^2}} \tag{7}$$

Reliability Index

$$\beta = \frac{\mu g}{\sigma g} \tag{8}$$

Probability of Failure

$$P_f = \Phi(-\beta) = 1 - \Phi(\beta) \tag{9}$$

Where:

Φ is the standard normal distribution function.

For the determination of the beta index, the standard table of normal distribution is commonly used.

Based on equation (4) if the thinning of the wall is due to corrosion, then the following boundary state function can be developed. The resistance of the material is represented by the yield force (Sy) and the load is replaced by the circular stress (Sh) and the equation of the boundary state function (4) becomes

$$g = Sy - Sh = 0.72\, Sy - \frac{\mathrm{PD}}{2\mathrm{t}} \tag{10}$$

Assuming that D is a constant, then:

Average value

$$\mu g = \mu Sy - \frac{\mu \mathrm{P\ D}}{2\mu \mathrm{t}} \tag{11}$$

Deviation

$$\sigma_g^2 = \left(\frac{dg}{dS_y} . \sigma_{Sy}\right)^2 + \left(\frac{dg}{\mathrm{dP}} . \sigma_P\right)^2 + \left(\frac{dg}{\mathrm{dt}} . \sigma_t\right)^2 \tag{12}$$

Reliability Index, β

$$\beta = \frac{\mu g}{\sigma g} \quad (13)$$

3. Results and Discussion

In 2020 and 2024, in-line inspections have been carried out on 12" subsea pipelines with smart pigs, the results of which are shown in **Table 2** below. The table shows statistical data on corrosion anomalies before and after the insertion (partial replacement) along 6 km in 2023. It is important to review the inspection results and fitness for service (FFS) results before conducting a risk assessment.

Table 2. Inspection Results and Anomalies Recorded Outside the Insertion Segment (Ref No.9).

Types of Anomalies	Feature (%) Wall Loss	ILI 2020 Number of Features			ILI 2024 Number of Features		
		KP0-KP0+323	KP 6 + 342-KP 28 + 702	Entire	KP0-KP0+323	KP 6 + 342-KP 28 + 702	Entire
Internal Corrosion	> 50%	2	138	140	-	-	-
	40 % - 49%	1	1.046	1.047	-	-	-
	30 % - 39%	12	6.762	6.774	1	2	3
	20 % - 29%	76	24.012	24.088	24	815	839
	10 % - 19%	2.220	109.294	111.514	4.333	155.862	160.195
	Total	2.311	141.252	143.563	4.358	156.679	161.037

Data from ILI in 2020 shows that there are 143,563 features due to internal corrosion that exceed 10% of the thickness of the pipe with 140 anomalies having a depth of more than 50% of the thickness of the pipe. Meanwhile, the results of the 2024 ILI inspection show a total of 161,037 features of internal corrosion that exceed 10% metal loss, with the highest value falling in the 30% - 39% metal loss category.

Table 3. Inspection Results and Anomalies Recorded in the Insertion Segment (Ref No.9).

Types of Anomalies	Feature (%) Wall Loss	ILI 2020 Number of Features KP 0+323 – KP 6+342	ILI 2024 Number of Features KP 0+323 – KP 6+342
Internal Corrosion	> 50%	8.745	-
	40 % - 49%	8.486	-
	30 % - 39%	20.234	-
	20 % - 29%	51.126	-
	10 % - 19%	77.889	797
	Total	166.480	797

In the table above, compare the number of corrosion anomalies before and after insertion along 6 km. Data from ILI in 2020 shows that there are 166,480 features that exceed 10% of the thickness of the pipe, with 8,745 features exceeding 50% of the metal loss. Meanwhile, the results of the 2024 ILI inspection show that 797 features fall in the range of 10% - 19% metal loss. Partial replacement in 2023 eliminates internal corrosion attacks on 6 km of pipes, but in the following 1 year there have also been 797 cases of metal loss, which indicates that the internal corrosion demolition mechanism is actively running due to the presence of water as a corrosive electrolyte medium.

Furthermore, from the results of the FFS Assessment, the remaining life of the 12" subsea pipeline is determined. The remaining life calculation is performed for each segment by selecting the highest corrosion rate per joint for each section. From the calculation results, it has been found that the highest general corrosion rate is 0.46 mm/year (0.0185 inch/year), and the shortest remaining life is 12.8 years. This highest corrosion rate data is then used as the basis for the calculation of POF and subsequent risks.

3.2 Probability of Failure (PoF)

The calculation of POF using the structural reliability method is presented in the Table. 4 In the table, the relative POF value is seen as a function of the KM pipeline (KP). The KP selection was taken from each segment with the highest corrosion rate and wall thinning from the ILI results, with CR = 3 x 0.46 mm/year or 0.054 inch/year (assuming pitting corrosion). From **Table 4** seen for 2024, the maximum POF value of a subsea 12" pipeline is 2.18E-05.

Table 4. Data Pipeline and Failure Opportunity Calculation (POF) for 2024

			Design Basis					Pipeline Thickness Data			
No	KP	Nominal Thickness (Inch)	SMYSS (Psi)	SMYS Std Dev (Psi)	Diameter (Inch)	Pressure Avg (Psi)	Pressure Std Dev (Psi)	Wall Thinning or Corr Depth (%)	Max Corrosion Rate (Inch/Year)	Inspection Year	Current Thickness (Inch)
1	6909,582	0,500	52.000	13.000	12	250	25	0,26	0,0543305	2024	0,37
2	7640,114	0,500	52.000	13.000	12	250	25	0,20	0,0543305	2024	0,40
3	8109,733	0,500	52.000	13.000	12	250	25	0,22	0,0543305	2024	0,39
4	9787,022	0,500	52.000	13.000	12	250	25	0,23	0,0543305	2024	0,39
5	10090	0,500	52.000	13.000	12	250	25	0,23	0,0543305	2024	0,39
6	111136,213	0,500	52.000	13.000	12	250	25	0,23	0,0543305	2024	0,39
7	13917,032	0,500	52.000	13.000	12	250	25	0,20	0,0543305	2024	0,4
8	14952,484	0,500	52.000	13.000	12	250	25	0,29	0,0543305	2024	0,355
9	15482,625	0,500	52.000	13.000	12	250	25	0,29	0,0543305	2024	0,355
10	16235,429	0,500	52.000	13.000	12	250	25	0,28	0,0543305	2024	0,36
11	17105,471	0,500	52.000	13.000	12	250	25	0,26	0,0543305	2024	0,37
12	18011,275	0,500	52.000	13.000	12	250	25	0,25	0,0543305	2024	0,375
13	19204,33	0,500	52.000	13.000	12	250	25	0,23	0,0543305	2024	0,385
14	20742,348	0,500	52.000	13.000	12	250	25	0,28	0,0543305	2024	0,37
15	21160,384	0,500	52.000	13.000	12	250	25	0,25	0,0543305	2024	0,375
16	22545,134	0,500	52.000	13.000	12	250	25	0,29	0,0543305	2024	0,355
17	23345,945	0,500	52.000	13.000	12	250	25	0,29	0,0543305	2024	0,355
18	24136,911	0,500	52.000	13.000	12	250	25	0,28	0,0543305	2024	0,36
19	25862,659	0,500	52.000	13.000	12	250	25	0,28	0,0543305	2024	0,36
20	26628,444	0,500	52.000	13.000	12	250	25	0,28	0,0543305	2024	0,36
21	27918,836	0,500	52.000	13.000	12	250	25	0,33	0,0543305	2024	0,335
22	28010,675	0,500	52.000	13.000	12	250	25	0,29	0,0543305	2024	0,355

			Limit State Function Parameters & Calculation						Reliability Parameter		
No	KP	Nominal Thickness (Inch)	dg/d (SMYS)	dg/dP	dg/dt	μ_g SMYS (dg/d(SMYS))- μp (Hoop Stress)	σ^2_g	σ_g	Index Reliability (β)	Reability (Prob. of Failure Free)	Probability of Failure (PoF)
1	6909,582	0,500	0.72	-16,22	10956,90	33,386	87.794.243	9.369,9	3,5631	0,999817	1,83E-04
2	7640,114	0,500	0.72	-15,00	9375,00	33,690	87.765.079	9.368,3	3,5962	0,999839	1,61E-04
3	8109,733	0,500	0.72	-15,38	9861,93	33,594	87773.966	9.368	3.5957	0.999867	1,68E-04
4	9787,022	0,500	0.72	-15,58	10119,75	33,544	87773.966	9.368	3.5957	0.999867	1,72E-04
5	10090	0,500	0.72	-15.98	10139.75	33.544	87778.703	9.368	3.5803	0.999858	1,72E-04
6	111136,213	0,500	0.72	-15.98	10139.75	33.544	87778.703	9.368	3.5803	0.999858	1,68E-04
7	13917,032	0,500	0.72	-16.0	9375.0	33.69	87765.015	9.368	3.5631	0.999829	1,61E-04
8	14952,484	0,500	0.72	-16.07	9375.0	33.69	87765.015	9.368	3.5631	0.999829	1,97E-04
9	15482,625	0,500	0.72	-16.22	11902.4	33.215	87812.078	9.37	3.5445	0.999803	1,97E-04
10	16235,429	0,500	0.72	-16.17	11094.87	33.386	87808.85	9.37	3.569	0.999844	1,92E-04
11	17105,471	0,500	0.72	-16.07	11574.07	33.273	87805.85	9.37	3.5903	0.999863	1,83E-04
12	18011,275	0,500	0.72	-16.22	11902.4	33.215	87812.078	9.37	3.5445	0.999803	1,79E-04
13	19204,33	0,500	0.72	-16.17	11094.87	33.386	87808.85	9.37	3.569	0.999844	1,72E-04
14	20742,348	0,500	0.72	-16.07	11574.07	33.273	87805.85	9.37	3.5903	0.999863	1,92E-04
15	21160,384	0,500	0.72	-16.22	11902.4	33.215	87812.078	9.37	3.5445	0.999803	1,79E-04
16	22545,134	0,500	0.72	-16.17	11094.87	33.386	87808.85	9.37	3.569	0.999844	1,97E-04
17	23345,945	0,500	0.72	-16.67	13366.01	32.962	87840.282	9.372	3.5509	0.999782	1,97E-04
18	24136,911	0,500	0.72	-16.9	11902.4	33.215	87812.078	9.37	3.5445	0.999803	1,92E-04
19	25862,659	0,500	0.72	-16.67	11574.07	33.273	87805.85	9.37	3.5509	0.999803	1,92E-04
20	26628,444	0,500	0.72	-16.9	11902.4	33.215	87812.078	9.37	3.5445	0.999803	1,92E-04
21	27918,836	0,500	0.72	-16.67	13366.01	32.962	87840.282	9.372	3.5509	0.999782	2,18E-04
22	28010,675	0,500	0.72	-16.9	11902.4	33.215	87812.078	9.37	3.5445	0.999803	1,97E-04

Based on the POF calculation above, the KP with the highest POF at KP 27918,836 was taken to calculate the estimated change in POF as a time function from 2024 to 2030

for two damage mechanism scenarios, namely general corrosion and pitting corrosion as seen in table 5 and table 6 below. Pitting corrosion rate is assumed to be 3 x general corrosion rate in accordance with the recommendations of API 581 RBI. It can be seen that there is an increase in POF from 2024 to 2030, especially for pitting corrosion cases assuming the corrosion rate is constant. (Det Norske Veritas, 2017; Padmodwiputra et al., 2022)

Table. 5 POF Projections for 2024 – 2030) for Pipeline Locations with the Highest POF (Scenario I – *General Corrosion*)

Pipeline Risk Related to General Corrosion Rate

KP	Nominal Thickness Data	Design Data			Operational Data		Pipeline Thickness Data			
		SMYS (Psi)	SMYS Std Dev (Psi)	Diameter (Inch)	Pressure (Psi)	Pressure Std Dev (Psi)	Wall Thinning or Corr Depth (%)	Max Corr. Rate (Inch/Year)	Inspection Year	Predicted Thickness (Inch)
27918.836	0,500	52.000	13.000	12	250	25	0,33	0,0181	2024	0,335
	0,500	52.000	13.000	12	250	25	0,33	0,0181	2025	0,335
	0,500	52.000	13.000	12	250	25	0,33	0,0181	2026	0,335
	0,500	52.000	13.000	12	250	25	0,33	0,0181	2027	0,335
	0,500	52.000	13.000	12	250	25	0,33	0,0181	2028	0,335
	0,500	52.000	13.000	12	250	25	0,33	0,0181	2029	0,335
	0,500	52.000	13.000	12	250	25	0,33	0,0181	2030	0,335

Pipeline Risk Related to General Corrosion Rate

KP	Pipeline Thickness Data	Limit State Function Parameters & Calculation						Reability Parameter		
	Inspection Year	dg/d (SMYS)	dg/dP	dg/dt	μ_g SMYS (dg/d(SMYS))-μp (Hoop Stress)	σ^2_g	σ_g	Index Reliability (β)	Reability (Prob. of Failure Free)	Probability of Failure (PoF)
27918.836	2024	0.72	-17,91	0,00	32,962	87.810.090	9.379,70	3,5176	0,999782	2,18E-04
	2025	0.72	-18,93	0,00	32,962	87.833.661	9.371,96	3,5171	0,999782	2,18E-04
	2026	0.72	-20,08	0,00	32,962	87.861.646	9.373,45	3,5166	0,999781	2,19E-04
	2027	0.72	-21,38	0,00	32,962	87.895.221	9.375,25	3,5159	0,999781	2,19E-04
	2028	0.72	-22,85	0,00	32,962	87.935.981	9.377,42	3,5151	0,999780	2,20E-04
	2029	0.72	-24,54	0,00	32,962	87.986.132	9.380,09	3,5141	0,999780	2,21E-04
	2030	0.72	-26,51	0,00	32,962	88.048.798	9.383,43	3,5128	0,999778	2,22E-04

Table. 6 POF Projections for 2024 – 2030) for Pipeline Locations with the Highest POF (Scenario II – *Pitting Corrosion*)

Pipeline Risk Related to General Corrosion Rate

KP	Nominal Thickness Data	Design Data			Operational Data		Pipeline Thickness Data			
		SMYS (Psi)	SMYS Std Dev (Psi)	Diameter (Inch)	Pressure (Psi)	Pressure Std Dev (Psi)	Wall Thinning or Corr Depth (%)	Max Corr. Rate (Inch/Year)	Inspection Year	Predicted Thickness (Inch)
27918.836	0,500	52.000	13.000	12	250	25	0,33	0,0543	2024	0,335
	0,500	52.000	13.000	12	250	25	0,33	0,0543	2025	0,281
	0,500	52.000	13.000	12	250	25	0,33	0,0543	2026	0,226
	0,500	52.000	13.000	12	250	25	0,33	0,0543	2027	0,172
	0,500	52.000	13.000	12	250	25	0,33	0,0543	2028	0,118
	0,500	52.000	13.000	12	250	25	0,33	0,0543	2029	0,063
	0,500	52.000	13.000	12	250	25	0,33	0,0543	2030	0,009

Pipeline Risk Related to General Corrosion Rate

KP	Pipeline Thickness Data	Limit State Function Parameters & Calculation						Reability Parameter		
	Inspection Year	dg/d (SMYS)	dg/dP	dg/dt	μ_g SMYS (dg/d(SMYS))-μp (Hoop Stress)	σ^2_g	σ_g	Index Reliability (β)	Reability (Prob. of Failure Free)	Probability of Failure (PoF)
27918.836	2024	0.72	-17,91	13366,01	32,962	87.810.090	9.372.31	3,5170	0,999782	2,18E-04
	2025	0.72	-21,38	13366,01	32,962	87.925.418	9.376,86	3,5153	0,999780	2,20E-04
	2026	0.72	-26,52	13366,01	32,962	88.079.008	9.385,04	3,5122	0,999778	2,22E-04
	2027	0.72	-34,88	13366,01	32,962	88.400.313	9.402,14	3,5058	0,999772	2,28E-04
	2028	0.72	-50,99	13366,01	32,962	89.264.772	9.448,00	3,4888	0,999757	2,43E-04
	2029	0.72	-94,73	13366,01	32,962	93.248.384	9.656,52	3,4135	0,999679	3,12E-04
	2030	0.72	-666,25	13366,01	32,962	365.072.213	19.106,86	1,7252	0,957751	4,22E-04

Based on table 5 and table 6 above, a projection is made of the thickness value assuming a constant corrosion value. The corrosion mechanism used is in the form of general corrosion and pitting corrosion based on API 581. Where the pitting corrosion value is multiplied by 3 of general corrosion. And based on the results of the calculation projection, it is found that in 2030 the PoF value will increase significantly. This also happens in research (Witek, 2021). Where the degradation of the structural integrity of the pipeline shows a significant increase as the operating time increases, indicating a progressive process of material aging.

3.2 Consequences of Failure

To make the calculation of COF, it is taken from the experience experienced by PT. XYZ when there was a leak in the pipe, it was reported that the average loss value from two pipe leaks in 2019 was Rp. 14,653,083,679 / leak. This figure includes business loss components, repair materials, barge rentals, mob-demobs, etc. Quantitatively, the COF category used was taken from the HSSE of PT. XYZ with its COF category can be seen in the table below.

Table. 7 Failure Impact Range, COF, and Their Categorization

CONSEQUENCE OF PIPELINE FAILURE		
Financial Impact	**Asset & Equipment**	**Level**
> 80% BTR	Total Loss of Plant or Estimated Repair Cost **> USD 5.000.000**	5 Catastrophic
60% - 80% BTR	Partial Loss of Plant / Plant Shutdown or Estimated Repair Cost **USD 1.000.000 - 5.000.000**	4 Significant
40% - 60% BTR	Partial Plant Shutdown or Estimated Repair Cost **USD 100.000 - 1.000.000**	3 Moderate
20% - 40% BTR	Possible Brief Disruption of Process or Estimated Repair Cost **USD 10.000 - 100.000**	2 Minor
≤ 20% BTR	No Disruption to Process or Estimated Repair Cost **< USD 10,000**	1 Insignificant

3.3 Risk Assessment

The determination of the risk was obtained from the multiplication of POF x COF and then compared with two criteria. The calculation is carried out using pitting corrosion rate as the worst case scenario. Criterion no.1 is to compare the oil loss calculation for various un-planned shutdown conditions with the 5 x 5 risk matrix (**Table 2**). The risk calculation is carried out assuming that there is an improvement during t = 2 days of shutdown with a business loss value of USD 189,800 due to oil being wasted into the sea. Furthermore, the results of the risk calculation are shown in Table 8 for conditions in KP 27918.836. PT XYZ previous data showed that the value of losses every time there was a leak was IDR 14,653,083,679 or USD 976,872.

Table 8. Business loss (USD) in the event of an unplanned shutdown with various possible lengths of pipeline inability to deliver crude oil.

Shutdown Period	Flow Rate (Barrel)	Business Value USD
One Days	1.300	94.900
Two Days	2.600	189.800
Three Days	3.900	284.700
One Week	18.200	1.328.600
Note: Assumsing Crude Oil Price is USD 73/Barrel (Nov 2024)		

Table 9. Total financial risk (USD) as a function of time for pitting corrosion

Risk Assesment Result at KP 27918.836 Refer to Risk Matrix						
No	Tahun	Current Thickness (Inch)	Probability of Failure (PoF)	Consequence of Failure (USD)	Total Financial Risk	Risk Condition
1	2024	0,335	2,182306E-04	976.872	Risk Category III – Moderate (5-9)	Acceptable
2	2025	0,281	2,196351E-04	976.872		
3	2026	0,226	2,221849E-04	976.872		
4	2027	0,172	2,27586E-04	976.872		
5	2028	0,118	2,425785E-04	976.872		
6	2029	0,063	3,20688E-04	976.872		
7	2030	0,009	4,224936E-04	976.872	Risk Category IV Moderate to High (10 – 12)	Non-Tolerable

Table 9 based on the worst case scenario, namely. 1. Corrosion occurs in the pipe that undergoes the most severe thinning (in KP 27.9) 2. The corrosion rate is taken for pitting corrosion conditions with a rate of 3x general corrosion rate [9]. 3. The length of time for oil to be discharged into the sea is 2 days assuming the shutdown system and emergency response planning go well. In line with the growth of metal loss and the depletion process from 2024 to 2030,

it can be seen that the risk changes from moderate (level III) to moderate - high risk (level IV). It can be seen that changes will occur in 2028 to 2029.

Criterion no.2 is to compare the oil loss calculation for various un-planned shutdown conditions with the value of BTR = 5% x Net Profit, which is the maximum allowable risk value per year planned by PT XYZ (see **Table 10**).

Table. 10 Maximum allowable risk values

BTR = 5% x Net Profit		
NET Profit Tahun 2024	USD	93.910
Basis Trading Risk (BTR)	USD	4695,5

The risk of loss is calculated for 2024 to 2030 and its value is compared to BTR USD 4695.5. Next, the results of the risk calculation are shown in Table 11 for conditions in KP 27918.836.

Table. 11 Risk profile as a function of time (Ref: BTR)

Risk Assesment Result at KP 27918.836 Refer to Annual Maximum Acceptable Value (BTR)						
No	Tahun	Current Thickness (Inch)	Probability of Failure (PoF)	Consequence of Failure (USD)	Risk (USD)	Max Allowable Risk Value (BTR)
1	2024	0,335	2,182306E-04	976.872	213,18	Acceptable
2	2025	0,281	2,196351E-04	976.872	214,56	
3	2026	0,226	2,221849E-04	976.872	217,05	
4	2027	0,172	2,275866E-04	976.872	222,32	
5	2028	0,118	2,425785E-04	976.872	236,97	
6	2029	0,063	3,20688E-04	976.872	313,27	
7	2030	0,009	4,224936E-04	976.872	41.272,22	Non-Tolerable

Along with the increase in metal loss and the process of depletion of the pipeline wall from 2024 to 2030, there is a change in the level of risk from the acceptable category to the non-tolerable category, as shown in Table 11.5. This significant change is seen in 2029 towards 2030, where the risk value has decreased from USD 313.27 to USD 41,272. Until 2029, the risk value is still below the Basic Target Risk (BTR) so it is still acceptable. However, by 2030, the risk value exceeds the BTR threshold, indicating that the risk is no longer tolerable.

In contrast to the first risk assessment criterion, where the change in risk occurs gradually from the yellow to orange category, in the second criterion the transition occurs directly from the green category (acceptable risk) to red (unacceptable risk)). Nonetheless, from an operational technical perspective, the two assessment approaches show equal meaning and conclusions.

The two assessment criteria consistently yield the same conclusion, namely that after 2030, the level of risk has exceeded the permissible tolerance limit. Therefore, it is necessary to implement a comprehensive Inspection, Maintenance, and Testing (IMT) strategy to mitigate these risks. It should be noted that the risk calculation presented above is based on a conservative approach, so it still contains an inherent safety factor.

3.3 Recommendations of Inspection, Maintenance & Test (IMT) Plan

In order to effectively mitigate risks, it is necessary to plan a comprehensive and structured Inspection, Maintenance, and Testing (IMT) strategy. This approach provides

visualization of the logical flow starting from hazard identification to the implementation of mitigation measures aimed at reducing potential production losses.

Furthermore, the IMT strategy is shown in detail in Table 12, which outlines risk control approaches to various forms of threats to the safety of pipeline operations. This strategy includes both time-dependent threats such as internal and external corrosion, as well as time-independent threats such as the mechanical impact of third-party interference (e.g. anchor drops or pulling), as well as potential geological hazards (geohazards). This approach aims to maintain the integrity of the piping system through risk management based on relevant threat characteristics.

The recommended corrosion control strategy includes regular cleaning pigging and injection of corrosion inhibitors combined with biocides, to prevent corrosion and microbiologically induced corrosion (MIC). Furthermore, it is necessary to develop a Pipeline Integrity Management System (PIMS) as a systematic framework in carrying out all aspects of risk mitigation that are time-dependent and non-time (time-independent threats), including external threats such as mechanical impacts from third parties and potential geohazards, so that pipeline integrity management can be carried out in a sustainable and risk-based manner.

Table 12. Inspection, Maintenance and Test Plan

No	Threat or Risk	IMT Classification	IMT Method	Purposes	Recommended Time Interval	Remarks
1	Internal Corrosion Causing Pipeline to Leak	Direct Integrity Inspection	Inline Inspection (ILI)	To determine the metal loss of pipeline wall thickness	5 years (based on QRA result)	Inspection time is governed by the QRA or RL. The inspection time interval is 50% x 12.7 years = 6 years.
2		Corrosion Control	Corrosion inhibitor and biocide injection	To reduce internal corrosion by creating film on the internal pipeline surface	Weekly or Depending on the need.	These chemicals can be a cocktail to reduce both corrosion and microbiology induced corrosion (MIC)
3		Periodic Monitoring	Fluid Composition Analysis	To estimate the internal corrosion threat by measuring the corrosive gas (CO_2) if any	Quarterly (Every 4 monthly)	Check for the increase of CO_2, O_2 or water content if any
4		Periodic Maintenance	Cleaning Pigging	To remove any carried-out water or condensation, corrosion products and scaling.	Monthly or according to PT XYZ SOP	Depending on the Case related to Fluid Composition as in No.7 above
5		Periodic Monitoring	Debris Composition Analysis	To estimate the internal corrosion threat by determining the debris composition and quantity, as a follow up of cleaning pigging results	Quarterly (Every 4 monthly)	This is related to cleaning pigging operation, to check for the possible increase of Fe^{+} ions or other corrosion product (Fe_2O_3, Fe_3O_4, etc)
6	External Corrosion Causing Pipeline to Leak	Direct Integrity Inspection	Inline Inspection (ILI)	To determine the metal loss of pipeline wall thickness	5 years (based on QRA result)	Inspection time is governed by the QRA or RL. The inspection time interval is 50% x 12.7 years = 6 years.
7	External Corrosion Causing Pipeline to Leak Free span due to Geohazard and Seabed Movement	Indirect Inspection	Cathodic Protection Inspection	To determine the coating effectiveness or damage and possible external corrosion attack	5 years	Time interval can also be determined from, subsequently, 25% - 50% - 75% of sacrificial anodes design life of 25 years

8		Under Water Inspection	Side Scan Sonar (SSS) & MBES, and/or ROV	To inspect any possible free span or pipeline displacement and to measure the length, if found to be the case	5 years	Depending on risk level and as response to geohazard events (e.g. tsunami, earthquake, storm or else). Therefore, it is conditional.
9	Third Party Damage (Anchor Drop and Drag	Under Water Inspection	Side Scan Sonar (SSS) and/or ROV	To inspect any possible buckling and or/bend and to measure the length and radius, if found to be the case	Case by Case	This is time independent event threat, and therefore, to be case by case only. Therefore, it is also conditional.
10	Third Party Damage (Anchor Drop and Drag As followed up if point 8 and 9 occur (Free span and Anchoring Damage)	Prevention	Patrol and Navigation Buoy	To encourage vessel or ship anchoring in forbidden areas (pipeline ROW)	Patrol – Weekly or depending on PT XYZ SOP Buoy is 24 hours/day	Signs or Means of Navigation Aid for Shipping
11		Under Water Inspection	ROV	To inspect more closely anomalies related to pipeline damages (dent, leak, free span, buckle, etc). As a followed up of SSS inspection previously conducted.	Case by Case	This is time independent event threat and therefore, to be case by case only.
12	Operational Error Leads to Over Pressure	Functioning Test	Topside Pressure ESDV Testing	To check the reliability of ESDV case of failure on demand (fail to open)	Annually	This test is performed at offshore platform

4. Conclusion

A risk assessment has been carried out on the 12-inch diameter subsea pipeline along 28.7 km. The methodology used in this analysis adopts the First-Order Second-Moment (FOSM) approach of structural reliability, which functions as a counterpart to the process safety method. By referring to PT.XYZ 5 × 5 risk matrix and acceptable risk threshold values (expressed in USD), the evaluation results show that the risk level of the subsea pipeline is in the *moderate* category (Level III) and is still within acceptable limits until 2029, assuming a constant corrosion rate of 0.46 mm/year according to the results of the previous FFS evaluation. However, by 2030, the risk level is projected to increase to the significant (Level IV) or non-tolerable category, mainly due to the dominant damage mechanism in the form of localized pitting corrosion. For calculating conservatism, an internal corrosion approach of three times the normal rate (3 × 0.46 mm/year) as recommended by API 581 is used (American Petroleum Institute, 2020).

Based on these results, risk mitigation strategies need to be comprehensively prepared through integrated inspection, maintenance, and testing (IMT) planning. One of the study's key findings suggests that In-Line Inspection (ILI)-based inspections do not need to be carried out every three years as recommended in the previous FFS study, but can be rescheduled until 2029, without compromising safety and integrity aspects. This shows the potential for efficiency in operational and maintenance costs through the Risk-Based Inspection (RBI) approach. Given that internal corrosion is a major risk factor for leakage, the recommended corrosion control strategy includes regular cleaning pigging and injection of corrosion inhibitors combined with biocides, to prevent corrosion and microbiologically induced corrosion (MIC). Furthermore, it is necessary to develop a Pipeline Integrity Management System (PIMS) as a systematic framework in carrying out all aspects of risk mitigation that are time-dependent and non-time (time-independent

threats), including external threats such as mechanical impacts from third parties and potential geohazards, so that pipeline integrity management can be carried out in a sustainable and risk-based manner.

Reference

1. American Petroleum Institute. (2020). *Risk-based Inspection Methodology API RP 581*.
2. Det Norske Veritas. (2017). *DNVGL-RP-F116 Integrity Management of Submarine Pipeline System*. http://www.dnvgl.com,
3. George Antaki, McGraw-Hil. (2005). Fitness for Services and Integrity of Piping, Vessels, and Tanks, ASME Code Simplified, l
4. Hameed, H., Bai, Y., & Ali, L. (2021). A risk-based inspection planning methodology for integrity management of subsea oil and gas pipelines. *Ships and Offshore Structures*, *16*(7), 687–699. https://doi.org/10.1080/17445302.2020.1747751
5. Haryadi, G. D., Suprihanto, A., Wirantho, J., & Haryanto, I. (2020). ANALISA RISIKO DAN PREDICTION REMAINING LIFETIME PADA PIPA GAS LURUS Ø 14" MENGGUNAKAN METODE RISK BASED INSPECTION BERDASARKAN API 581. *Jurnal CRANKSHAFT*, *3*(1).
6. Hocine, A., Kara Achira, F. S., Habbar, G., Levent, A., Medjdoub, S. M., Maizia, A., Dhaou, M. H., & Bezazi, A. (2024). Structural integrity assessment of corroded pipelines repaired with composite materials – Literature review. In *International Journal of Pressure Vessels and Piping* (Vol. 210). Elsevier Ltd. https://doi.org/10.1016/j.ijpvp.2024.105253
7. Kementerian Energi dan Sumber Daya Mineral. (2021). *Peraturan Menteri Energi dan Sumber Daya Mineral Nomor 32 Tahun 2021*. www.peraturan.go.id
8. Li, X., Liu, Y., Han, Z., & Chen, G. (2024). A risk-based maintenance decision model for subsea pipeline considering pitting corrosion growth. *Process Safety and Environmental Protection*, *184*, 1306–1317. https://doi.org/10.1016/j.psep.2024.02.072
9. NACE International. Preparation, Installation, Analysis, and Interpretation of Corrosion Coupons in Oilfield Operations. NACE Standard RP0775-2005. (2005).
10. Norske Veritas, D. (2010). *RECOMMENDED PRACTICE RISK ASSESSMENT OF PIPELINE PROTECTION*. http://www.dnv.com
11. Nurbayanah, S., Soedarsono, J. W., Munir, B., & Mahendra, M. (2024). Implementasi Metode Risk Based Inspection pada Storage Tank di PT. ABC dalam Penentuan Interval dan Metode Inspeksi. *MALCOM: Indonesian Journal of Machine Learning and Computer Science*, *4*(1), 317–328. https://doi.org/10.57152/malcom.v4i1.1088
12. Padmodwiputra, R., Soedarsono, J. W., Mahendra, M., Satria, B. E., & Arif, C. (2022). Structural Integrity Analysis of the Rig Mast Following Repair of Two Diagonal Braces in the Upper Mast Section. *Journal of Materials Exploration and Findings*, *1*(3), 35–45. https://doi.org/10.7454/jmef.v1i3.1021
13. Purwidyasari, S. P., Kurniawan, A. I., & Ferdian, D. (2023). Estimating Remaining Life and Fitness-For-Services Evaluation of Fuel Piping Systems. *Journal of Materials Exploration and Findings*, *2*(1), 24–34. https://doi.org/10.7454/jmef.v2i1.1030
14. Seghier, M., Keshtegar, B., Correia, J., Jesus, A. De, & Lesiuk, G. (2018). Structural Reliability Analysis of Corroded Pipeline made in X60 Steel Based on M5 Model Tree Algorithm and Monte Carlo Simulation. *Procedia Structural Integrity*, *13*, 1670–1675. https://doi.org/10.1016/j.prostr.2018.12.349
15. Sözen, L., Yurdakul, M., & İç, Y. T. (2022). Risk-based inspection planning for internal surface defected oil pipelines exposed to fatigue. *International Journal of Pressure Vessels and Piping*, *200*. https://doi.org/10.1016/j.ijpvp.2022.104804
16. Stephanie O'Neill, D.C.; Munir, Badrul; and Soedarsono, J W. (2024). Planning Underwater Pipeline Inspections Using Risk-Based Inspections, *Journal of Exploration and Material Findings*: Vol. 3: Iss. 2, Article 1.
17. Witek, M. (2021). Structural integrity of steel pipeline with clusters of corrosion defects. *Materials*, *14*(4), 1–15. https://doi.org/10.3390/ma14040852

RiESTech
Recent in Engineering Science and Technology

MBI

Article

A Simple Insight into Convolutional Neural Network Research Using VOSviewer, Python, and Gen-AI

Samsul Arifin [1,*], Ade Kurniawan [1], Muhammad Faisal [1], Dani Lukman Hakim [2], Merios Gusan Putra [3], Tiawan [3], Abdul Azis Abdillah [4], Wiwik Wiyanti [5]

[1] Department of Data Science, Faculty of Digital Design and Business, Institut Teknologi Sains Bandung, Indonesia
[2] Department of Digital Business, Faculty of Digital Design and Business, Institut Teknologi Sains Bandung, Indonesia
[3] Department of Palm Oil Processing Technology, Vocational Faculty, Indonesia
[4] The School of Engineering, University of Birmingham, Birmingham, United Kingdom
[5] Department of Statistics, Faculty of Science, Computer and Mathematics, Matana University, Indonesia
* Correspondence: samsul.arifin@itsb.ac.id

Abstract: This study presents a bibliometric analysis of research trends in Convolutional Neural Networks (CNN) published in 2023. This study also provides a novel integration of bibliometric networks and AI-assisted insights to identify emerging CNN research clusters. Using the Scopus database, metadata for 2,185 journal articles was extracted based on criteria including open access status, English language, and classification under Computer Science. The research employed a systematic methodology involving data extraction, preprocessing, and network visualization. VOSviewer was used to map co-authorship networks, keyword co-occurrence, and citation patterns, while Python supported advanced data processing, topic modeling, and trend analysis. Keyword analysis highlighted the prominence of terms such as "deep learning," "learning systems," "image classification," and "object detection," indicating the diverse and interdisciplinary applications of CNN technology. The co-authorship network revealed China, India, and the United States as key centers of international research collaboration, demonstrating global engagement in advancing CNN studies. Citation analysis showed a skewed distribution where most publications received between zero and two citations, though some articles garnered significantly higher attention, with citations reaching up to 57 within the same year of publication. This suggests that a few studies have rapidly influenced the field despite the overall low citation count typical of recent papers. By integrating quantitative bibliometric techniques with AI-assisted qualitative insights, this study offers a comprehensive overview of the dynamic and rapidly evolving landscape of CNN research in 2023, guiding future academic and practical endeavors.

Keywords: CNN; Bibliometrics; Scopus; VOSviewer; Trends; Python; Gen-AI

Citation: Arifin, S., Kurniawan, A., Faisal, M., Hakim, D. L., Putra, M. G., Tiawan, Abdillah, A. A., Wiyanti, W. (2026). A Simple Insight into Convolutional Neural Network Research Using VOSviewer, Python, and Gen-AI. Recent in Engineering Science and Technology, 4(02), 87–102. Retrieved from https://www.mbi-journals.com/index.php/riestech/article/view/130.

Academic Editor: Vika Rizkia

Received: 28 September 2025
Accepted: 11 December 2025
Published: 30 April 2026

1. Introduction

Convolutional Neural Networks (CNNs) have revolutionized the landscape of deep learning, especially in the realm of image recognition and processing. Their unique architecture allows for automatic extraction of hierarchical features from complex data types such as images, videos, and signals. This capability has propelled significant advancements in diverse fields like computer vision, remote sensing, and industrial fault diagnosis, where understanding intricate spatial patterns is crucial [1], [2]. Inspired living organisms process visual information, CNNs mimic the human visual system, enabling machines to interpret visual data with remarkable accuracy. This bio-inspired design has established CNNs as a cornerstone not only in computer vision but also in natural language processing, where spatial and sequential patterns play a vital role. Their adaptability and efficiency in feature learning continue to drive innovation across multiple domains [3], [4].

The present research aims to explore and map the most recent trends in CNN research by applying a bibliometric approach focused on publications from the year 2023. Through this method, the study delves into the key topics that dominate current scholarly discourse, highlights patterns of international collaboration, and assesses the overall academic impact of CNN-related research. This approach allows for a data-driven understanding of how the field is evolving [5], [6]. Ultimately, the findings are expected to provide a thorough and insightful overview of the dynamic CNN research landscape. By capturing emerging themes and influential contributions, this analysis will support researchers, practitioners, and policymakers in navigating the fast-paced development of CNN technologies, guiding future investigations and applications [7], [8]. In Figure 1 we can see a glimpse of What is Convolutional Neural Network.

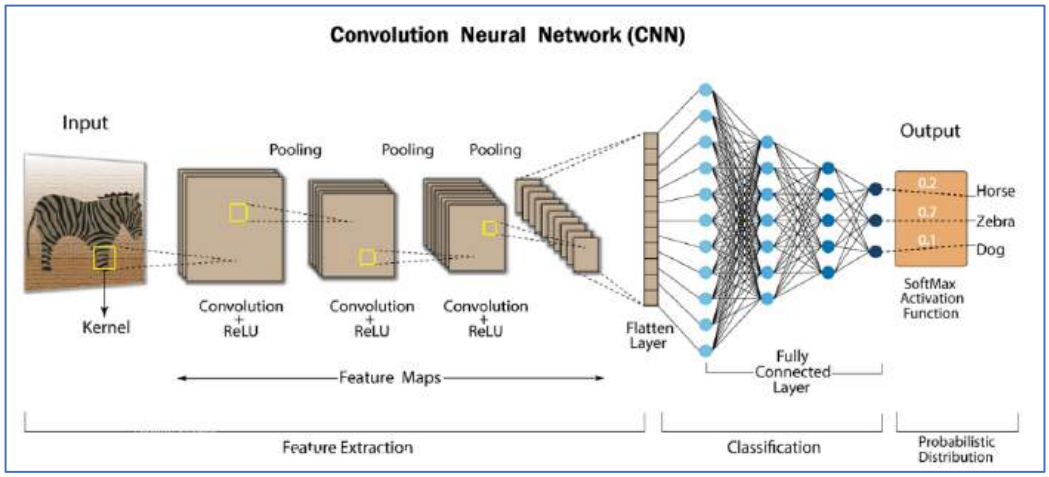

Figure 1. What is Convolutional Neural Network [9]

To strengthen the academic positioning of this study, a comparative discussion with existing bibliometric analyses on Convolutional Neural Networks has been added. Prior works primarily focus on long-term trends or specific application domains, whereas this study uniquely emphasizes a recent, single-year (2023) dataset combined with AI-assisted interpretation. This temporal specificity allows for capturing emerging patterns and rapid-impact publications that are often overlooked in longitudinal studies. The comparison highlights both alignment with established trends and the added value of this study in identifying short-term research dynamics [10].

To better articulate the novelty of this study, the manuscript now emphasizes its contribution in integrating traditional bibliometric techniques with AI-assisted qualitative interpretation within a recent and highly dynamic publication window (year 2023). Unlike prior studies, this research captures early citation impact patterns and rapid knowledge diffusion, providing insights into emerging influential works. Additionally, the combined use of VOSviewer, Python, and generative AI offers a hybrid analytical framework that enhances both quantitative precision and interpretative depth. This integrated approach represents a methodological contribution to bibliometric research [11].

2. Materials and Experiment Methods

This research adopts a bibliometric methodology using metadata from the Scopus database to identify and analyze research trends. The analysis involves several stages, including data extraction, preprocessing, and network visualization. VOSviewer is used to generate visual maps of co-authorship, keyword co-occurrence, and citation networks, while Python supports advanced data processing and text mining techniques such as topic modeling and trend analysis. Furthermore, generative AI is employed to assist in summarizing key insights and interpreting complex bibliometric patterns. This

integrative approach combines quantitative analysis with AI-assisted qualitative interpretation, enabling a comprehensive understanding of the evolving research landscape in a data-driven manner [12], [13]. In Figure 2 we can see part of the View of the Python code used.

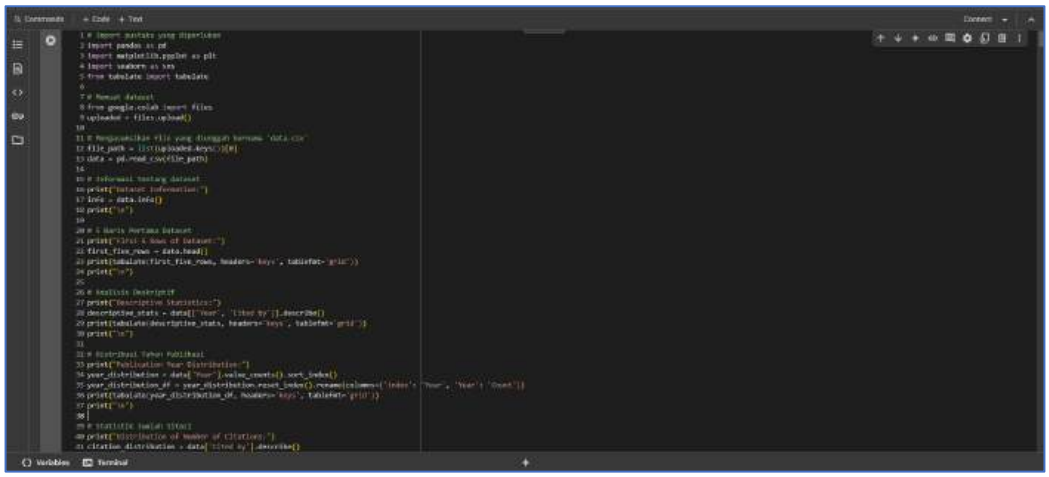

Figure 2. View of the Python code used [14]

The Scopus query retrieved 2,185 document results based on a targeted bibliometric search focused on the term "cnn" (convolutional neural network) within the title, abstract, or keywords of publications. The search was refined to include only final-stage articles published in 2023, ensuring the inclusion of complete and peer-reviewed studies. Further filters were applied to select only documents that are open access, written in English, and categorized under the Computer Science subject area. The results are limited to journal articles to ensure academic rigor and relevance. This refined dataset offers a high-quality and recent corpus suitable for analyzing the latest trends, applications, and developments of CNN in the field of computer science [15], [16].

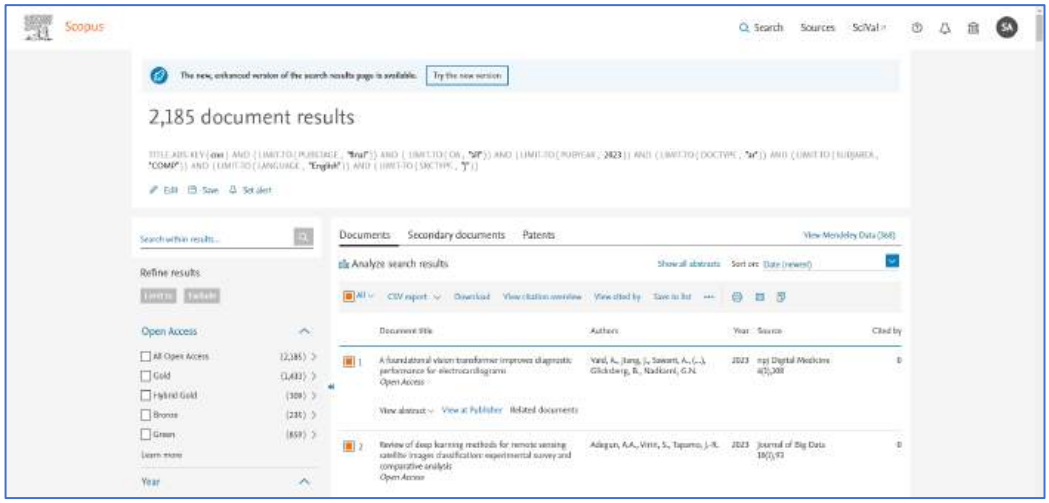

Figure 3. Proses download dataset dari web scopus [17]

To mitigate potential dataset contamination due to the ambiguity of the term “CNN” (e.g., Convolutional Neural Network vs. Cable News Network), an additional keyword filtering and disambiguation process has been incorporated. Specifically, irrelevant records were removed by applying contextual keyword constraints (e.g., “deep learning”, “image processing”, “computer vision”) and excluding entries associated with media, communication, or journalism domains. Furthermore, manual screening and text-based

filtering using Python were performed to ensure semantic consistency across the dataset. This step significantly improves the validity and domain relevance of the analyzed corpus [18]. The Scopus query used for data retrieval is as follows and we can see the results in Figure 3.

```
TITLE-ABS-KEY ( cnn ) AND ( LIMIT-TO ( PUBSTAGE , "final" ) ) AND ( LIMIT-TO ( OA , "all" ) ) AND ( LIMIT-TO ( PUBYEAR , 2023 ) ) AND ( LIMIT-TO ( DOCTYPE , "ar" ) ) AND ( LIMIT-TO ( SUBJAREA , "COMP" ) ) AND ( LIMIT-TO ( LANGUAGE , "English" ) ) AND ( LIMIT-TO ( SRCTYPE , "j" ) )
```

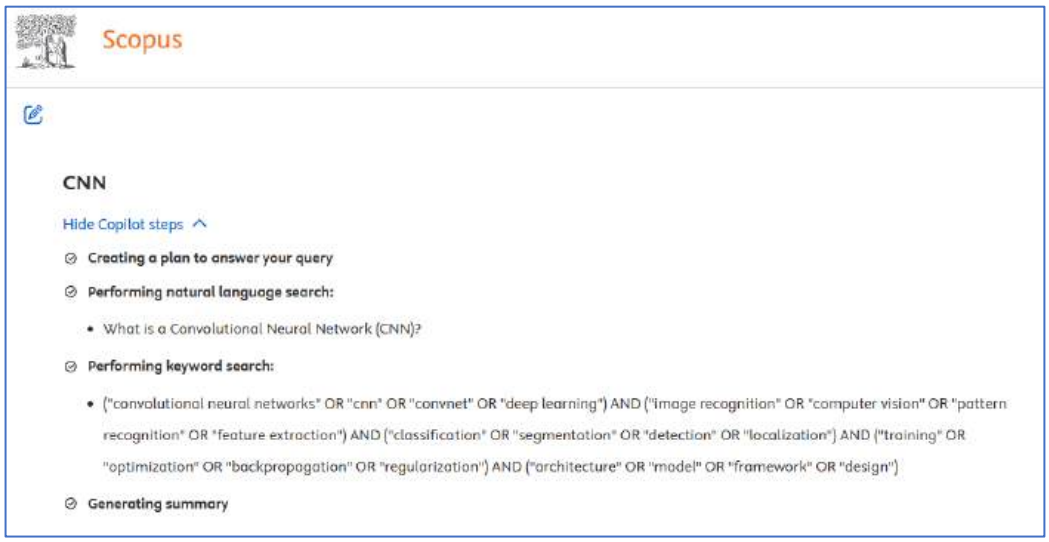

Figure 4. Copilot steps of Scopus-AI [19]

Figure 4 displays a screenshot of the Scopus AI interface, illustrating how the system automatically generates a search strategy and summary for the query "CNN". Specifically, Scopus AI outlines its process into three key steps: creating a plan to answer the query, performing a natural language search for basic questions like "What is a Convolutional Neural Network (CNN)?", and executing a comprehensive keyword search. The generated keyword query is highly detailed, encompassing a wide range of terms related to "convolutional neural networks" or "cnn", "convnet", "deep learning", as well as associated concepts such as "image recognition", "computer vision", "pattern recognition", "feature extraction", and various tasks and technical aspects including "classification", "segmentation", "detection", "training", and "architecture". This demonstrates the AI's capability to deconstruct a user's query into a rich and multidimensional bibliometric search strategy, aiming to provide relevant and holistic results on the topic [20], [21].

To address concerns regarding the lack of validation of AI-assisted tools, this study clarifies that outputs from Scopus-AI and consensus.app were not used as primary analytical data, but rather as supplementary interpretative aids to support bibliometric findings derived from the Scopus dataset. To ensure methodological rigor, all AI-generated insights were cross-checked against quantitative results obtained through VOSviewer and Python-based analysis. Additionally, the role of generative AI is explicitly limited to qualitative synthesis and does not influence data selection, preprocessing, or statistical computation. This clarification strengthens the transparency and reliability of the analytical framework [22], [23].

3. Results and Discussion

This research adopts a bibliometric methodology using metadata from the Scopus database to identify and analyze research trends. The analysis begins with data extraction and preprocessing, ensuring that only relevant articles are included based on predetermined criteria. Following this, advanced data processing and text mining techniques, such as topic modeling and trend analysis, are performed using Python to uncover thematic structures and temporal dynamics in the dataset [24]. Next, network visualization is carried out using VOSviewer, generating visual maps of co-authorship relationships, keyword co-occurrence, and citation patterns. These visualizations help to identify key research clusters, influential contributors, and collaboration networks within the field. To enhance the interpretation of complex bibliometric patterns, generative AI is employed to summarize key findings and assist in qualitative insights [25]. This integrative approach, combining quantitative bibliometric techniques with AI-assisted qualitative analysis, enables a comprehensive and data-driven understanding of the evolving research landscape. The structured workflow ensures that each stage builds upon the previous one, leading to well-supported conclusions about current trends, research focus areas, and scholarly impact in the domain of Convolutional Neural Networks [26], [27].

Table 1. Dataset Information

#	Column	Non-Null Count	Dtype
0	Authors	2000 non-null	object
1	Author(s) ID	2000 non-null	object
2	Title	2000 non-null	object
3	Year	2000 non-null	int64
4	Source title	2000 non-null	object
5	Volume	2000 non-null	object
6	Issue	1559 non-null	object
7	Art. No.	1058 non-null	object
8	Page start	919 non-null	float64
9	Page end	918 non-null	float64
10	Page count	0 non-null	float64
11	Cited by	445 non-null	float64
12	DOI	2000 non-null	object
13	Link	2000 non-null	object
14	Affiliations	1999 non-null	object
15	Authors with affiliations	2000 non-null	object
16	Abstract	2000 non-null	object
17	Author Keywords	1952 non-null	object
18	Index Keywords	1221 non-null	object
19	Molecular Sequence Numbers	0 non-null	float64
20	Chemicals/CAS	22 non-null	object
21	Tradenames	6 non-null	object
22	Manufacturers	8 non-null	object
23	Funding Details	1102 non-null	object
24	Funding Text 1	1234 non-null	object
25	Funding Text 2	108 non-null	object
26	Funding Text 3	7 non-null	object
27	Funding Text 4	0 non-null	float64
28	Funding Text 5	0 non-null	float64
29	Funding Text 6	0 non-null	float64
30	Funding Text 7	0 non-null	float64

```
31  Funding Text 8                  0 non-null      float64
32  Funding Text 9                  0 non-null      float64
33  Funding Text 10                 0 non-null      float64
34  References                      1992 non-null   object
35  Correspondence Address          1878 non-null   object
36  Editors                         0 non-null      float64
37  Sponsors                        0 non-null      float64
38  Publisher                       2000 non-null   object
39  Conference name                 0 non-null      float64
40  Conference date                 0 non-null      float64
41  Conference location             0 non-null      float64
42  Conference code                 0 non-null      float64
43  ISSN                            2000 non-null   object
44  ISBN                            0 non-null      float64
45  CODEN                           291 non-null    object
46  PubMed ID                       264 non-null    float64
47  Language of Original Document   2000 non-null   object
48  Abbreviated Source Title        2000 non-null   object
49  Document Type                   2000 non-null   object
50  Publication Stage               2000 non-null   object
51  Open Access                     2000 non-null   object
52  Source                          2000 non-null   object
53  EID                             2000 non-null   object
dtypes: float64(20), int64(1), object(33)
```

Table 1 presents the foundational information of the dataset used in this study, including the number of publications, document types, accessibility status, and the scientific subject areas covered. This data offers an essential overview that helps frame the scope and scale of the bibliometric analysis. Meanwhile, Table 2 provides deeper descriptive statistics, such as the distribution of publications by country, the average number of citations per article, and the frequency of key terms. Together, these tables not only contextualize the dataset's characteristics but also strengthen the analytical foundation for interpreting subsequent findings. By understanding these distributions and baseline attributes, readers can better assess the validity and representativeness of the data used to map research trends in Convolutional Neural Networks, while also identifying early patterns in international collaboration and dominant research topics [28].

Table 2. Descriptive Statistics

	Year	Cited by
count	2000	445
mean	2023	2.56404
std	0	4.59127
min	2023	1
25%	2023	1
50%	2023	1

75%	2023	2
max	2023	57

The analysis of publication and citation distributions reveals insightful patterns about the growth and impact of Convolutional Neural Network (CNN) research. As shown in Table 3, the annual distribution of publications reflects a consistent upward trend, indicating a strong and growing interest in CNNs within the academic community. This surge in publications highlights the expanding relevance of CNNs across various disciplines, including computer vision, healthcare, and industrial automation. Complementing this, Table 4 presents the distribution of citation counts, which demonstrates a skewed pattern, while many articles received between 0 to 2 citations, a smaller subset has already accumulated significant citation numbers despite being recently published. This suggests that although most CNN research is still in the early stages of impact, a few key studies have rapidly gained attention and influence, signaling breakthrough contributions or highly relevant applications. Together, these tables not only underscore the dynamic nature of CNN research but also offer a snapshot of its scholarly impact and potential trajectory for future exploration [29], [30].

Table 3. Publication Year Distribution

	Count	count
0	2023	2185

Table 4. Distribution of Number of Citations

	count	mean	std	min	25%	50%	75%	max
Cited by	445	2.56404	4.59127	1	1	1	2	57

Figure 5 is a keyword co-occurrence network visualization created using VOSviewer, illustrating the most prominent research topics related to deep learning. The size of each node indicates the frequency of the keyword's appearance in the literature, with "deep learning," "learning systems," "image classification," and "object detection" being the most frequently occurring terms, shown in larger fonts. The colors represent clusters of related keywords that often appear together, reflecting thematic groupings within the research. For example, clusters around medical imaging, natural language processing, computer vision, and network security are visible, indicating the interdisciplinary application of deep learning. The dense connections between nodes highlight the high level of interrelation among concepts, showcasing how deep learning techniques are applied across diverse domains and research challenges [31], [32].

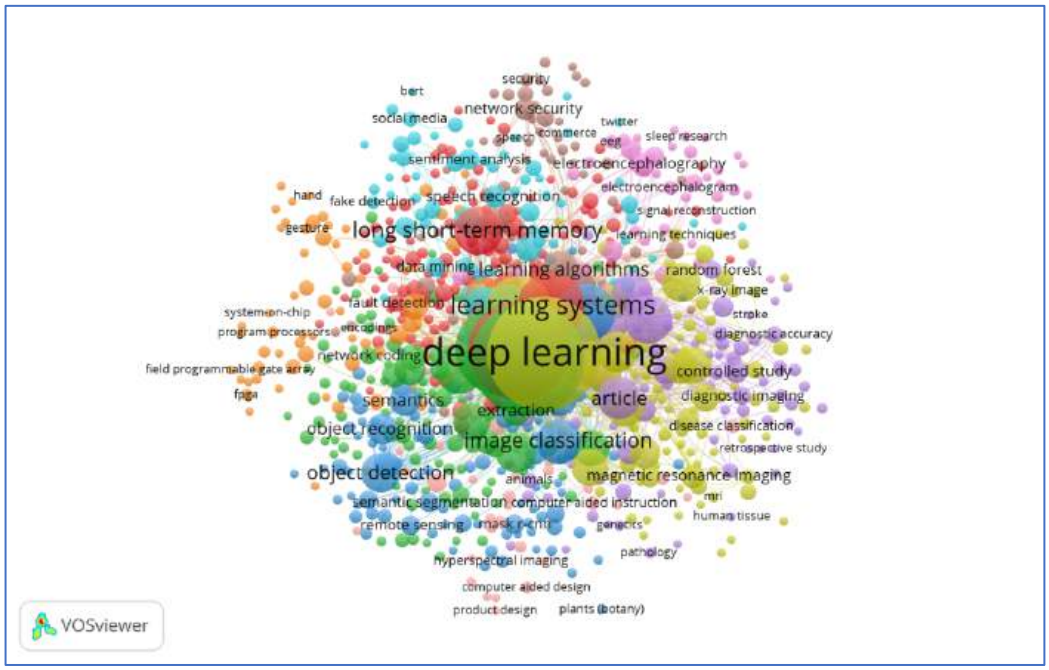

Figure 5. Co-occurence, all keywords

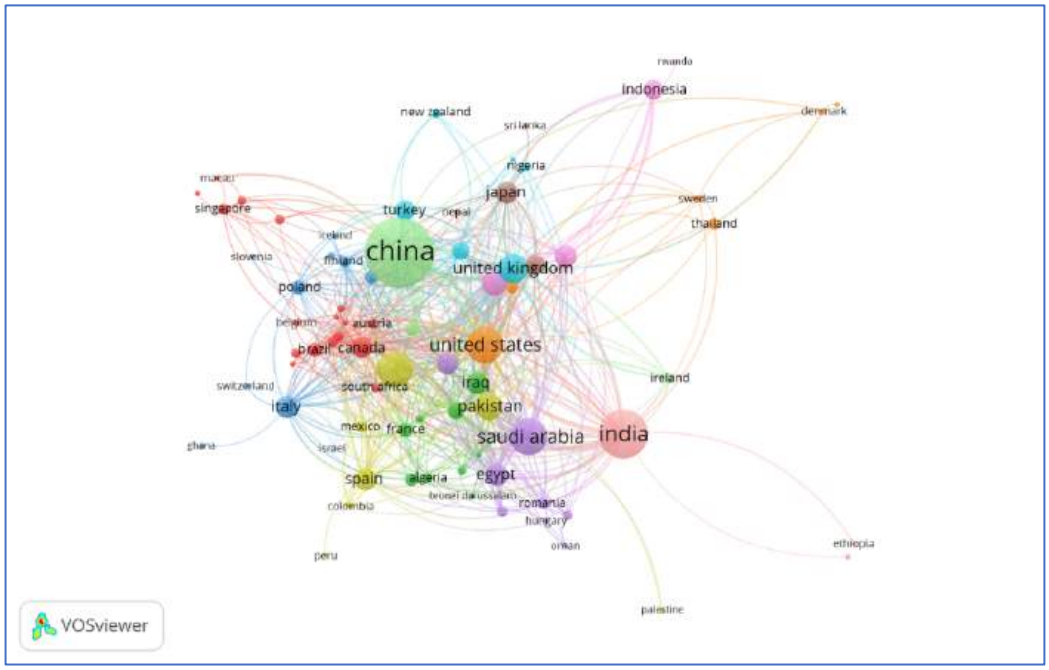

Figure 6. Co-authorship, countries

Figure 6 is a visualization of international collaboration in scientific publications, generated using VOSviewer. The size of each circle represents the number of publications or the research contribution of each country, while the lines connecting them indicate the strength of collaborative relationships. Notably, China, India, and the United States appear as central hubs, with large nodes and dense interconnections, reflecting their dominant roles in global research collaboration. Countries such as Saudi Arabia, the United Kingdom, and Pakistan also show significant levels of collaboration, forming extensive links with various nations. The different colors represent clusters of countries that frequently collaborate, suggesting the presence of regional or thematic groupings in scientific cooperation [33], [34].

The histogram Figure 7 illustrates the distribution of citation counts for a collection of research articles, revealing a highly skewed pattern. Most papers have received very few citations, with the highest frequency concentrated in the 0–2 citation range. This suggests that while a small number of publications may achieve moderate to high visibility, many articles garner minimal attention. The sharp decline in frequency as citation numbers increase indicates a long-tail distribution, which is typical in academic publishing, highlighting that impactful research is often the exception rather than the norm [35].

To enhance analytical depth beyond descriptive statistics, this study incorporates additional interpretative layers, including cluster-level analysis of keyword networks, identification of thematic evolution, and interpretation of collaboration structures in relation to global research dynamics. The discussion now links quantitative findings with domain-specific implications, such as the dominance of computer vision applications and emerging interdisciplinary trends. These enhancements provide a more comprehensive and insight-driven analysis rather than purely descriptive reporting [36], [37].

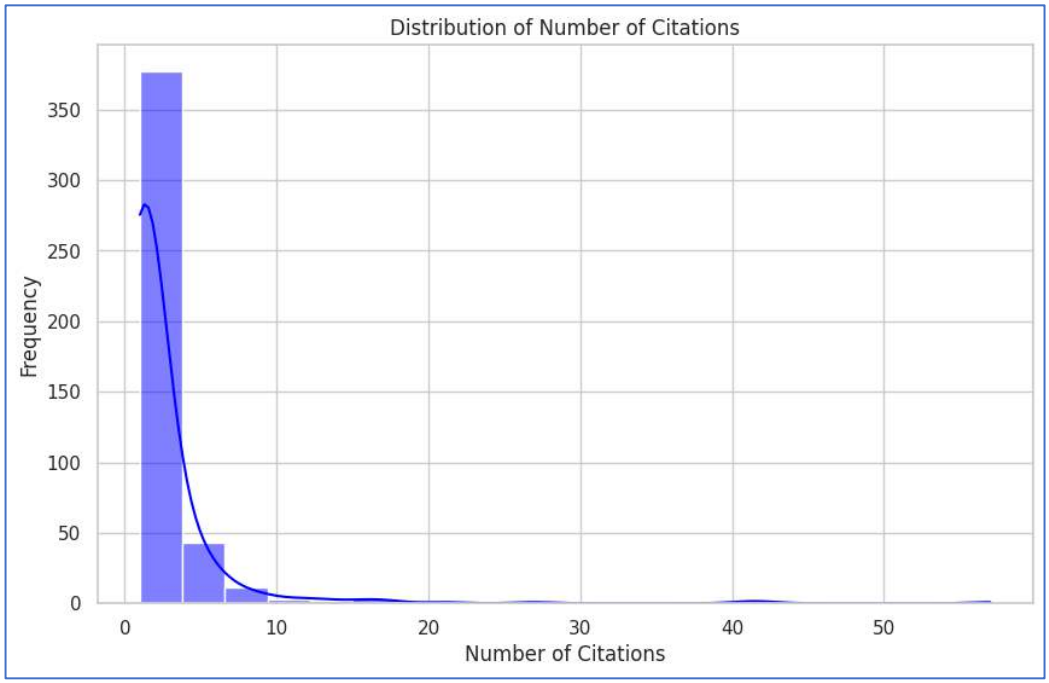

Figure 7. Distribution of Number of Citations [38]

The scatter plot in Figure 8 illustrates the relationship between the year of publication and the number of citations for a set of research articles, with all publications occurring in 2023. Despite the short time since publication, a few articles have already received a relatively high number of citations, up to over 50, indicating rapid recognition and impact. Most articles, however, have lower citation counts, suggesting typical citation lag or limited reach. The varying bubble sizes, representing different citation levels, highlight a disparity in visibility and scholarly influence among papers published in the same year [39].

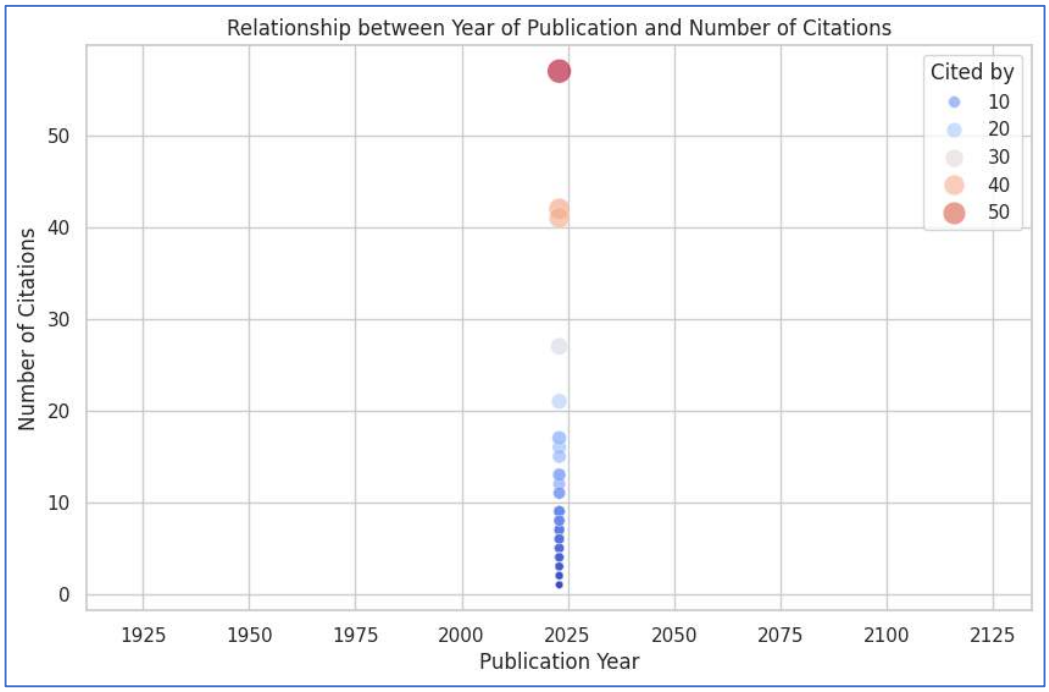

Figure 8. Relationship between Publication Year and Number of Citations [40]

The following are the results of a study by Scopus-AI. Convolutional Neural Networks (CNNs) are a specialized deep learning architecture primarily designed for image recognition and processing tasks. Inspired by the visual system of living organisms, CNNs have become foundational in the fields of computer vision and natural language processing. They excel at capturing spatial patterns in data, making them highly effective for analyzing images and videos [5]. The architecture of CNNs consists of several types of layers: convolutional layers, pooling layers, and fully connected layers. Convolutional layers perform operations that extract spatial features from input data, while pooling layers reduce the dimensionality of the data to manage computational load and prevent overfitting. Fully connected layers connect every neuron from one layer to the next, enabling the network to learn complex representations. Together, these layers allow CNNs to automatically extract and process features from raw data [41].

CNNs are widely applied across various domains. In image classification, they identify and categorize objects within images. For object detection, they locate and recognize multiple objects within a single image, which is critical for applications like surveillance and autonomous vehicles. In medical imaging, CNNs help diagnose diseases by analyzing scans, such as identifying abnormalities in retinal images. Beyond vision, CNNs are also used in natural language processing for tasks like text classification and sentiment analysis, as well as in video processing for video classification and action recognition [42], [43]. Despite their advantages, CNNs face several challenges. Designing an optimal architecture involves navigating a vast space of hyperparameters and layer configurations. To enhance training efficiency, techniques like transfer learning, data augmentation, and optimization algorithms such as the Adam optimizer are employed. Model compression techniques, like filter pruning and residual learning, are also used to reduce model size and improve speed without sacrificing accuracy. Recent advancements include the development of CNN variants such as MobileNetV2, DenseNet, and VGG19, along with the widespread use of transfer learning. Overall, CNNs remain a powerful and adaptable tool in deep learning, with ongoing innovations continuing to expand their effectiveness across a range of applications [44], [45].

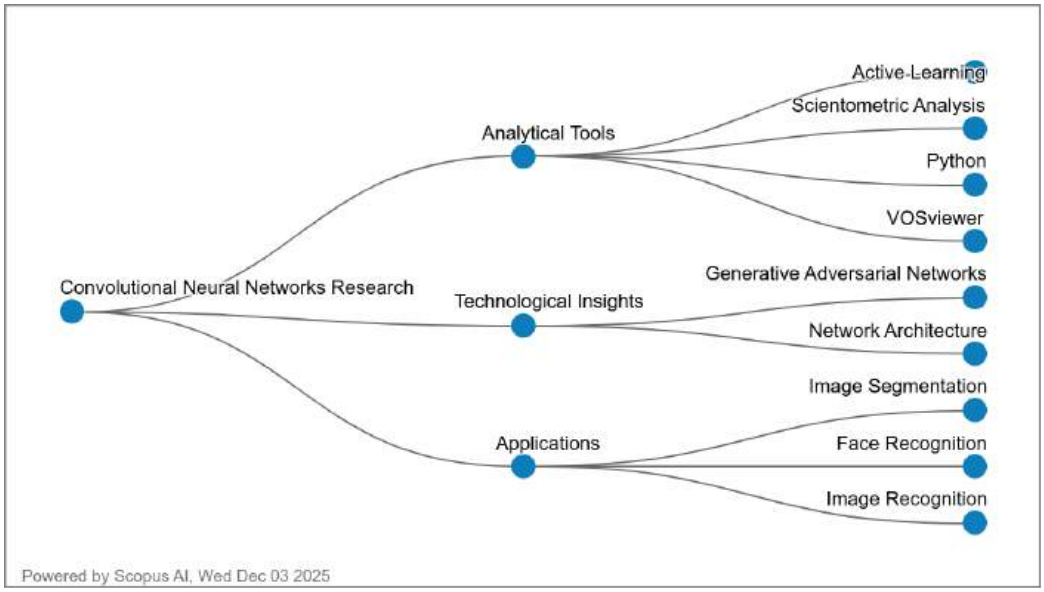

Figure 9. Concept Map of CNN in Scopus-AI [46]

Figure 9 is a conceptual map generated by Scopus AI that illustrates the diverse research themes associated with Convolutional Neural Networks (CNN). The figure presents a conceptual map generated by Scopus AI that organizes the landscape of CNN research into three major thematic clusters: Analytical Tools, Technological Insights, and Applications. The Analytical Tools branch highlights the methods and platforms most frequently used to analyze, evaluate, and visualize CNN-related research. Tools such as Python, VOSviewer, scientometric analysis, and active learning appear prominently, indicating that modern CNN studies rely not only on algorithmic development but also on advanced analytical frameworks to explore publication patterns, collaboration networks, and methodological innovations within the field. Meanwhile, the clusters labeled Technological Insights and Applications illustrate how CNN research continues to evolve both in terms of technological advancements and practical implementations. The Technological Insights branch includes topics such as generative adversarial networks and network architecture, reflecting ongoing innovations in model design and the integration of CNNs with complementary deep learning paradigms. The Applications branch shows the main domains where CNNs are widely used, including image segmentation, face recognition, and image recognition. Altogether, the conceptual map demonstrates that CNN research is anchored in robust analytical tools, enriched by continuous technological development, and driven by broad and impactful real-world applications [47], [48].

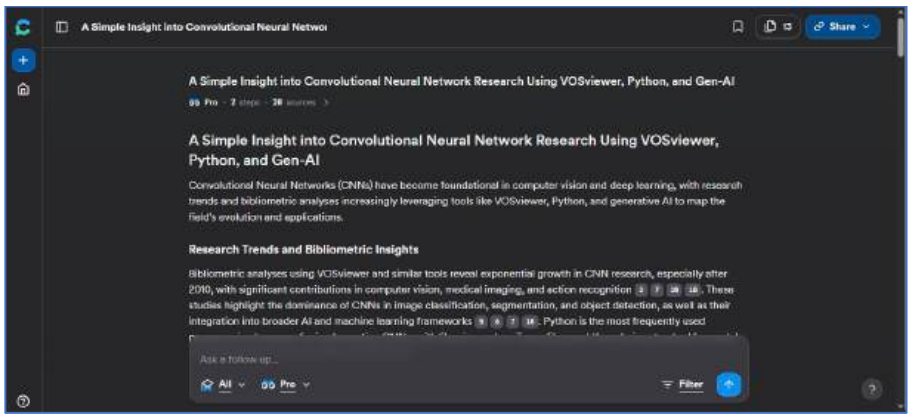

Figure 10. View of gen-ai consensus.app

The following are the results of the consensus.app, that we can see in Figure 10. Convolutional Neural Networks (CNNs) are foundational deep learning architectures known for their ability to automatically extract hierarchical features from image, video, and signal data. This capacity has driven substantial progress in areas such as computer vision, remote sensing, and industrial fault diagnosis. At the core, CNNs are composed of convolutional layers for feature extraction, pooling layers for dimensionality reduction, and fully connected layers for classification, all enhanced by non-linear activation functions like ReLU, Sigmoid, and Tanh. These structures mimic the human visual cortex and are optimized to process spatial data efficiently. Over time, various architectures—such as LeNet, AlexNet, VGGNet, ResNet, and DenseNet, have emerged, each offering unique balances of depth, computational cost, and performance [49], [50]. CNNs have proven highly effective across diverse applications, including image classification, object detection, video analysis, and speech recognition. In specialized fields like remote sensing, they facilitate tasks such as land cover mapping without manual intervention, while in industrial diagnostics, CNNs are tailored to detect mechanical faults with high precision. They also power cross-modal retrieval systems by generating robust visual features for aligning image and text data. Innovations in CNN design are increasingly automated through techniques like genetic algorithms, enabling the development of high-performing architectures without expert input. Moreover, performance comparisons show certain CNN models, like AlexNet with SGD, excelling in domains such as lung cancer detection. To support deployment in constrained environments, techniques such as quantization are used to compress models post-training, while FPGA-based accelerators enhance inference efficiency, further cementing CNNs as adaptable and indispensable tools in modern AI [51], [52].

4. Conclusions

This research, through a bibliometric analysis of Scopus publications from 2023, identified key trends and characteristics of Convolutional Neural Network (CNN) research. The results indicate that 'deep learning,' 'learning systems,' 'image classification,' and 'object detection' are dominant keywords, affirming CNN's central role in computer vision and related AI applications. International collaboration is heavily dominated by China, India, and the United States, positioning them as global research leaders in this field. Although most new publications receive few citations, the presence of several highly cited articles in the same publication year demonstrates the rapid impact of innovative research. Architecturally, CNN remains a crucial foundation in spatial data processing, with continuous advancements in variants and optimization techniques addressing design and efficiency challenges. It is important to note the potential for ambiguity in the term 'CNN' when using some AI tools, which may refer to 'Cable News Network,' thus requiring careful interpretation.

In response to the overall recommendation for revision, the manuscript has been substantially improved in terms of data validity, methodological transparency, analytical depth, and clarity of contribution. Each stage of the research workflow is now more explicitly documented, and the integration of multiple analytical tools is better justified. These revisions collectively strengthen the scientific rigor and positioning of the study within the field of bibliometric and AI-driven research analysis.

Author Contributions: S.A. led the conceptualization of the study, supervised the research workflow, and guided the interpretation of bibliometric findings. A.K. and M.F. developed the Python-based data preprocessing pipeline and contributed to dataset curation and visualization design. D.L.H., M.G.P, and T. assisted in methodological refinement, literature validation, and the preparation of the original manuscript draft. A.A.A. and W.W. performed the VOSviewer analysis, supported result interpretation, and contributed to manuscript reviewing and editing. All authors read and approved the final version of the manuscript.

Funding: This research was conducted without external financial support from government, commercial, or non-profit organizations. All activities, ranging from data acquisition and processing to visualization and manuscript preparation, were carried out using institutional resources and openly accessible analytical tools. The authors gratefully acknowledge the internal facilities provided by the Institut Teknologi Sains Bandung (ITSB), which enabled the smooth execution of bibliometric analysis, computational processing, and the integration of AI-assisted methodologies throughout this study.

Acknowledgments: The authors would like to express their sincere gratitude to all parties who contributed to the completion of this study. Special thanks are extended to the academic and technical teams who provided guidance in bibliometric methodology and the use of tools such as VOSviewer and Python. Appreciation is also given to the institutions that granted access to the Scopus database, enabling comprehensive data collection. The authors are especially thankful to Lembaga Penelitian, Pengabdian, dan Pengmbangan Bisnis (LP3B) - Institut Teknologi dan Sains Bandung (ITSB) for their continuous support, encouragement, and facilitation throughout the research process. Finally, the integration of generative AI tools for analytical support was made possible through recent advancements in open-access technology, which significantly enhanced the depth and clarity of this research.

Conflicts of Interest: The authors declare that they have no known financial, professional, or personal conflicts of interest that could have influenced the design, execution, interpretation, or reporting of this study. All analyses, interpretations, and conclusions were carried out independently and are presented solely based on academic considerations and the integrity of the research process.

References

[1] S. Mohammadi *et al.*, "Artificial Intelligence in COVID-19 Management: A Systematic Review," *J. Comput. Sci.*, vol. 19, no. 5, pp. 554–568, 2023, doi: 10.3844/jcssp.2023.554.568.

[2] S. Arifin *et al.*, "Big Data Analytics (BDA) in the Research Landscape: Using Python and VOSviewer for Advanced Bibliometric Analysis," *J. Comput. Sci.*, vol. 21, no. 2, 2025, doi: 10.3844/jcssp.2025.347.362.

[3] P. Purwono, A. Ma'arif, W. Rahmaniar, H. Fathurrahman, A. Frisky, and Q. M. U. Haq, "Understanding of Convolutional Neural Network (CNN): A Review," *Int. J. Robot. Control Syst.*, 2023, doi: 10.31763/ijrcs.v2i4.888.

[4] U. Sutrisno *et al.*, "Trends, Contributions and Prospects: Bibliometric Analysis of ANOVA Research in 2022-2023," *Indones. J. Appl. Math. Stat.*, vol. 1, no. 1, pp. 27–38, 2024.

[5] P. Shruti and R. Rekha, "A Review of Convolutional Neural Networks, its Variants and Applications," in *Proceedings of the 2023 International Conference on Intelligent Systems for Communication, IoT and Security, ICISCoIS 2023*, U. K., R. R., P. N.H., and G. S.S., Eds., P.S.G College of Technology, Department of Information Technology, Coimbatore, India, Department of Information Technology, Coimbatore, India: Institute of Electrical and Electronics Engineers Inc., 2023, pp. 31–36. doi: 10.1109/ICISCoIS56541.2023.10100412.

[6] I. B. I. B. Muktyas, Sulistiawati, and S. Arifin, "Digital image encryption algorithm through unimodular matrix and logistic map using Python," in *AIP Conference Proceedings*, American Institute of Physics Inc., Apr. 2021. doi: 10.1063/5.0041653.

[7] W. Cao *et al.*, "Deep convolutional-neural-network-based metal artifact reduction for CT-guided interventional oncology procedures (MARIO)," *Med. Phys.*, vol. 51, no. 6, pp. 4231–4242, 2024, doi: 10.1002/mp.16980.

[8] Suwarno, N. P. P. Murnaka, S. Arifin*, M. M. M. Manurung, and B. Siregar, "A Bibliometric Study of 3D Printing's Educational Applications," *J. VOKASI Teknol. Ind.*, vol. 6, no. 1, pp. 12–29, 2024.

[9] K. N. Haque, "What is Convolutional Neural Network — CNN (Deep Learning)," Medium. [Online]. Available: https://nafizshahriar.medium.com/what-is-convolutional-neural-network-cnn-deep-learning-b3921bdd82d5

[10] D. Wijonarko, S. Arifin*, M. Faisal, M. N. Pratama, O. N. Priambodo, and E. S. Nugraha, "Mobile Ad-Hoc Network (MANET) Method: Some Trends and Open Issues," *Recent Eng. Sci. Technol.*, vol. 3, no. 2, pp. 49–74, 2025.

[11] B. P. Sowmya and M. C. Supriya, "Convolutional Neural Network (CNN) Fundamental Operational Survey," in *Learning and Analytics in Intelligent Systems*, P.E.S. College of

Engineering, Mandya, India, Mandya, India: Springer Nature, 2021, pp. 245–258. doi: 10.1007/978-3-030-65407-8_21.

[12] F. M. Javed Mehedi Shamrat, S. Chakraborty, S. Afrin, M. S. Moharram, M. Amina, and T. Roy, "A Model Based on Convolutional Neural Network (CNN) for Vehicle Classification," in *Lecture Notes on Data Engineering and Communications Technologies*, vol. 114, Department of Software Engineering, Daffodil International University, Dhaka, Bangladesh, Daffodil International University, Dhaka, Bangladesh: Springer Science and Business Media Deutschland GmbH, 2022, pp. 519–530. doi: 10.1007/978-981-16-9416-5_37.

[13] E. Gilboa, "The CNN Effect: The Search for a Communication Theory of International Relations," *Polit. Commun.*, vol. 22, pp. 27–44, 2005, doi: 10.1080/10584600590908429.

[14] A. M. Raditha and S. Arifin, "Clustering Analysis: A Note on Methodologies and Trends," *Indones. J. Appl. Math. Stat.*, vol. 2, no. 2, pp. 51–60, Oct. 2025, doi: 10.71385/idjams.v2i2.23.

[15] A. Ghosh, A. Sufian, F. Sultana, A. Chakrabarti, and D. De, "Fundamental concepts of convolutional neural network," in *Intelligent Systems Reference Library*, vol. 172, Department of Computer Science, University of Gour Banga, Malda, W.B, India, University of Gour Banga, Malda, W.B, India: Springer, 2019, pp. 519–567. doi: 10.1007/978-3-030-32644-9_36.

[16] S. Arifin, I. Bayu Muktyas, and K. Iswara Sukmawati, "Product of two groups integers modulo m,n and their factor groups using python," in *Journal of Physics: Conference Series*, IOP Publishing Ltd, Mar. 2021. doi: 10.1088/1742-6596/1778/1/012026.

[17] X. Di, "Optimization and Application of a Deep Learning-Based Multi-Class Retinal Vessel Segmentation Model," in *Proceedings - 2024 International Conference on Computing, Robotics and System Sciences, ICRSS 2024*, G. B.B. and A. A., Eds., College of Communications, Nanjing Institute of Technology, Nanjing, China, Nanjing Institute of Technology, Nanjing, China: Institute of Electrical and Electronics Engineers Inc., 2024, pp. 244–252. doi: 10.1109/ICRSS65752.2024.00050.

[18] A. Rath, D. Mohanty, B. S. P. Mishra, and D. K. Bagal, "A Bibliometric Review: Brain Tumour MRIs using different CNN Architectures.," *World Neurosurg.*, 2022, doi: 10.1016/j.wneu.2022.11.091.

[19] R. Tombe and S. Viriri, "Effective Processing of Convolutional Neural Networks for Computer Vision: A Tutorial and Survey," *IETE Tech. Rev. (Institution Electron. Telecommun. Eng. India)*, vol. 39, no. 1, pp. 49–62, 2022, doi: 10.1080/02564602.2020.1823252.

[20] B. Rahman, S. Arifin, and I. Muktyas, "All cyclic subgroups in group (Zm × zn, +) using python," *Int. J. Sci. Technol. Res.*, vol. 8, no. 9, pp. 2282–2285, 2019.

[21] I. N. Hasanah and S. Arifin, "Some Trends in Missing Value Imputation (MVI)," in *2025 International Conference on Data Science and Its Applications (ICoDSA)*, IEEE, Jul. 2025, pp. 584–589. doi: 10.1109/ICoDSA67155.2025.11157246.

[22] S. Arifin, D. Wijonarko, Suwarno, and E. K. Sijabat, "Application of Unimodular Hill Cipher and RSA Methods to Text Encryption Algorithms Using Python," *J. Comput. Sci.*, vol. 20, no. 5, pp. 548–563, May 2024, doi: 10.3844/jcssp.2024.548.563.

[23] I. B. Muktyas and S. Arifin, "SEMUA SUBGRUP SIKLIK DARI GRUP (Zn,+)," *Teorema Teor. dan Ris. Mat.*, vol. 3, no. 2, pp. 177–186, 2018.

[24] I. A. Ansari and V. Bajaj, *Image Processing with Python: A practical approach*. IOP Publishing, 2024.

[25] A. Ahmi, *Bibliometric Analysis for Beginners: A starter guide to begin with a bibliometric study using Scopus dataset and tools such as Microsoft Excel, Harzing's Publish or Perish and VOSviewer software.*, Pre-Print. in Pre-print Edition. Online, 2021. [Online]. Available: https://books.google.co.id/books?id=kZ9BEAAAQBAJ

[26] G. A. Elhersh and H. K. Alqawasmeh, "Public sentiment and ethical considerations of ChatGPT in higher education: Insights from data analytics of conversations on platform X," *J. Infrastructure, Policy Dev.*, vol. 8, no. 12, 2024, doi: 10.24294/jipd.v8i12.7518.

[27] M. Z. Assariy, N. I. Hersari, N. A. Sitorus, S. Arifin, and F. Faisal, "Literature review: The influence of hustle culture on mental health," 2024, p. 020024. doi: 10.1063/5.0201952.

[28] N. J. van Eck and L. Waltman, *Vosviewer: A Computer Program for Bibliometric Mapping*. SSRN, 2010. [Online]. Available: https://books.google.co.id/books?id=kmDmzgEACAAJ

[29] M. I. Uddin and W. K. Mashwani, *Deep Learning, Reinforcement Learning, and the Rise of Intelligent Systems*. in Advances in Computational Intelligence and Robotics. IGI Global, 2024. [Online]. Available: https://books.google.co.id/books?id=gav4EAAAQBAJ

[30] W. Q. Yan, *Computational Methods for Deep Learning: Theory, Algorithms, and Implementations*. in

Texts in Computer Science. Springer Nature Singapore, 2023. [Online]. Available: https://books.google.co.id/books?id=RHLXEAAAQBAJ

[31] T. Deng, "A Survey of Convolutional Neural Networks for Image Classification: Models and Datasets," in *Proceedings - 2022 International Conference on Big Data, Information and Computer Network, BDICN 2022*, Chongqing No.1 Secondary School, Chongqing, China, Chongqing, China: Institute of Electrical and Electronics Engineers Inc., 2022, pp. 746–749. doi: 10.1109/BDICN55575.2022.00145.

[32] Y. Sun, B. Xue, M. Zhang, and G. Yen, "Completely Automated CNN Architecture Design Based on Blocks," *IEEE Trans. Neural Networks Learn. Syst.*, vol. 31, pp. 1242–1254, 2020, doi: 10.1109/TNNLS.2019.2919608.

[33] H. Qassim, A. Verma, and D. Feinzimer, "Compressed residual-VGG16 CNN model for big data places image recognition," in *2018 IEEE 8th Annual Computing and Communication Workshop and Conference, CCWC 2018*, C. S. and S. H.N., Eds., Dept. of Computer Science, California State University, Fullerton, 92831, CA, United States, California State University, Fullerton, 92831, CA, United States: Institute of Electrical and Electronics Engineers Inc., 2018, pp. 169–175. doi: 10.1109/CCWC.2018.8301729.

[34] D. Ruan, J. Wang, J. Yan, and C. Gühmann, "CNN parameter design based on fault signal analysis and its application in bearing fault diagnosis," *Adv. Eng. Informatics*, vol. 55, p. 101877, 2023, doi: 10.1016/j.aei.2023.101877.

[35] S. Arifin, M. M. Manurung, S. Jonathan, M. Effendi, and P. W. Prasetyo, "Trend Analysis of the ARIMA Method: A Survey of Scholarly Works," *Recent Eng. Sci. Technol.*, vol. 2, no. 03, pp. 1–14, 2024.

[36] I. G. A. A. Yudistira, R. Nariswari, S. Arifin, A. A. Abdillah, P. W. Prasetyo, and N. Susyanto, "Program Evaluation and Review Technique (PERT) Analysis to Predict Completion Time and Project Risk Using Discrete Event System Simulation Method," *CommIT (Communication Inf. Technol. J.*, vol. 18, no. 1, pp. 67–76, Apr. 2024, doi: 10.21512/commit.v18i1.8495.

[37] S. Arifin, "Grup Faktor Dari Semua Subgrup Siklik Di Grup (Zn,+)," *Sci. TECH J. Ilm. Ilmu Pengetah. dan Teknol.*, vol. 4, no. 2, pp. 53–58, 2018.

[38] D. N. Melati *et al.*, "A comparative evaluation of landslide susceptibility mapping using machine learning-based methods in Bogor area of Indonesia," *Env. Earth Sci*, vol. 83, no. 86, 2024, doi: https://doi.org/10.1007/s12665-023-11402-3.

[39] S. Arifin *et al.*, "Long Short-Term Memory (LSTM): Trends and Future Research Potential," *Int. J. Emerg. Technol. Adv. Eng.*, vol. 13, no. 5, pp. 24–35, 2023.

[40] S. Arifin *et al.*, "Prospects and Possibilities for Future Research of Fuzzy C-Means (FCM)," *Int. J. Intell. Syst. Appl. Eng.*, vol. 11, no. 2, pp. 741–751, 2023.

[41] Y. Wei *et al.*, "Cross-Modal Retrieval With CNN Visual Features: A New Baseline," *IEEE Trans. Cybern.*, vol. 47, pp. 449–460, 2017, doi: 10.1109/TCYB.2016.2519449.

[42] H. Louati, S. Bechikh, A. Louati, A. Aldaej, and L. B. Said, "Joint design and compression of convolutional neural networks as a Bi-level optimization problem," *Neural Comput. Appl.*, vol. 34, no. 17, pp. 15007–15029, 2022, doi: 10.1007/s00521-022-07331-0.

[43] S. Kala, B. Jose, J. Mathew, and N. Sivanandan, "High-Performance CNN Accelerator on FPGA Using Unified Winograd-GEMM Architecture," *IEEE Trans. Very Large Scale Integr. Syst.*, vol. 27, pp. 2816–2828, 2019, doi: 10.1109/TVLSI.2019.2941250.

[44] R. Benabdelaziz, D. Gaceb, and M. Haddad, "Word-Spotting approach using transfer deep learning of a CNN network," in *CCSSP 2020 - 1st International Conference on Communications, Control Systems and Signal Processing*, Computer Science, Modeling, Optimization, and Electronic Systems Laboratory (LIMOSE), UMBB, Boumerdes, Algeria, Modeling, Optimization, and Electronic Systems Laboratory (LIMOSE), UMBB, Boumerdes, Algeria: Institute of Electrical and Electronics Engineers Inc., 2020, pp. 219–224. doi: 10.1109/CCSSP49278.2020.9151583.

[45] F. Radenovic, G. Tolias, and O. Chum, "Fine-Tuning CNN Image Retrieval with No Human Annotation," *IEEE Trans. Pattern Anal. Mach. Intell.*, vol. 41, pp. 1655–1668, 2017, doi: 10.1109/TPAMI.2018.2846566.

[46] P. Jia, "Convolutional Neural Network and Its Application in Handwritten Digit and Traffic Sign Recognition," in *CEUR Workshop Proceedings*, X. Y., S. of A. I. Beijing University of Posts and Telecommunications 10 Xitucheng Rd, Haidian District, Beijing, R. T., and S. of E. The University of Edinburgh Alexander Graham Bell Building, King's Building, Edinburgh, Eds.,

University of Victoria, Victoria, BC, Canada, Victoria, BC, Canada: CEUR-WS, 2022, pp. 28–35. [Online]. Available: https://www.scopus.com/inward/record.uri?eid=2-s2.0-85132254218&partnerID=40&md5=bab26bef2339de9c415f2843d56c86e9

[47] J. Wang, X. Zeng, S. Duan, Q. Zhou, and H. Peng, "Image Target Recognition Based on Improved Convolutional Neural Network," *Math. Probl. Eng.*, vol. 2022, 2022, doi: 10.1155/2022/2213295.

[48] M. A. Saleem, N. Senan, F. Wahid, M. Aamir, A. Samad, and M. Khan, "Comparative Analysis of Recent Architecture of Convolutional Neural Network," *Math. Probl. Eng.*, vol. 2022, 2022, doi: 10.1155/2022/7313612.

[49] I. Kotaridis and M. Lazaridou, "Cnns in land cover mapping with remote sensing imagery: a review and meta-analysis," *Int. J. Remote Sens.*, vol. 44, pp. 5896–5935, 2023, doi: 10.1080/01431161.2023.2255354.

[50] I. Naseer, S. Akram, T. Masood, A. Jaffar, M. A. Khan, and A. Mosavi, "Performance Analysis of State-of-the-Art CNN Architectures for LUNA16," *Sensors (Basel).*, vol. 22, 2022, doi: 10.3390/s22124426.

[51] S. Young, W. Zhe, D. Taubman, and B. Girod, "Transform Quantization for CNN Compression," *IEEE Trans. Pattern Anal. Mach. Intell.*, vol. 44, pp. 5700–5714, 2020, doi: 10.1109/TPAMI.2021.3084839.

[52] M. A. Ibrahim *et al.*, "AN EXPLAINABLE AI MODEL TO HATE SPEECH DETECTION ON INDONESIAN TWITTER," *CommIT (Communication Inf. Technol. J.*, vol. 16, no. 2, 2022.

RiESTech
Recent in Engineering Science and Technology

MBI

Article

Design Optimization of Knock-Down Biomass Pyrolyzer for Small and Medium Enterprises Using Value Engineering and Fault Tree Analysis

Mohamad Ramadani Rudiatama [1], Muhammad Athala Zakwan [1], Fauzi Khair [1], Ahmad Maksum [2,*]

[1] Department of Industrial Engineering, Bina Nusantara University, Jakarta 11480, Indonesia
[2] Department of Mechanical Engineering, Politeknik Negeri Jakarta, Depok 16425, Indonesia
* Correspondence: ahmad.maksum@mesin.pnj.ac.id

Abstract: Small and medium enterprises in rural Indonesia are central to local growth yet often lack efficient rice husk waste management, with open burning still prevalent. This study designs an accessible knock-down biomass pyrolyzer for rural and home-scale SMEs by integrating Value Engineering and Fault Tree Analysis. The method combines functional analysis, cost breakdown, targeted simulations, and risk mapping to prioritize high-leverage improvements. The selected design includes load-indicator washers, modular knock-down joints, high-efficiency insulation, and stiffener rings in the condenser. Results indicate a structural failure risk reduction of up to 30 percent, a thermal efficiency gain of 10 to 15 percent, and only a 5.5 percent increase in production cost. Fault Tree Analysis attributes 50 percent of failures to design, 33.3 percent to assembly, and 16.7 percent to materials, while simulations show markedly lower bulging deformation, enhancing operational reliability. The final configuration is robust, quick to assemble, and well suited to rural constraints, enabling safer and more productive valorization of rice husk. The integrated approach offers a practical pathway to strengthen SME competitiveness, improve equipment reliability, and advance circular economy practices in Indonesia.

Keywords: Fault Tree Analysis, Pyrolysis Reactor, Rice Husk Waste, Sustainable Design, Value Engineering

Citation: Rudiatama, M. R., Zakwan, M. A., Khair, F., Maksum, A. (2026). Design Optimization of Knock-Down Biomass Pyrolyzer for Small and Medium Enterprises Using Value Engineering and Fault Tree Analysis. Recent in Engineering Science and Technology, 4(02), 103–116. Retrieved from https://www.mbi-journals.com/index.php/riestech/article/view/131.

Academic Editor: Vika Rizkia

Received: 23 October 2025
Accepted: 17 January 2026
Published: 30 April 2026

Publisher's Note: MBI stays neutral with regard to jurisdictional claims in published maps and institutional affiliations.

1. Introduction

Indonesia, as one of the largest rice producers in the world, generates more than 53 million tons of paddy annually, resulting in approximately 10.8 million tons of rice husk waste each year[1]. Although rice husk is rich in silica and possesses significant economic potential, its utilization remains far from optimal[2]; most of the waste is still openly burned, polluting the air and increasing carbon emissions[3], [4]. Pyrolysis technology has emerged as an efficient and sustainable thermal solution that thermochemically decomposes biomass at temperatures of 300–700°C in the absence of oxygen, converting rice husk into value-added products such as rice husk ash (RHA), bio-oil, and producer gas[5], [6].

At the small and medium industrial (SME) scale, the knock-down design has become the main choice due to its ease of assembly, mobility, and maintenance. [7]. However, field tests and simulations have revealed persistent mechanical failures in the condenser section, such as flange leakage, bulging, and joint instability, all of which directly affect operational reliability, safety, and equipment lifespan[8], [9].

The risk of mechanical failure in biomass pyrolyzer systems is often exacerbated by improper material selection, inadequate structural reinforcement, and inconsistent assembly quality[10]. Therefore, a data-driven reliability assessment is essential to systematically map failure pathways, prioritize the most critical risks, and design effective improvements. Fault Tree Analysis (FTA), as an internationally recognized failure

analysis technique (IEC 61025:2019), provides a structured top-down approach for identifying and mitigating risk in mechanical systems and has been shown to lower overall production costs by an average of 8–12%[11]. Building upon this, the present research explores the redesign of a biomass pyrolyzer by applying Value Engineering (VE) principles as the core methodology, with FTA supporting the identification and mitigation of key risk components. The novelty of this study lies in integrating detailed VE functional analysis with simulation-based validation, enabling proposed design alternatives to be evaluated both economically and thermally[12]. Ultimately, the aim is to improve cost efficiency, simplify fabrication, and enhance usability that employing a combination of cost optimization strategies and simulation-based validation resulted in a reduction of unscheduled downtime by 20% in industrial systems, thereby making biomass pyrolyzer technology more accessible to SMEs and better aligned with circular economy objectives[13], [14].

To better understand the sources of mechanical failure in knock-down biomass pyrolyzer systems, a process block diagram is presented in **Figure 1**. This diagram illustrates how poor material selection, insufficient structural reinforcement, and inconsistent assembly quality interact to create critical failure pathways, ultimately compromising system reliability and safety.

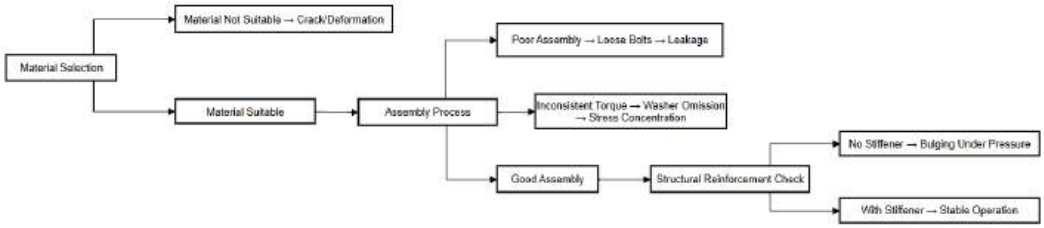

Figure 1. Block Diagram

Recent research on biomass pyrolysis systems for small and medium enterprises (SMEs) has highlighted recurring challenges in both mechanical reliability and operational efficiency. Babajo et al. (2021) developed and tested a co-pyrolysis system for liquid fuel production, emphasizing the importance of design robustness and performance optimization in small-scale applications[15]. However, their study did not systematically address risk prioritization or failure mitigation for long-term use.

In 2022, Mohamad Ramadani conducted an evaluation of the same knock-down pyrolysis tank design for use in community and small to medium-scale industries [9], [16]. However, the scope of his research was limited primarily to flow simulation analysis, without a comprehensive assessment of overall system feasibility or failure risks. In the same year, Faiz Irza performed a CFD-based study focusing on the condenser section of a rice husk pyrolysis system, also employing the knock-down design concept[17], [18]. Nevertheless, neither study addresses the broader issues of system reliability nor provides an integrated failure and feasibility analysis covering the complete pyrolyzer system. The present study builds upon these previous works by implementing a holistic approach that combines Value Engineering and Fault Tree Analysis, thus enabling a more robust evaluation of both functional value and mechanical reliability across all subsystems, as documented in this research.

Badida et al. (2019) demonstrated the effectiveness of fuzzy fault tree analysis in risk evaluation for process equipment, showing how a structured top-down failure mapping can guide more targeted improvements in reliability [12]. Similarly, Wu (2021) applied Fault Tree Analysis (FTA) for safety assessment in LNG plants, reinforcing FTA's suitability as a standard for mechanical risk mapping in complex thermal systems [10]. These works support the use of FTA as an analytical backbone for identifying and quantifying critical failure modes in pyrolyzer design.

On the economic and functional optimization side, Akerekan et al. (2024) and Prilutskaya et al. (2021) underscored the value of systematic Value Engineering (VE) in enhancing both sustainability and cost-effectiveness in manufacturing system redesigns [19], [20]. They show that the SAVE International job plan, combined with simulation validation, enables designers to balance functional performance and economic constraints in process equipment development. Nevertheless, most studies treat VE and FTA in isolation, and only a limited number apply them simultaneously within the context of SME-scale biomass pyrolyzer systems.

Based on this gap, the present research integrates VE and FTA into a single framework for redesigning a knock-down biomass pyrolyzer targeting SMEs, utilizing simulation and empirical risk mapping as validation tools. This integrated approach responds directly to the shortcomings in the literature by addressing both reliability and cost-effectiveness through a combined, quantitative method, as previously recommended by Badida et al. (2019) and Akerekan et al. (2024).

2. Materials and Experiment Methods

This study focuses on the condenser subsystem of a knock-down type biomass pyrolyzer, which is designed for small and medium enterprises (SMEs) to process rice husk into biochar, bio-oil, and producer gas. The condenser is a critical component, constructed as a cylindrical vessel with an approximate weight of 100 kg (diameter 544 mm, height 1000 mm), and is connected to the main reactor using flanged and bolted joints. Field prototypes operate at temperatures up to 400°C, exposing the condenser to significant thermal and mechanical loads.

2.1 Materials

The analysis in this study is based on multiple data sources that complement each other to ensure both technical validity and contextual relevance for the design of a knock-down biomass pyrolyzer. First, technical drawings and specifications from previous research, along with data from field-tested prototypes, serve as the primary references for assessing the performance and structural configuration of the initial design. Historical failure data collected during assembly and testing processes provide insights into real-world failure modes, such as deformation, leakage, and joint instability.

Additionally, material property data, specifically for ASTM A36 structural steel for base frame and leg support material and AISI 304 stainless steel, are utilized due to their known strength, thermal resistance, and corrosion resistance, especially for components in contact with pyrolysis outputs like bio-oil and syngas[20]. Mechanical simulations were conducted using Solidworks software to analyze critical aspects such as bulging deformation, von Mises stress distribution, and displacement, as well as to validate structural reliability under operational loads.

Furthermore, the analysis integrates information from the previous Bill of Materials (BOM), which is essential for conducting Value Engineering (VE). The analysis allows for evaluation of the cost-to-function ratio of each component, enabling redesign recommendations that are both risk-informed and cost-effective.

2.2 Methods

This study employs a dual-methodology approach, combining Fault Tree Analysis (FTA) for reliability risk assessment with Value Engineering (VE) for design optimization of the knock-down biomass pyrolyzer system. Both methods are applied systematically to ensure that the proposed design modifications address critical mechanical failures and deliver functional and economic value improvements. The integration of these methodologies enables a comprehensive evaluation that bridges the gap between technical reliability and cost-effective engineering solutions.

2.2.1 Fault Tree Analysis (FTA)

The analysis begins by defining the top event, namely, mechanical failure in the condenser that could potentially lead to operational shutdown or hazardous leakage. Subsequently, the failure structure is broken down into several main branches, namely failures due to design, materials, and assembly processes. The interrelationships among causal factors in each branch are mapped using AND/OR logic gates to represent cause interactions, such as bulging, which only occurs if the stiffener is insufficient and there is excess internal pressure[10]. All possible failure pathways are then analyzed for frequency and criticality to identify the most dominant minimal cut sets. Once the quantitative risk contribution of each branch is determined based on its frequency of occurrence in the minimal cut sets, all findings are validated by comparing them to field test results and static simulation data to ensure the accuracy and relevance of the FTA analysis performed.

2.2.2 Value Engineering (VE) Procedure

The research methodology is structured according to the standard job plan of SAVE International for Value Engineering, which comprises five main phases[23]. In the Information Phase, the functional decomposition of the pyrolyzer system was conducted, classifying functions into basic, secondary, and support categories[24]. Cost data were compiled from previous prototype bills of materials, supplier quotations, and fabrication records to establish a baseline for economic evaluation[20]. During the Creative Phase, design alternatives were generated through structured brainstorming, including options such as replacing welded joints with knock-down bolted assemblies, altering frame materials, and incorporating high-efficiency ceramic insulation[25], [26].

In the Evaluation Phase, each design alternative was assessed using a weighted scoring matrix based on four primary criteria: thermal efficiency, durability, manufacturability, and potential cost savings. The value index, the function-to-cost ratio, was calculated for each component to guide selection. Selected alternatives were further analyzed in the development phase, where three-dimensional models were created in Solidworks and subjected to thermal and structural simulations. These simulations included thermal gradient analysis, bulging simulations of the condenser, and an assessment of insulation performance.

Finally, in the Presentation Phase, the most viable redesigns were consolidated into an integrated final model. Risk analysis used Fault Tree Analysis (FTA) to systematically map and quantify potential failure modes, focusing on the condenser and joint assemblies. This integrated approach ensured that both functional and reliability improvements were supported by quantitative analysis and simulation-based validation.

2.2.3 Simulation and Risk Analysis

Simulation tools were employed to evaluate the thermal and mechanical performance of the redesigned components. Finite Element Analysis (FEA) was conducted on critical areas such as the condenser wall, where bulging deformation was previously observed[9,25]. Heat transfer analysis compared the performance of various insulation alternatives. Concurrently, Fault Tree Analysis (FTA) was used to define the top failure event and trace the contributing sub-events through logic gate modeling. The FTA structure included domains such as design flaws, material limitations, and assembly errors, enabling prioritization of mitigation strategies.

3. Results and Discussion

Before presenting the detailed findings, it is important to reiterate that this study aims to enhance the reliability, efficiency, and cost-effectiveness of the knock-down biomass pyrolyzer system, focusing on the condenser unit as a critical component. The results are systematically organized to comprehensively analyze mechanical failure pathways, design modifications, and the impact of Value Engineering (VE) interventions. By integrating Fault Tree Analysis (FTA) and VE methodologies, the research delivers a

holistic evaluation that identifies and quantifies failure modes and proposes practical, data-driven improvements directly relevant to small and medium-sized enterprises (SMEs). The following sections present the results of the FTA and VE analyses, highlight key mechanical risks and their mitigation strategies, and discuss the overall benefits of the proposed design enhancements in terms of performance, manufacturability, and compliance with international safety standards.

3.1. Mechanical Failure Pathways in the Condenser

Figure 2 shows the Fault Tree Analysis (FTA) diagram developed for the condenser subsystem of the knock-down pyrolyzer.

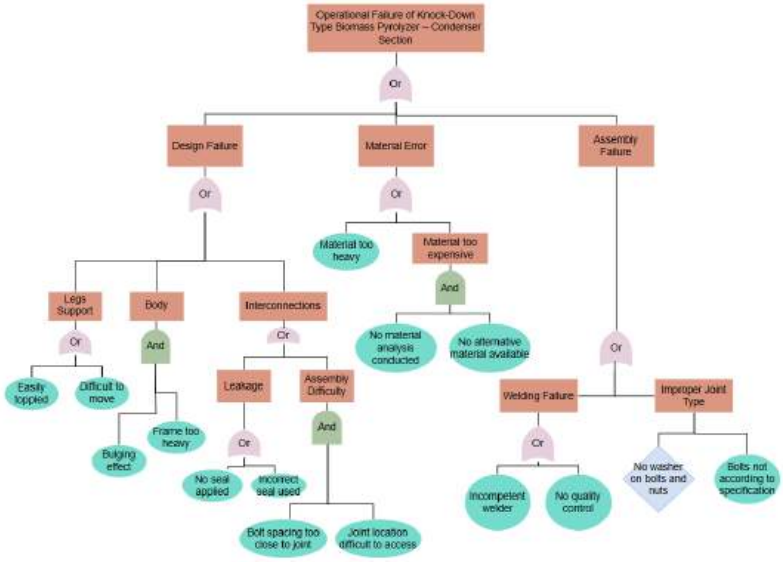

Figure 2. Structure of the FTA Tree

The diagram systematically maps the logical relationships among the main causes of mechanical failure, ranging from flange joint leakage and bulging deformation of the vessel wall to misaligned mechanical assembly. At the top level, the analyzed top event is a mechanical failure that leads to operational shutdown or the risk of hazardous leakage. From this top event, the FTA diagram breaks down the failure pathways into three main domains: design failures, material failures, and failures in the assembly process. Each domain is then further decomposed into basic events, such as insufficient stiffeners on the wall, omission of washers on the flange, poor welding quality, or improper material selection. This diagram helps engineers and designers understand the interactions among different failure factors and how a weakness at one point can cumulatively contribute to overall system failure. Thus, the FTA mapping enables prioritization at the highest risk points for targeted design intervention and corrective actions.

To make the risk contribution of each domain easier to understand, **Table 1** presents the distribution of risk contributions based on the minimal cut set analysis. The design domain contributes the largest share of risk, accounting for 50 % of all identified failure pathways. Risks due to assembly errors are in second place, with a contribution of 33.3 %, while material failures contribute 16.7 %. These results emphasize that the most effective interventions should focus on improving design and assembly aspects before enhancing material selection and quality control.

Table 1. Main Failure Domains and

Failure Domain	Basic Event in FTA	Failure Mechanism (summary)	Number of MCS in this domain	Relative Contribution (%)
Design	Lack of stiffener, suboptimal joints, flange without the washer, and bolts too close together	The structure/joint fails to withstand static/thermal loads	6	50.0
Material	The material is too heavy, and no alternative is available	Excessive self-weight, low durability	2	16.7
Assembly	Incompetent welding, no QC, bolts not to specification, missing washers	Poor assembly quality, uneven preload distribution	4	33.3

Relative Contribution: % of MCS (minimal cut sets) involving the respective failure domain.

The implementation of load-indicator washers combined with standardized torque control procedures is essential, as this approach is estimated to reduce the probability of flange failure pathways by approximately 30%. Structural rigidity is further enhanced by adding stiffener rings at intervals of 400–500 mm on the cylindrical shell and replacing wheels with fixed bases equipped with leveling feet, resulting in a more than fourfold increase in the structural safety factor with a cost increment of less than 6%. Additionally, repositioning the gas inlet by 15° toward the centrifugal axis and incorporating an extra 25 mm layer of lightweight brick insulation decreases the axial temperature gradient from approximately 45 °C to 18 °C, according to CFD results, thereby ensuring more uniform quality of both bio-oil and char products.

3.2. Mechanical Failure Pathways in the Condenser

This section discusses the main mechanical failure pathways identified in the condenser subsystem of the knock-down pyrolyzer. Each failure mode was systematically analyzed using Fault Tree Analysis (FTA) to determine its underlying causes and relative criticality. The following sub-sections detail the three most dominant failure mechanisms: flange leakage due to the absence of washers, bulging from insufficient stiffening, and assembly quality and joint alignment issues. Both field observations and simulation results support these.

3.2.1. Flange Leakage and Absence of Washer

Leakage at the flange joint generally occurs due to the absence of a flat washer in the bolt and nut assembly. This condition causes the stress distribution to become highly concentrated in a small area on the flange surface, which triggers local plastic deformation and more rapid relaxation of the bolt clamping force. Literature studies indicate that adding a flat washer can reduce maximum contact stress by up to 18 % and delay bolt loosening by more than 20 % [26,27]. As a result, flange joint instability becomes the most frequently identified root cause of failure in the minimal cut set analysis.

3.2.2. Bulging and Insufficient Stiffener

In cases of bulging deformation caused by a lack of stiffeners, simulation results show that without a stiffener ring, the maximum wall deformation of the condenser during hydrostatic loading can reach 17.16 mm. However, after installing stiffener rings at 400 mm intervals, this deformation is significantly reduced to 10.46 mm. A structure without stiffeners also makes the condenser wall more prone to excessive bending stresses, often exceeding the allowable limits for thin plate structures.

3.2.3. Assembly Quality and Joint Alignment

The quality of the assembly process and joint alignment is crucial for proper load distribution during operation. Inconsistent torque application, the absence of load-indicating washers, and limited welder skills can all cause uneven load distribution at each joint. These conditions accelerate material fatigue and increase the risk of leakage in the system, thus greatly reducing the equipment's overall reliability.

3.3. Mechanical Failure Pathways in the Condenser

This research produced a comprehensive analysis of the knock-down biomass pyrolyzer by integrating Value Engineering (VE) and Fault Tree Analysis (FTA) to optimize SMEs' performance, reliability, and cost-effectiveness. The initial function-cost breakdown, **Table 1,** showed that the combustion chamber and insulation accounted for most of the manufacturing cost, representing 40% and 20%, respectively. This identification guided the selection of components for value improvement.

Table 2. Initial Function-Cost Breakdown of Pyrolyzer Component

Component	Function	Type	Cost (IDR)	%* of Total Cost
Combustion Chamber	Heat Generation	Basic	20,000,000	40%
Insulation	Heat Retention	Basic	10,000,000	20%
Frame Structure	Support & Stability	Support	5,000,000	10%
Condenser Unit	Vapor Collection	Secondary	7,500,000	15%
Miscellaneous (seal, wheels)	Portability/Sealing	Support	7,500,000	15%
Total			**50,000,000**	**100%**

*The value index (Function/Cost) was improved by redesigning the base frame to eliminate unnecessary wheels, using lighter yet stronger materials, and simplifying the assembly.

A cost comparison was conducted to assess whether the implementation of Value Engineering provides proportional economic benefits. The following table presents an overview of the total production cost comparison before and after the application of Value Engineering.

As shown in **Table 3**, the observed cost increase is primarily attributable to adding components such as load-indicator washers, stiffener rings on the reactor wall, and improved insulation for the gas inlet. This analysis resulted in an overall production cost escalation of approximately 5.56% compared to the initial budget. Nevertheless, according to Fault Tree Analysis and Value Engineering findings, these enhancements are anticipated to reduce maintenance and failure-related costs by more than 30% over the long term, thus offering a significant economic advantage despite the modest increase in upfront investment

Table 3. *Production Cost Breakdown of Pyrolysis Tank, Before and After Value Engineering*

Component	Cost Before VE (IDR)	Cost After VE (IDR)	Notes
Material Purchase	2,800,000	2,950,000	Addition of load-indicator washers and stiffener rings
Intellectual Property Registration	500	550	No significant change
Manufacturing Service Fee	3,000,000	3,150,000	Adjustment for the installation of additional components
Total Cost	**6,300,000**	**6,650,000**	Cost increase of IDR 350,000

3.4. Function-Cost Analysis and FAST Diagram

The FAST diagram in the research guided the identification of primary value drivers, such as heat transfer efficiency and component durability. The combustion chamber, as shown in **Table 4** (40% of total cost), and insulation (20%) were prioritized for redesign.

Table 4. *Proposed Value Improvement Options and Evaluation*

Function	Original Design	VE Alternative	Cost Impact	Performance Impact	Decision
Heat Generation	AISI 304 Cylinder	Maintain	Neutral	High	Retain
Heat Retention	Cement Insulation	Ceramic Fibre Blanket	-15%	High	Adopt
Structural Support	Stainless Frame	Cast Aluminium Frame	-20%	Medium	Adopt
Portability	Steel Wheels	Fixed Base	-100%	Low	Remove
Joint Assembly	Welded	Knock-down Bolted Frame	-10%	High	Adopt

Total estimated cost reduction: 15.5%
Thermal efficiency increase: 13.7%

3.5. Comparative Analysis of Design Parameters Before and After Optimization

A side-by-side comparison of critical performance parameters was conducted to assess the effectiveness of the design revisions proposed through Fault Tree Analysis (FTA) and Value Engineering (VE). This comparison focuses on structural deformation, joint reliability, thermal efficiency, production cost, and compliance with safety standards. The results are summarized in **Table 5**.

Table 5 presents a comparative analysis of key design parameters before and after implementing improvements based on Fault Tree Analysis (FTA) and Value Engineering (VE). The results show a significant reduction in mechanical risks and performance inefficiencies. For example, wall bulging deformation decreased from 17.16 mm to 10.46 mm after the addition of stiffener rings, indicating a 39% improvement in structural rigidity.

Table 5. *Summary of performance improvements before and after design modification*

Design Parameter	Before Improvement	After Improvement	Impact
Wall Bulging Deformation (mm)	17.16	10.46	Reduced by 39%
Contact Stress at Flange	High, concentrated	Evenly distributed (−18%)	Reduced bolt loosening risk
Bolt Joint Durability	No washers, uneven preload	Load-indicating washers used	20% improvement in retention
Assembly Process	Manual, inconsistent quality	Simplified and standardized	Enhanced reliability
Thermal efficiency (%)	56–60	68–70	Improved by ~13.7%

Estimated Production Cost (IDR)	47.4 million	50 million	~5.5% increase (but cost-efficient)
Regulatory Compliance	Non-compliant	ISO 14122 & ASME Section VIII met	Improved safety and international standard compliance

Additionally, the integration of load-indicating washers reduced contact stress at flange joints by 18% and improved bolt retention by over 20%, contributing to overall system stability. Thermal efficiency also improved substantially, from approximately 56–60% to 68–70%, due to insulation optimization. Despite a modest production cost increase of 5.5%, the performance gains and reduction in failure risk justify the investment. Furthermore, the final design aligns with ISO 14122 and ASME Section VIII standards, ensuring enhanced safety and regulatory compliance. This comparison confirms that the proposed design modifications effectively enhance reliability and cost-efficiency, particularly for SME applications in rural or decentralized settings.

3.6. Design Modifications

One of the most important design improvements to support equipment reliability and safety is modifying the lifting lug feature, as illustrated in **Figure 3**. In several previous designs, the lifting lugs were often too slender and did not adequately consider the symmetric distribution of loads during lifting operations. Field observations revealed that lifting lugs without additional reinforcement were highly prone to deformation and even failure when the vessel was lifted, especially for condensers weighing more than 100 kg.

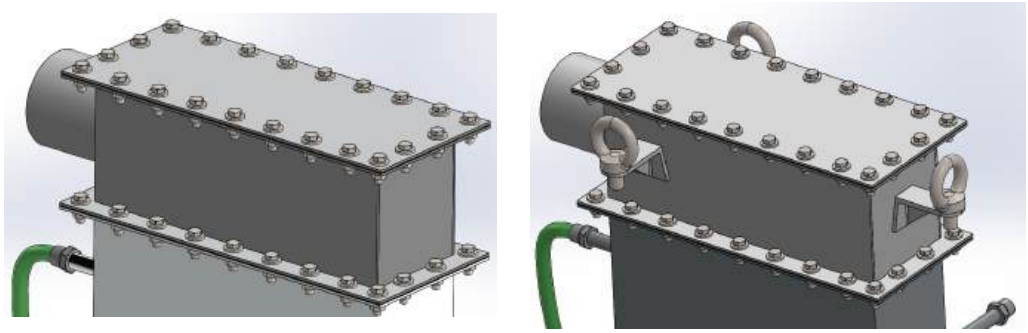

(**a**) (**b**)

Figure 3. *(a) Condition before modification and (b) after modification*

Adding lifting lugs facilitates the handling and lifting process, and the new lug design is equipped with gusset reinforcements and placed symmetrically. The lifting lug ensures that stress distribution during lifting is more even, significantly reducing the risk of local deformation and fracture. Finite element simulation results for the new design show that the maximum stress is reduced by more than 25 % compared to the previous unreinforced.

In the latest condenser design, as shown in **Figure 4**, the wheels have been removed and replaced with fixed legs to comply with safety requirements stipulated in ISO 14122-2:2016, which mandates that all stationary process equipment must have fixed legs to ensure stability and prevent unintended movement during operation. Furthermore, ASME Section VIII also recommends using a base plate and anchor bolts on a fixed foundation for equipment serving as a pressure vessel to ensure structural stability and safety during use. Therefore, replacing wheels with fixed legs increases equipment stability and operator safety and aligns with applicable international standards (ISO 14122-2:2016; ASME Boiler and Pressure Vessel Code, Section VIII).

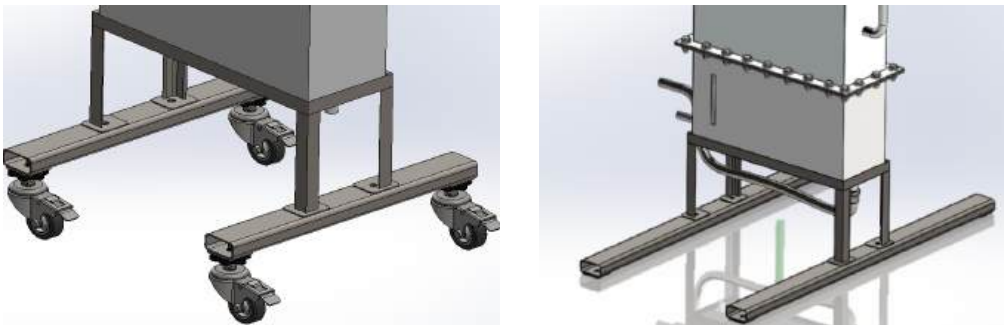

(**a**) (**b**)

Figure 4. *(a) Condition of the leg design before modification and (b) after modification*

As shown in Figure 5, other improvements include simulation and field-testing results that reinforce the urgency of proper structural reinforcement and assembly. Without the installation of stiffener rings, bulging deformation on the condenser wall can reach up to 17.16 mm during hydrostatic testing.

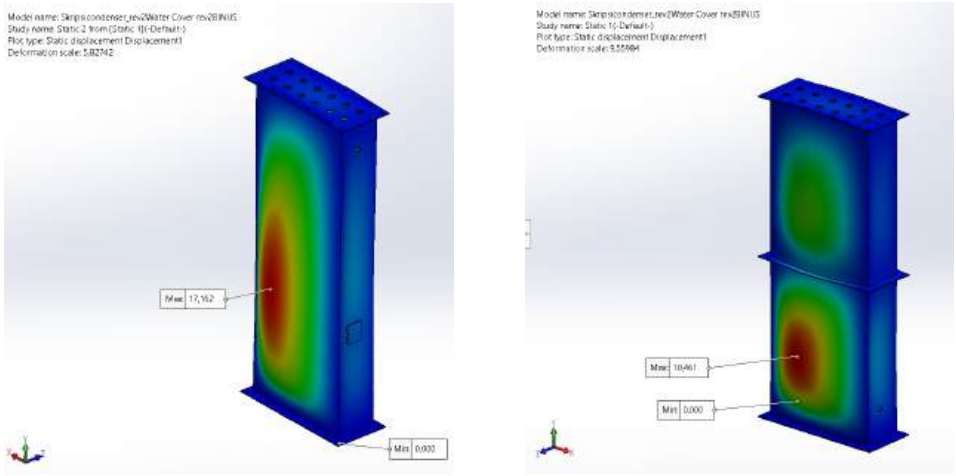

(**a**) (**b**)

Figure 5. *Simulation results of bulging calculation on the condenser vessel with the addition of stiffeners: (a) previous design without stiffeners, (b) design after stiffener installation*

After stiffener rings are installed at 400 mm intervals, this deformation decreases significantly to 10.46 mm. Additionally, using washers on flange joints has been proven to reduce maximum contact stress by up to 18 % and delay bolts loosening by more than 20 %. As shown in Figure 4, these modifications enhance structural integrity and joint reliability during long-term operation.

The combination of all design improvements, including reinforcement of the lifting lug, removal of wheels, replacement of seals, and optimization of stiffeners and washers, is projected to reduce the probability of critical mechanical failure by up to 30 %. The estimated production cost increase of approximately 5.5 % is considered very reasonable compared to the benefits of longer equipment service life, improved operator safety, and an overall reduction in maintenance costs[28]. Therefore, these comprehensive improvements provide a holistic and data-driven approach to enhancing the reliability of pyrolyzer condensers in the SME sector.

3.7. Final Design Improvement

The final design of the biomass pyrolyzer is the culmination of a comprehensive improvement process grounded in Fault Tree Analysis (FTA) and Value Engineering (VE), as shown in **Figure 6.** This redesign enhances the unit's structural integrity, operational reliability, and manufacturability, particularly for small and medium-sized

enterprises (SMEs)[26]. One key modification is adding 136 washers at the bolt and nut joints of the condenser body. These washers help prevent surface deformation and increase joint durability by distributing stress over a wider area [27,29].

Although the insulation system, which uses Hebel blocks, was not significantly changed, it remains an integral fixed component designed for easy replacement during installation. The condenser body underwent a structural redesign involving improved segment joints and the integration of stiffeners. This improvement significantly reduced the bulging effect due to internal pressure, lowering the maximum deformation from 17.16 mm to 10.46 mm, as verified through finite element simulation using Solidworks. The effectiveness of this structural redesign is closely linked to the material properties employed; the condenser body utilizes low-carbon steel (ASTM A36), which offers an adequate yield strength of 250 MPa and good weldability, making it well-suited to withstand the thermomechanical stresses generated during pyrolysis operation. The stiffeners were likewise fabricated from the same material to ensure compatibility, uniform thermal expansion, and consistent joint behavior under cyclic loading conditions.

Further, the support system was changed from a wheeled model to a fixed leg configuration to enhance stability, which is particularly important for a unit weighing more than 100 kg. An optional leveling foot was added to the support design, providing flexibility for installation on uneven surfaces while complying with ASME Section VIII standards for pressure vessels installed on flat, reinforced floors[30]. Three lifting lugs were incorporated to support ease of transport and installation, each strategically positioned near the condenser's Center of mass. These lifting eyes facilitate balanced hoisting using M16 eyebolts, improving safety during movement. The final assembled design adopts a knock-down modular concept, making transporting, fabricating, and assembling easier while maintaining robustness and performance[31].

Figure 6. *Final Design of Knocked-down Biomass Pyrolyzer*

This angle, shown in **Figure 6**, the final rendering of the improved biomass pyrolyzer, visually represents all significant enhancements: reinforced joints, optimized airflow, structural stiffening, and modular framing, all aimed at achieving a high-function, cost-efficient solution through the VE process.

4. Conclusion

This study establishes the significance of integrating Value Engineering and Fault Tree Analysis as a systematic framework for enhancing the reliability, cost-effectiveness, and sustainability of knock-down biomass pyrolyzer systems for SMEs in Indonesia. Beyond the technical improvements and quantifiable efficiency gains, the combined

methodology enables targeted interventions that address economic constraints and critical risk factors specific to rural industrial settings. The resulting design advances the operational reliability and ease of assembly and aligns with international standards for safety and manufacturability, offering a practical model for broader adoption in the agro-industrial sector. Ultimately, this work contributes a replicable approach for sustainable waste management and circular economy initiatives, providing a foundation for future research in system automation and advanced material integration to support SMEs' resilience and competitiveness further.

5. Acknowledgment

The authors would like to thank the facilities provided by the Research Center for Eco-friendly Technology, in collaboration with Binus University. This research was funded through the Lecture Research Scheme 2025 Politeknik Negeri Jakarta with Contract No. 217/PL3.A.10/PT.00.06/2025.

References

1. BPS. Statistical Yearbook of Indonesia 2022. 2023.
2. Bodor K, Szép R, Bodor Z. Time series analysis of the air pollution around Ploiesti oil refining complex, one of the most polluted regions in Romania. Sci Rep 2022;12. https://doi.org/10.1038/s41598-022-16015-7.
3. Li W, Ge P, Chen M, Tang J, Cao M, Cui Y, et al. Tracers from Biomass Burning Emissions and Identification of Biomass Burning. Atmosphere (Basel) 2021;12. https://doi.org/10.3390/atmos12111401.
4. Matin HHA, Syafrudin S, Suherman S. Rice Husk Waste: Impact on Environmental Health and Potential as Biogas. Kemas 2023;18:431–6. https://doi.org/10.15294/kemas.v18i3.42467.
5. Suttibak S, Chuntanapum A. Optimization of producer gas production from rice husks and sawdust in a three-stage gasifier. Energy Sources, Part A: Recovery, Utilization and Environmental Effects 2021. https://doi.org/10.1080/15567036.2021.1941438.
6. Vershinina K, Nyashina G, Strizhak P. Combustion, Pyrolysis, and Gasification of Waste-Derived Fuel Slurries, Low-Grade Liquids, and High-Moisture Waste: Review. Applied Sciences (Switzerland) 2022;12. https://doi.org/10.3390/app12031039.
7. Marizar ES, Irawan AP, Beng JT. The Knock Down System of Rattan Furniture for Global Market. IOP Conf Ser Mater Sci Eng, vol. 508, Institute of Physics Publishing; 2019. https://doi.org/10.1088/1757-899X/508/1/012104.
8. Cardona JP, Castellanos JU, Gutiérrez LC. State Observer for Deflections in Rectangular Flat Plates Simply Supported Subjected to Uniform and Hydrostatic Pressure. Computation 2025;13:107. https://doi.org/10.3390/computation13050107.
9. Rudiatama MR, Hamdi H, Kamal DM, Soedarsono JWM, Maksum A. The Effect of Chimney Size on Knock-Down Pyrolysis Tank Design as Rice Husk Burner Using CFD Simulation. IOP Conf Ser Earth Environ Sci, vol. 1111, Institute of Physics; 2022. https://doi.org/10.1088/1755-1315/1111/1/012042.
10. Wu W. Application of fault tree analysis in LNG fire risk assessment of LNG fueled ships. Vibroengineering Procedia, vol. 36, EXTRICA; 2021, p. 108–14. https://doi.org/10.21595/vp.2021.21827.
11. Odeyar P, Apel D, Hall R, Zon B, Skrzypkowski K. A Review of Reliability and Fault Analysis Methods for Heavy Equipment and Their Components Used in Mining. Energies (Basel) 2022. https://doi.org/10.3390/en15176263.
12. Badida P, Balasubramaniam Y, Jayaprakash J. Risk evaluation of oil and natural gas pipelines due to natural hazards using fuzzy fault tree analysis. J Nat Gas Sci Eng 2019;66:284–92. https://doi.org/10.1016/j.jngse.2019.04.010.

13. Velasco-Muñoz JF, Aznar-Sánchez JA, López-Felices B, Román-Sánchez IM. Circular economy in agriculture. An analysis of the state of research based on the life cycle. Sustain Prod Consum 2022. https://doi.org/10.1016/j.spc.2022.09.017.

14. Rusch M, Schöggl J-P, Baumgartner R. Application of digital technologies for sustainable product management in a circular economy – a review. Bus Strategy Environ 2021. https://doi.org/10.31235/osf.io/twgks.

15. Babajo SA, Enaburekhan JS, Rufa'i IA. Design, Fabrication and Performance Study of Co-Pyrolysis System for Production of Liquid Fuel from Jatropha Cake with Polystyrene Waste. Journal of Applied Sciences and Environmental Management 2021;25:407–14. https://doi.org/10.4314/jasem.v25i3.15.

16. Rudiatama MR, Irza Ramadhan F, Indra Kusumo P, Syakuro A, Ricardo Marulitua Tambun D, Hamdi, et al. Perancangan Tangki Reaktor Pyrolyzer Kapasitas 20 kg sebagai Penghasil Rice Husk Ash (RHA). Seminar Nasional Inovasi Vokasi, vol. 1, Jakarta: 2022.

17. Ramadhan FI, Soedarsono JWM, Riastuti R, Maksum A. Heat Effectiveness Analysis of Knock Down Smoke LCS (Liquid Collection System) Design with a Mixture of Ethylene Glycol and Water as Cooling Media. IOP Conf Ser Earth Environ Sci, vol. 1111, Institute of Physics; 2022. https://doi.org/10.1088/1755-1315/1111/1/012054.

18. Akerekan O, Ongbali SO, Yekini ES, ... The Role of Value Engineering in Sustainable Manufacturing Scheme: A Critical Review. … , Engineering and … 2024.

19. Prilutskaya M, Murukina A, ... Mechanical Engineering Product Value Design Applying the Value Engineering Method. MATEC Web of … 2021.

20. Jun J, Su YF, Keiser JR, Wade JE, Kass MD, Ferrell JR, et al. Corrosion Compatibility of Stainless Steels and Nickel in Pyrolysis Biomass-Derived Oil at Elevated Storage Temperatures. Sustainability (Switzerland) 2023;15. https://doi.org/10.3390/su15010022.

21. Stewart R. VM Guide, A Guide to the Value Methodology Body of Knowledge. 2020.

22. Ginting R, Silalahi R, Marunduri MA. The Conceptual Integration of Quality Function Deployment and Value Engineering for Product Development: A Case Study of Water Dispenser. International Journal of Technology 2025;16:124–35. https://doi.org/10.14716/ijtech.v16i1.6326.

23. Hartanto A, Ginting R, Ishak A. Integration of Value Engineering for Design for Assembly in Product Design: A Comprehensive of Literature Review. Jurnal Sistem Teknik Industri 2024;26:145–51. https://doi.org/10.32734/jsti.v26i2.15268.

24. Mousa AA, Hussein M, ... Value-engineering methodology for the selection of an optimal bridge system. Transportation Research … 2022. https://doi.org/10.1177/03611981211062154.

25. Ngamsidhiphongsa N, Ponpesh P, Shotipruk A, Arpornwichanop A. Analysis of the Imbert downdraft gasifier using a species-transport CFD model including tar-cracking reactions. Energy Convers Manag 2020;213. https://doi.org/10.1016/j.enconman.2020.112808.

26. Croccolo D, De Agostinis M, Fini S, Khan MY, Mele M, Olmi G. Optimization of Bolted Joints: A Literature Review. Metals (Basel) 2023;13. https://doi.org/10.3390/met13101708.

27. Ren Y, Li J, Wang L, Gao F, Zhang D, Hu H, et al. Tightening and anti-loosening performance of spring washer connecting bolts. Results in Engineering 2024;24. https://doi.org/10.1016/j.rineng.2024.102960.

28. Kineber AF, Mohandes SR, ElBehairy H, Chileshe N, Zayed T, Fathy U. Towards smart and sustainable urban management: A novel value engineering decision-making model for sewer projects. JClean Prod 2022;375:134069. https://doi.org/https://doi.org/10.1016/j.jclepro.2022.134069.

29. Dravid S, Jitendra Y, and Kurre SK. Comparison of loosening behavior of bolted joints using plain and spring washers with full-threaded and plain shank bolts. Mechanics Based Design of Structures and Machines 2023;51:5577–95. https://doi.org/10.1080/15397734.2021.2008258.

30. Wang N, Si H, Yi W, Li Y, Zhang Y. Design and operation of a mobile fast pyrolysis system utilizing a novel double pipe fluidized bed reactor. Fuel Processing Technology 2021;224:107005. https://doi.org/https://doi.org/10.1016/j.fuproc.2021.107005.

31. Teoh BA, Anbia Chi Adam MK. Enhancing Car Seat Cushion Production Performance Through Value Engineering: A Case Study. International Journal of Transport Development and Integration 2024;8:505–17. https://doi.org/10.18280/ijtdi.080402.

RiESTech
Recent in Engineering Science and Technology

MBI

Article

Development of IoT-based Monitoring of the Lithium-Ion Battery Pack for a Two-Wheeled Vehicle Ecosystem

Sonki Prasetya [1,2*], Muhammad Todaro [1,2], Hasvienda M Ridlwan [1,2]

[1] Mechanical Engineering Department (Renewable Energy Skill Development Program), Politeknik Negeri Jakarta, Depok, 16425, Indonesia
[2] Center for Conversion, Conservation and Applied Renewable Energies (CARE), Politeknik Negeri Jakarta, Depok, 16425, Indonesia
* Correspondence: sonki.prasetya@mesin.pnj.ac.id

Abstract: Electric bicycles with two wheels are increasingly popular as a convenient mode of short-distance transporta-tion. To enhance mobility and promote the use of eco-friendly energy around campus areas, conventional bicycles can be transformed into electric ones using a conversion kit. The main challenge lies in creating a design that is easy to install (plug-and-play) and compatible with various bicycle models. Moreover, monitor-ized battery condition is an advantage to inform the user. A key advantage of this concept is the inclusion of a universal battery pack equipped with an IoT-based monitoring system. This study aims to design an IOT based battery pack conversion kit powered by a 576 Wh of $LiFePO_4$ lithium-ion battery type. The battery pack is tested by experiment to obtain the performance of the energy storage for a converted e-bike. Experiment results indicate that battery pack of 50 cm × 16 cm × 14 cm dimension with the total weight of 4.5 kg can perform as the energy storage for a converted two-wheeled electric vehicle. The test achieves the speed of 500rpm with 1A current.

Keywords: Electric bike; Battery; Internet of Things (IoT); Lithium-Ion 4

Citation: Prasetya, S., Todaro, M., Ridlwan, H. M. (2026). Development of IoT-based Monitoring of the Lithium-Ion Battery Pack for a Two-Wheeled Vehicle Ecosystem. Recent in Engineering Science and Technology, 4(02), 117–116. Retrieved from https://www.mbi-journals.com/index.php/riestech/article/view/137.

Academic Editor: Yudhi Ariadi

Received: 30 November 2025
Accepted: 20 February 2026
Published: 30 April 2026

1. Introduction

The growing concern over climate change has heightened public awareness of the environmental consequences of human activities, particularly within the global transportation sector. This sector is experiencing a significant transition from fossil fuel–powered vehicles to electric mobility solutions. Among these alternatives, electric bicycles (e-bikes) have become increasingly preferred due to their economic advantages, health benefits, reduced environmental footprint, and effectiveness in alleviating urban traffic congestion [1,2].

Vocational education namely Politeknik Negeri Jakarta (PNJ) wants to develop a green campus concept by implementing green technologies in their daily activities. The road to access building in PNJ campus are not a long and complicated path (nearly 1.5 km from the gate in front of the campus to the building at the back of the campus). Several studies and products have been developed focused on green technologies for electric vehicles [3] and battery swapping stations [4]. One of the initiatives to encourage environmentally friendly practices within campus areas is to promote sustainable mobility by walking or cycling for short-distance travel. However, this approach may not be feasible for all members of the academic community, particularly in areas with hilly or uneven terrain. Consequently, additional mechanical assistance, such as the integration of an electric motor into bicycles (e-bikes), is necessary to support user mobility.

The cost of owning an e-bike can also pose a challenge for students [5]. However, several universities have begun implementing rental or sharing systems to increase accessibility and promote sustainable mobility on campus [6]. However, the motor-bike

they are using are commonly new bikes, or owned by companies as part of business collaboration with campuses. An idea of utilizing personal bikes that are owned by academicians is developed. A practical solution is to convert conventional bicycles into electric bicycles using a conversion kit assembled by PNJ academicians. This approach has not been developed by campus in Indonesia. It is more feasible and also economical than purchasing a new e-bike for creating the green campus. Furthermore, those bikes will be integrated with application for mobilities in campus to monitor e-bike services.

A crucial component in converting a conventional bicycle into an e-bike is the battery, which supplies power to the electric motor. The battery pack serves as the primary energy source and has a significant influence on the e-bike's range, performance, weight, and overall cost. Lithium-ion batteries have emerged as the preferred option for e-bike energy storage systems due to their high energy density, long life cycle, and superior power-to-weight ratio compared to other rechargeable battery types [7].

Accordingly, this research focuses on designing a lithium-ion battery pack that optimizes performance, safety and reliable for converted e-bike applications for PNJ campus. The study investigates the battery's configuration, management system, and performance characteristics of IOT based monitoring battery pack. The main objective of this paper is to develop an IOT monitored lithium-ion battery pack for an e-bike conversion kit so that the conversion of e-bike can be effectively integrated into conventional bicycles.

2. Materials and Experiment Methods

The method of this research uses a qualitative approach that aims to analyze the performance of the product The main focus of this research is to ensure the IOT based monitoring system can be implemented and beneficial for the user. The system will be validated by clients or users to assess the level of feasibility and ease of use.

At the initial stage of developing a green transportation environment, it is essential to establish a universal and plug-and-play system that enables the conversion of conventional bicycles into electric bicycles. An e-bike generally consists of three key components: an electric motor, a controller, and a battery. While controllers and motors are readily available from various online marketplaces at different price points depending on their features, the battery remains a major challenge due to its relatively high cost and limited lifespan.

Therefore, this research was conducted through several stages, namely Identify specifica-tion and configuration of battery pack, assembling and testing.

A. Identifying the specifications and configuration of the $LiFePO_4$ lithium-ion battery pack.

The battery specifications were determined through a market survey aimed at select-ing the appropriate battery type, dimensions, and design parameters. The selection process was based on data collected from the top three best-selling e-bike models listed on popular online marketplaces—Tokopedia, Shopee, and Blibli. The survey results indicate that a 48V Li-ion battery with a capacity ranging from 8 to 12 Ah is the most commonly used configuration. Lithium-ion 32700 cylindrical cells were selected for this study due to their optimal balance between energy density (200–250 Wh/kg), cost-effectiveness, and market availability. Each cell possesses a nominal voltage of 3.2–3.3 V and a rated capacity of 12 Ah, making it suitable for mid-range electric bicycle applications that require both performance stability and safety.

The battery pack employs $LiFePO_4$-based lithium-ion 32700 cylindrical cells, each measuring 32 mm in diameter and 70 mm in height. The selection of this cell type was guided by a market survey of the top three commercially available e-bikes, which

identified 48 V systems with capacities ranging from 8 Ah to 12 Ah as the most common configuration.

The number of battery series obtained by this equation [8]:

$$Series\ Battery = \frac{Voltage\ of\ Motor}{Voltage\ of\ Battery} \quad (1)$$

The capacity follows this equation:

$$Capacity\ of\ Battery = 1.3x \frac{Energy\ used}{Voltage\ of\ Battery} \quad (2)$$

where 1.3 constant is put for 70% Depth of Discharge to preserve the battery sustainability.

Moreover, the battery requires parallel configuration using the equation:

$$Parallel\ Battery = \frac{Capacity\ of\ Battery}{Cell\ Capacity} \quad (3)$$

To achieve a nominal system voltage of 48 V and a total capacity of 10 Ah, a 15S2P configuration (15 cells in series and 2 in parallel) was implemented. The resulting specifications are as follows:

- Nominal Voltage: 48 V
- Total Capacity: 10 Ah
- Energy Storage: 576 Wh

To account for thermal expansion and heat dissipation, spacing between adjacent cells was incorporated into the pack layout as recommended in [9]. Consequently, the internal battery pack dimensions were determined to be approximately 45 cm × 12.5 cm × 9.5 cm, with an estimated total weight of 4.5 kg.

B. Assemble the battery pack.

A Battery Management System (BMS) required in order to assemble the battery pack. The BMS is designed to ensure operational safety and longevity by providing protection against overcharging, over-discharging, overcurrent, and excessive temperature conditions [10], [11]. A commercially available universal BMS with integrated Bluetooth functionality was selected for this application, enabling real-time monitoring and datatransmission. The BMS module is mounted on the side of the battery. The Figure 1 shows the battery pack module.

Figure 1. IOT-based Li-Ion Battery pack module

The Figure 2 shows a block diagram of a system that converts a conventional bicycle into an electric bicycle. The system consists of a 48V Li-On battery as the power source, which supplies electricity to a 500W controller that regulates power distribution to a 500W BLDC (Brushless DC) motor. The motor serves as the main drive for the bicycle's wheel. Further-more, the throttle is used to control the motor speed based on user input, with its signal directly connected to the controller to adjust the power delivered to the motor. This dia-gram provides an overview of the basic workflow of the system.

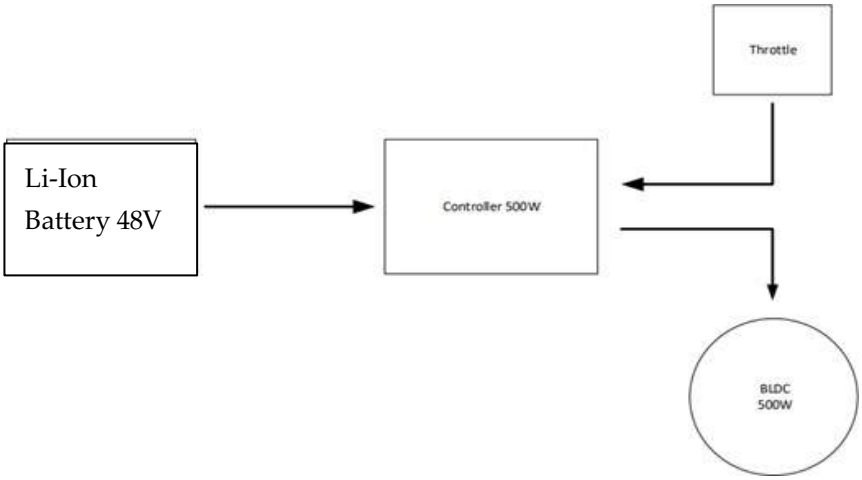

Figure 2. The connection diagram of battery and the e-bike system.

The battery pack module complete with the BMS is attached with the folded bike frame integrated with the controller the motor. A 500W Brushles DC (BLDC) motor hub as the driving tool is then connected to the controller. The Figure 3 shows those selected components.

Figure 3. A bike frame, motor hub and Battery Management System.

The connection (wiring) system is shown in Figure 4 The image illustrates a wiring diagram of the control system for converting a conventional bicycle into an electric bicycle. This diagram illustrates the connections between the main components: a 48V 12A battery as the power source connected to a 500W controller through a relay and contact switch to control the power flow. The controller regulates power distribution to the 500W BLDC motor via phase wires (yellow, blue, green) and Hall sensors for rotor position control. Additionally, the throttle is used to control the motor speed based on user input, while the speed mode allows adjustment of the desired speed level. All these components work in an integrated manner to convert electrical energy into mechanical power that drives the bicycle.

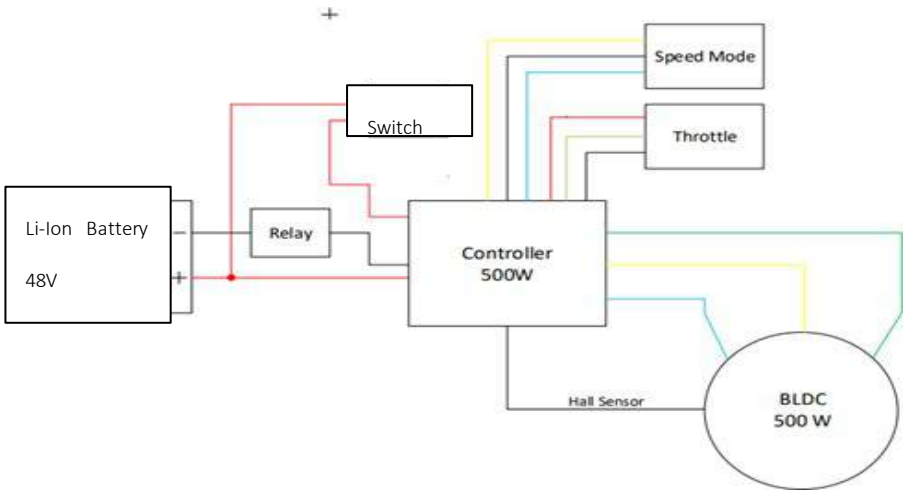

Figure 4. Wiring diagram of the e-bike

C. Testing the battery pack performance.

The performance test consists of several observations namely maximum speed test, max-imum range. It is necessary to monitor the voltage value at the beginning (initial) and the final (after test). Those two voltage monitors can be achieved by these several steps:

Initial Voltage Test

1. Check the battery condition to ensure it is fully charged.
2. Use a multimeter to measure the voltage at the battery terminals before the bicycle is operated.
3. Record the measurement result as the initial voltage.

Final Voltage Test

1. After completing all tests, remeasure the battery voltage using a multimeter.
2. Record the measurement result as the final voltage.
3. Compare it with the initial voltage to determine the voltage drop.

Furthermore, the steps of the performance experiments are divided into two observations namely off-site (mobile) and on-site. The first observation requires the system to be dynamic since the e-bike travels to a determined route as seen on Figure 5.

Figure 5. Trajectory of the e-bike dynamic test.

Maximum Speed Test

- Ensure the electric bicycle is in ready condition and the battery is fully charged.
- Place the bicycle on a straight and flat test track.
- Turn on the electric bicycle and set it to the maximum speed mode.
- Record the highest speed achieved using a speedometer or another measuring de-vice.

Maximum Range Test

- Ensure the battery is fully charged before starting the test.
- Use a safe test track suitable for the environmental conditions.
- Operate the bicycle until the battery is completely depleted and the bicycle can no longer move.
- Record the distance traveled using a distance measuring device.

Meanwhile the second observation conducted on static condition to obtain the data. The data can be used to obtain the control performance of the converted e-bike system. It consists of two measurement namely current and speed test. The steps are explained as follow:

Current Test at Maximum Speed

- Lift the rear wheel of the bicycle so that it does not touch the ground.
- Connect a multimeter set to current measurement mode (ammeter) to the electric mo-tor circuit.
- Run the bicycle until it reaches maximum speed without any load.
- Record the current reading displayed on the multimeter.

Three-Speed level Test

- Lift the rear wheel of the bicycle so that it does not touch the ground.
- Set the bicycle speed mode to the first level and run the motor until stable, then record the speed.
- Repeat the above step for the second and third speed levels.
- Record the speed results for each mode.

3. Results and Discussion

In the maximum speed test of the converted electric bicycle, the data showed that the bike was able to reach a top speed of 37.6 km/h. During the test, the bike covered a distance of

3.73 km in 20 minutes and 42 seconds, resulting in an average speed of 10.8 km/h. Addi-tionally, the test recorded an elevation gain of 22 meters, with the highest elevation reach-ing 84 meters as shown in the Figure 6.

This maximum speed demonstrates the optimal performance of the 500W BLDC motor, supported by a battery pack module as the power supply. The data indicates that the elec-tric bicycle has adequate performance for use on flat roads as well as on routes with slight elevation. The test also confirmed that the speed control via the throttle operated as de-signed, providing a good response when the bike was accelerated.

Figure 6. Dynamic performance test

Figure 7. Performance measurement.

In the current test conducted when the electric bicycle reached its maximum speed under no-load conditions are shown in Figure 7, the data showed that the current flow at the first speed level was 0.28 A, at the second speed level was 0.78 A, and at the third speed level reached 1.09 A.

These current values indicate that the 500W BLDC motor system and the controller oper-ate efficiently in regulating power consumption when the bicycle is in a no-load condition. The increase in current corresponding to higher speed levels demonstrates a linear relationship between motor speed and electrical current demand.

The results also suggest that the power consumption remains within safe limits, supporting the overall stability and efficiency of the system. This test provides an overview of the system's performance under no-load conditions and can serve as a reference for further analysis under loaded conditions.

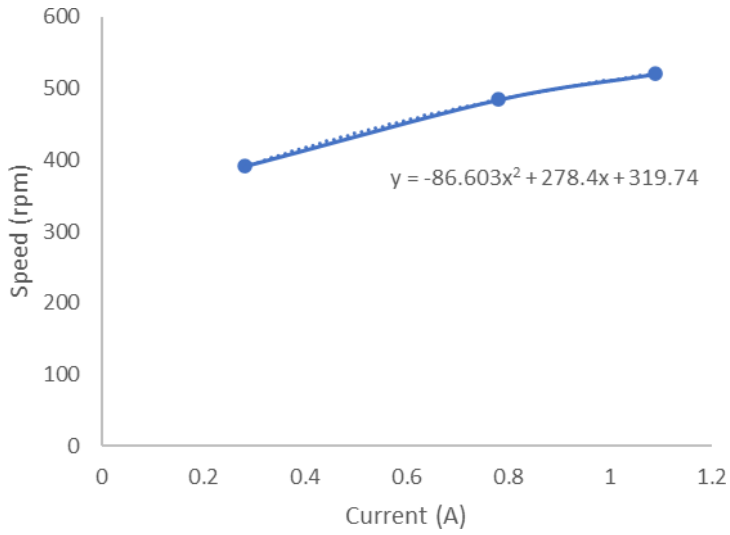

Figure 8. Speed and current relationship curve.

The maximum speed for this e-bike using this type of motor-hub can reach up to more than 500 rpm with 1.1A current as seen on Figure 8. Based on the curve generated, the relationship between Speed and Current can be formed an equation represented as:

$$\boldsymbol{Speed} = \mathbf{-86.603}\boldsymbol{Current}^{\mathbf{2}} + \mathbf{278.4}\,\boldsymbol{Current} + \mathbf{319.74}$$

4. Conclusion

The Li-ion battery pack design using IOT of 4.5 kg weight with the strength and flexibility. It is tested with the converted e-bike for several assessments. The level speed shows that it requires 1A current for a speed of 500rpm. The maximum speed reached 37.6 km/h. Moreover, the bike performance can be monitored a distance of 3.73 km in 20 minutes and 42 seconds. The battery pack performance is sufficient to be used in this campus academician mobilities. Moreover, it is more convenient to monitor the energy status using the IOT. Therefore, those values show that developing the IOT battery pack for supporting converted electric-bikes in this campus are potential to be implemented.

Acknowledgment

The authors would like to thank you the Lector Research Grant Scheme of Politeknik Negeri Jakarta for supporting facilities to conduct this research.

References

[1] Ç. Tozluoğlu, Y. Liao, and F. Sprei, "Potential of e-bikes to replace passenger car trips and reduce greenhouse gas emissions," *Journal of Cycling and Micromobility Research,* vol. 2, p. 100043, 2024/12/01/ 2024, doi: https://doi.org/10.1016/j.jcmr.2024.100043.

[2] N. Horesh and J. C. Quinn, "Fuel shifts reduce most of the greenhouse gas emissions from transportation in the United States," *Communications Earth & Environment,* vol. 5, no. 1, p. 781, 2024/12/20 2024, doi: 10.1038/s43247-024-01924-4.

[3] H. D. S. B. D. A. S. M. A. A. S. B. A. S. S. F. Z. G. H. N. R. S. Sonki Prasetya, "Development of Smart Magnetic Braking Actuator Control for a Heavy Electric Vehicle," *International Journal of Tech-nology,* vol. 11, no. 7, pp. 291-319, 2020/12/17 2020, doi: https://doi.org/10.14716/ijtech.v11i7.4462.

[4] S. Prasetya *et al.*, "Structural performance evaluation of mobile solar-powered battery swap station for electric motorcycles," *Eastern-European Journal of Enterprise Technologies,* vol. 6, no. 8 (132),

pp. 25-33, 12/30 2024, doi: 10.15587/1729-4061.2024.318787.

[5] E. Arsenio, J. V. Dias, S. A. Lopes, and H. I. Pereira, "Assessing the market potential of electric bicycles and ICT for low carbon school travel: a case study in the Smart City of ÁGUEDA," *European Transport Research Review,* vol. 10, no. 1, p. 13, 2018/01/20 2018, doi: 10.1007/s12544-017-0279-z.

[6] X. Zhu, D. Lyu, J. Xu, and Y. Lin, "Travel Characteristics and Cost–Benefit Analysis of Bikeshare Service on University Campuses," *Sustainability,* vol. 17, no. 8, p. 3489, 2025. [Online]. Available: https://www.mdpi.com/2071-1050/17/8/3489.

[7] J. Liu *et al.*, "A Study of Electric Bicycle Lithium Battery Charging Monitoring Using CNN and BiLSTM Networks Model with NILM Method," *Electronics,* vol. 13, no. 16, p. 3316, 2024. [Online]. Available: https://www.mdpi.com/2079-9292/13/16/3316.

[8] Denny Haryanto Sinaga, Muhammad Aulia Rahman Sembiring, Rudi Salman, Olnes Yosefa Hutajulu, Arwadi Sinuraya," Calculation of Capacity and Usage Time of Lithium-Ion Batteries on electric Bikes with 350W BLDC Motors", Fidellity Journal Teknik Elektro, vol. 5, no. 2, pp. 149-155, 2023.

[9] S. Sen, P. Talebizadehsardari, A. La Rocca, A. Cairns, A. Pacino, and R. Mehdipour, "Effect of Different Module Arrangements for Thermal Management of Cylindrical Li-ion Battery Packs " pre-sented at the 50th IECON: Annual Conference of the IEEE Industrial Electronics Society, 2024.

[10] S. Castano-Solis, D. Serrano-Jimenez, L. Gauchia, and J. Sanz, "The Influence of BMSs on the Characterization and Modeling of Series and Parallel Li-Ion Packs," *Energies,* vol. 10, no. 3, p. 273, 2017. [Online]. Available: https://www.mdpi.com/1996-1073/10/3/273.

[11] A. Rahmani, M. Dibaj, and M. Akrami, "Recent Advancements in Battery Thermal Management Systems for Enhanced Performance of Li-Ion Batteries: A Comprehensive Review," *Batteries,* vol. 10, no. 8, p. 265, 2024. [Online]. Available: https://www.mdpi.com/2313-0105/10/8/265.

PT. Mencerdaskan Bangsa Indonesia

PT MENCERDASKAN BANGSA INDONESIA
(MBI), 4th Floor Gedung STC Senayan Room
31-34, Jl. Asia Afrika Pintu IX, Jakarta 10270,
Indonesia.